REPORT NO. NADC–78226–30

ATLAS OF INFRARED IMAGERY OF THE SEA SURFACE

Prepared by:

Barbara J. Moser

SEMCOR, Inc.
under Contract
to
NAVAL AIR DEVELOPMENT CENTER
Warminster, Pennsylvania 18974

Contract N62269-77-C-0382

25 AUGUST 1978

Approved for Public Release; Distribution Unlimited

Prepared for:

NAVAL AIR SYSTEMS COMMAND
Department of the Navy
Washington, D.C. 20360

UNCLASSIFIED

SECURITY CLASSIFICATION OF THIS PAGE (When Data Entered)

REPORT DOCUMENTATION PAGE		READ INSTRUCTIONS BEFORE COMPLETING FORM
1. REPORT NUMBER NADC-78226-30	2. GOVT ACCESSION NO.	3. RECIPIENT'S CATALOG NUMBER
4. TITLE (and Subtitle) ATLAS OF INFRARED IMAGERY OF THE SEA SURFACE		5. TYPE OF REPORT & PERIOD COVERED Phase 6. PERFORMING ORG. REPORT NUMBER
7. AUTHOR(s) Barbara J. Moser		8. CONTRACT OR GRANT NUMBER(s) N62269-77-C-0382
9. PERFORMING ORGANIZATION NAME AND ADDRESS SEMCOR, Inc. Route 38 Moorestown, N.J. 08057		10. PROGRAM ELEMENT, PROJECT, TASK AREA & WORK UNIT NUMBERS
11. CONTROLLING OFFICE NAME AND ADDRESS Naval Air Development Center (Code 3011) Warminster, PA 18974		12. REPORT DATE 25 August 1978 13. NUMBER OF PAGES 122
14. MONITORING AGENCY NAME & ADDRESS(if different from Controlling Office)		15. SECURITY CLASS. (of this report) UNCLASSIFIED 15a. DECLASSIFICATION/DOWNGRADING SCHEDULE

16. DISTRIBUTION STATEMENT (of this Report)

Approved for public release; distribution unlimited

17. DISTRIBUTION STATEMENT (of the abstract entered in Block 20, if different from Report)

18. SUPPLEMENTARY NOTES

19. KEY WORDS (Continue on reverse side if necessary and identify by block number)

infrared	oceanography
thermal	ocean surface
imaging	sea surface
mapping	line scanner

20. ABSTRACT (Continue on reverse side if necessary and identify by block number)

This report is a collection of 192 examples of thermal imagery recorded from aircraft over bodies of water. These infrared pictures show the surface expressions of eddies, convection cells, currents, and thermal fronts in addition to sea ice, wind streaks, whitecaps, and waves. Explanatory information, such as portions of National Ocean Survey charts corresponding to some of the imagery, is provided. The imagery presented was recorded during the period

DD FORM 1 JAN 73 1473 EDITION OF 1 NOV 65 IS OBSOLETE

UNCLASSIFIED

SECURITY CLASSIFICATION OF THIS PAGE (When Data Entered)

May 1959 to May 1972 by seven airborne passive infrared line scanners (the Reconofax Camera; AN/AAD-2; Reconofax IV, Mark II; AN/AAR-30; AN/AAR-32; AN/AAR-35; and Reconofax XIIIA); brief descriptions of the equipment and a table of design and performance parameters are supplied. The imagery was recorded in the 3- to 5.5-μm and 8- to 14-μm spectral bands. Sensitivities of sets with the various detector types employed (Ge:Au, Ge:Cu, Ge:Hg, InSb, HgCdTe) ranged from 0.001 to 0.3 K; resolutions varied from 18.4 to 1.0 mrad.

PREFACE

During the period November 1958 to July 1972, the Naval Air Development Center conducted a number of classified flight trials of passive infrared imaging equipment. More than 325 flights were conducted over both land and water and a wealth of data, much of which has now been declassified, was amassed. Under Contract N62269-77-C-0382, SEMCOR, Inc. was engaged to review these data and prepare an atlas of infrared imagery of oceanographic phenomena. Of the 409 rolls of film recorded during the flights, selected portions, chosen for their technical interest, are presented in this report in an effort to illustrate a variety of ocean surface effects. Brief descriptions of the equipment employed and remarks on the interpretation of the imagery are also provided.

TABLE OF CONTENTS

LIST OF TABLES

LIST OF ILLUSTRATIONS

INTRODUCTION

Every object radiates electromagnetic energy at a rate that is proportional to both the fourth power of its absolute temperature and to the radiant efficiency (emissivity) of the radiating object. For objects at room temperature, approximately 2 percent and 37 percent of this energy is radiated in the 3- to 5.5-μm and the 8- to 14-μm portions, respectively, of the infrared spectrum. In general, objects in a given scene exhibit differences in temperature, emissivity, and reflectivity. Accordingly, it is possible for an imaging device operating in these portions of the spectrum to record pictures of objects by virtue of their infrared incandescence even in absolute darkness.

EQUIPMENT DESCRIPTIONS

The thermal pictures presented in this atlas were obtained with seven equipments manufactured by HRB-Singer, Inc. (the Reconofax Camera; AN/AAD-2; Reconofax IV, Mark II; AN/AAR-30; AN/AAR-32; AN/AAR-35; and Reconofax XIIIA). Because all the equipments are very similar, only the AN/AAD-2 infrared mapping set is described (see Figure 1).

The AN/AAD-2 was designed originally for use in U.S. Army Signal Corps drone aircraft and was modified by the Naval Air Development Center for high-sensitivity over-water use. It operates in the following manner. A small portion of the infrared radiation emitted or reflected by the objects under surveillance is intercepted by the plane 45^{o}-angle scanning mirror, which is mounted on a rotating shaft whose axis is parallel to the flight path of the aircraft. As this mirror rotates at a rate of 100 revolutions per second, radiant energy from each object point along a line perpendicular to the flight path is sampled sequentially and focused by means of a parabolic mirror onto a cooled infrared detector. The electrical signal generated in the detector is amplified and passed on to a glow tube which emits light whose intensity is proportional to the electrical signal impressed upon it. Light from the glow tube is focused to a small spot by means of a microscope objective, which is also mounted on the rotating shaft. The intensity-modulated spot of light scans across a piece of slowly advancing photographic film in synchronism with the scanning mirror. As the aircraft advances, a 120^{o} field of view of the terrain below is swept out by the scanner and recorded on photographic film in the form of a continuous strip map. In the infrared pictures included in this report, effectively warm areas are rendered in light tones and effectively cool areas are rendered in dark tones.

The other scanning equipments, except for slight differences, operate in the same manner. Design and performance parameters of these sets are provided in Table I.

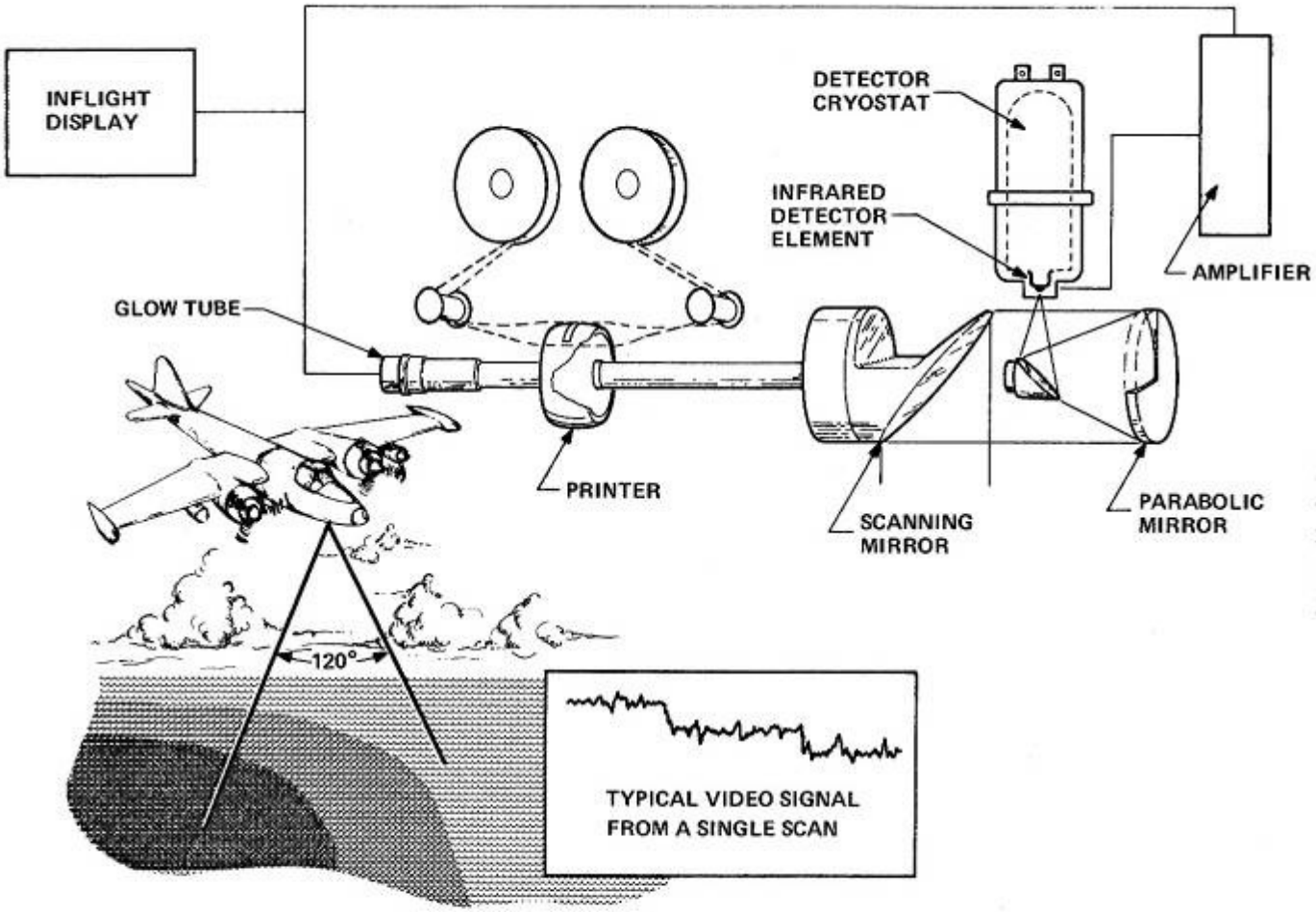

Figure 1. Schematic of AN/AAD-2 Operation

TABLE I. DESIGN AND PERFORMANCE PARAMETERS OF INFRARED IMAGING SETS

INFRARED IMAGING SET	RECONOFAX CAMERA	AN/AAD-2 AND RECONOFAX IV, MARK II	AN/AAR - 30	AN/AAR - 32	AN/AAR - 35	RECONOFAX XIIIA
EFFECTIVE OPTICAL APERTURE (cm2)	40	43.8	445	47	47.8	50
FOCAL LENGTH (mm)	153	153	381	153	153	100
FACETS ON SCAN MIRROR	1	1	1	1	1	6
SCAN SPEED (RPM)	180 - 3 000	6 000	1 080	6 000	11 100	12 000
LINES SCANNED PER SECOND	3-50	100	33	100	185	800
LATERAL FIELD OF VIEW (degrees)	140	120	140	120	120	120
DETECTOR TYPES	Ge:Au	(A,B,C) Ge:Cu (D) Ge:Hg (E) InSb (F) Ge:Au	(A,B,C) Ge:Cu (D,E,F,G) Ge:Hg (H) InSb (I) HgCdTe	Ge:Hg	Ge:Hg	(A,B,C) HgCdTe (D) InSb
SIZES OF DETECTORS	3.2 mm2 (CIRCULAR)	(A) 6.25 mm2 (CIRCULAR) (B) 6 x 6 mm (C) 0.5 mm (DIAMETER) (D) 2.5 x 2.5 mm (E) 2.5 x 2.5 mm (F) 3 mm2 (CIRCULAR)	(A) 6.25 mm2 (CIRCULAR) (B) 4.0 mm2 (CIRCULAR) (C) 0.5 mm (DIAMETER) (D) 4.0 mm2 (CIRCULAR) (E) 3 x 3 mm (F) 2.5 x 2.5 mm (G) 6.25 mm2 (CIRCULAR) (H) 7 x 7 mm (I) 0.45 x 0.43 mm	(A) 2.5 x 2.5 mm (B) 0.5 x 0.5 mm (C) 0.5 mm (DIAMETER)	0.3 x 0.3 mm	(A) 0.1 x 0.1 mm (B) 0.2 x 0.2 mm (C) 0.4 x 0.4 mm (D) 0.4 x 0.4 mm
SPECTRAL BAND (μm)	2-9	(A,B,C,D) 8-14 (E) 3-5.5 (F) 2-9	(A,B,C,D,E,F,G) 8-14 (H) 3-5.5 (I) 8-13	2-14, 8-14	2-14, 8-14	(A,B,C) 8-13 (D) 3-5.5
INSTANTANEOUS FIELD OF VIEW (mrad)	13.2	(A) 18.6 (B) 39.2 (C) 3.3 (D) 18.3 (E) 18.3 (F) 12.8	(A) 7.4 (B) 5.9 (C) 1.3 (D) 5.9 (E) 7.9 (F) 6.9 (G) 7.4 (H) 18.4 (I) 1.2	(A) 18.3 (B) 3.3 (C) 3.3	2.8	(A) 1.0 (B) 2.0 (C) 4.0 (D) 4.0
NOISE EQUIVALENT TEMPERATURE DIFFERENCE (K)	0.1	(A) 0.01 (B) 0.002 (C) 0.06 (D) 0.01 (E) 0.03 (F) 0.1	(A) 0.003 (B) 0.004 (C) 0.08 (D) 0.005 (E) 0.006 (F) 0.011 (G) 0.006 (H) 0.001 (I) 0.05	(A) 0.01 (B) 0.06 (C) 0.07	0.17	(A) 0.3 (B) 0.15 (C) 0.07 (D) 0.1
FILM WIDTH (mm)	70	70	127	70	70	70
STABILIZATION (ROLL AXIS ONLY) (degrees)	±35	±30	±30	±30	±30	±10

A Barnes model R-8B1 radiometer, an infrared device that senses ocean surface radiation and produces strip-chart recordings of the profiles of thermal patterns along the path of the aircraft, was also used during many of the flights. Table II lists relevant data pertaining to the Barnes radiometer.

TABLE II. DESIGN AND PERFORMANCE PARAMETERS OF THE BARNES RADIOMETER

Set	Radiometer Model R-8B1
Manufacturer	Barnes Engineering Company
Data recording	Clevite Brush Model 280 chart recorder
Optical aperture (cm^2)	99
Focal length (cm)	30.5
Detectors	Germanium immersed thermistor bolometers (two)
Signal produced by a temperature change of 1 K in an extended area blackbody	Approximately 250 μ V
Instantaneous field of view (deg)	0.4 X 2.0
Video bandwidth (Hz)	(a) 2.0 (b) 1.0 (c) 0.1
Noise equivalent temperature difference (K)	(a) 0.03 (b) 0.02 (c) 0.006
Scene area integrated per time constant (for aircraft velocity of 180 knots and altitude of 1000 ft)	Bandwidth (Hz) / Width (across track) (ft) / Length (along track) (ft) 2.0 / 35 / 32 1.0 / 35 / 57 0.1 / 35 / 510
Stabilization	None

INTERPRETATION OF THE IMAGERY

Water is very opaque to electromagnetic radiation in the intermediate and far infrared spectral bands concerned; accordingly, the thermal patterns pictured in this report represent effects occurring in the upper few hundredths of a millimeter of the water. Therefore, thermal profiles obtained with infrared imaging devices do not necessarily agree with bucket temperature measurements.

As mentioned previously, passive infrared imaging sensors respond to infrared radiation emitted by and reflected from the scene under surveillance. The radiation emitted is governed by the relation $W = \sigma \epsilon T^4$, in which W is the radiant power per unit area emitted from the surface, σ is the Stefan-Boltzmann constant (5.67×10^{-8} W/m^{2}K^4), T is the absolute temperature, and ϵ is the emissivity, a dimensionless quantity that is a measure of the "blackness" of a body. Emissivity is a function of the material, its surface quality, and angle of observation and has a value of zero for a perfect reflector and unity for a perfect absorber. Thus, variations in surface roughness and viewing angle may be recorded as variations in apparent temperature.

Reflectivity (ρ) and emissivity are interrelated by the expression $\rho = 1 - \epsilon$. Both of these quantities are plotted in Figure 2 as functions of the angle of observation relative to the normal. Because the emissivity decreases with increasing angle, the apparent temperature of the scene may vary as a function of scan angle, with the edges of the pictures appearing cold (dark) relative to the centers, unless some other factor dominates. One factor that could offset this effect would be the existence of a deck of low-altitude clouds whose temperature is greater than that of the ocean surface. In this case, as the angle at which the surface is viewed increases, a greater contribution of radiation is received from the clouds because of the increase in reflectivity with angle; this would tend to make the edges of the pictures appear warmer (lighter) than the centers.

Another characteristic of the recorded imagery is the greater prominence of ocean waves near the edges of the pictures than at the centers. This can be understood in terms of Figure 2. At angles of about 0° to 30°, there is very little variation in emissivity with angle. Thus, at near normal viewing angles, typical wave slopes of 20° or less produce very little variation in the amount of radiation emitted or reflected. However, at viewing angles of the order of 50°, the emissivity curve is much steeper and therefore the wave slopes give rise to larger variations in emissivity.

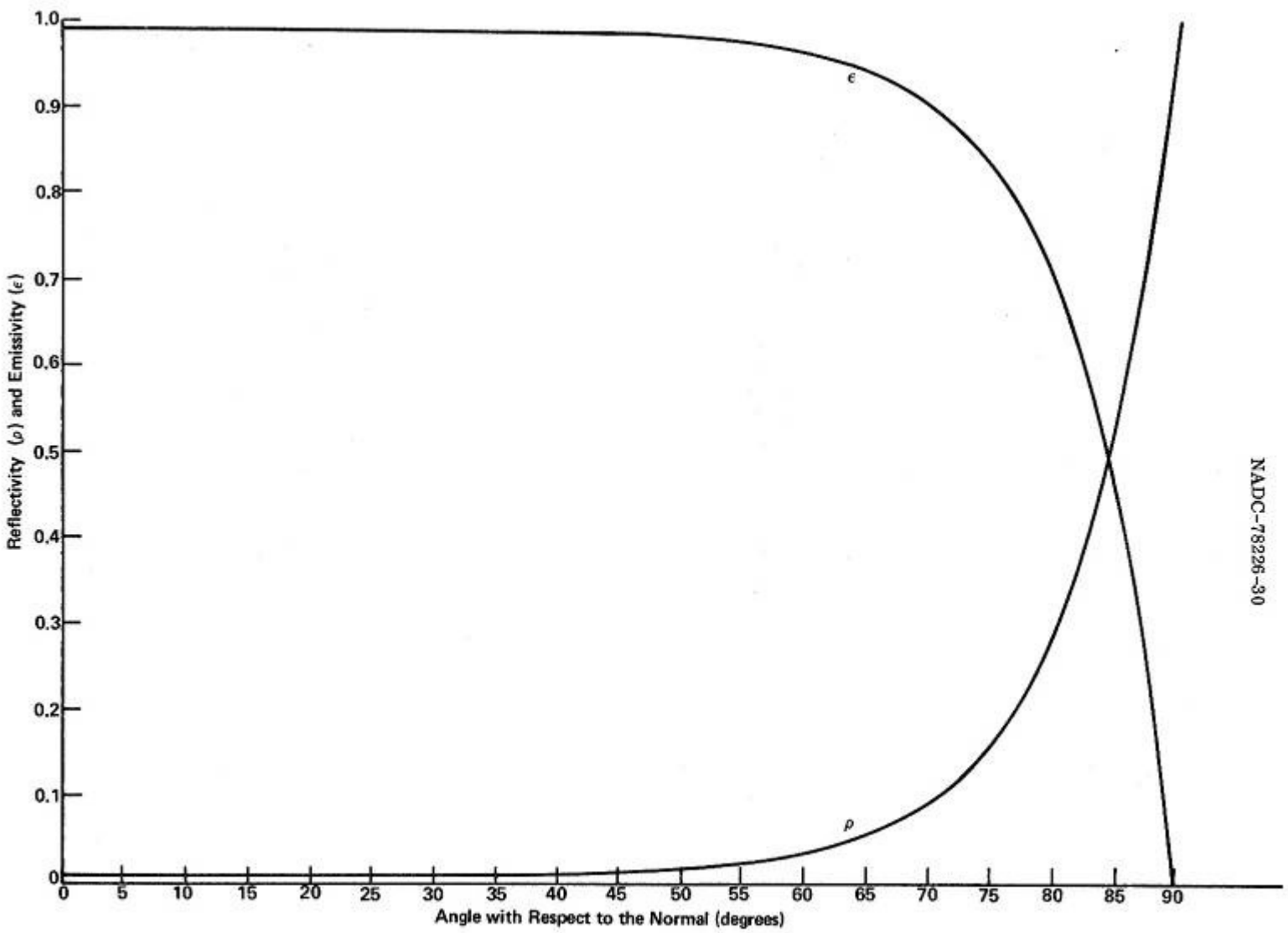

Figure 2. Reflectivity (ρ) and Emissivity (ϵ) of a Smooth Water Surface With Respect to Angle for 10 μm Radiation.

Another factor causing variations in the apparent scene temperatures recorded is the atmosphere between the sensor and the sea surface. Because the atmosphere is not perfectly transparent, it absorbs a certain amount of the radiation emitted by the sea surface that otherwise would have been intercepted by the sensor. Furthermore, the intervening atmosphere emits radiation that is detected by the infrared scanner. If the sea surface and the intervening atmosphere are at the same temperature, the atmosphere contributes an amount of radiation equal to that which it absorbs. If the atmosphere is cooler than the water, it absorbs more than it radiates and, conversely, if its temperature is greater than that of the water's surface, it radiates more than it absorbs. Since the path length through the atmosphere varies inversely as the cosine of the angle between the normal to the sea surface and the scanner's instantaneous viewing direction, such atmospheric effects are more pronounced at the edges of the pictures than at the center. Thus, an intervening atmosphere that is warmer than the water surface tends to cause the edges of the picture to appear warmer (lighter) than the center, and conversely.

Another factor influencing the appearance of the imagery stems from the fact that during each 360° of rotation of the scanning mirror, the detector views the inside of the scanner unit two-thirds of the time (240° of rotation) and the ocean surface one-third of the time (120°). Because of the dissipation of electrical energy in the scanner, the interior of the scanner housing is usually warmer than the sea surface. Thus, during each "inactive" portion of the scan cycle, the detector element may receive a burst of radiant energy from which it and the first stage of preamplification must recover during the "active" portion of the scan cycle. This recovery may appear on the pictures as a gradual monotonic shading from one edge to the other.

The infrared imaging sets employed are limited in dynamic range by their recording devices such that the largest temperature difference that can be recorded without saturation is about 100 times greater than the smallest. Thus, if the set were operating with a gain setting that would permit recording of temperature differences of 0.01 K, then temperature differences greater than 1.0 K would overload the system. Experience with high-sensitivity over-water infrared imaging devices has shown that, with the exception of whitecaps, temperature differences associated with large-area ocean surface patterns tend to be greater than those associated with small-area patterns. Accordingly, in a scene containing a wide range of pattern sizes, the large patterns may dominate to the exclusion of the small ones unless some form of compensation is applied.

The problem of variation in apparent scene temperature as a function of scan angle and the problem of limited dynamic range were addressed in the AN/AAD-2 by the simple artifice of replacing a preamplifier interstage coupling capacitor that passed frequencies as low as a few hertz with one of much smaller capacitance that, on a relative basis, "rolled off" the low-frequency response

and boosted the high-frequency response. Apparent temperature variations occurring at the scan frequency (100 Hz) and a few harmonics above it were then greatly suppressed and the small-area sea surface patterns, corresponding to frequencies of the order of 5 to 20 kHz, were enhanced. This change yielded pictures in which a wide range of sea surface pattern sizes could be seen, but denied the observer the ability to make simple inferences of the magnitudes of temperature differences characterizing them. In a later equipment, the AN/AAR-30, provisions were made for subtracting out effects occurring as a function of scan angle and for controlling in flight the frequency and slope of low-frequency roll-off. The effects of different roll-off settings on the imagery are illustrated in Figures 34 to 37.

An adverse effect of reducing the capacitance of the preamplifier interstage coupling capacitor is that that part of the circuit then acts as a differentiator and the output waveform represents the superposition of the input waveform and its first derivative. To illustrate this effect, suppose that the aircraft is flying along the edge of a sharply defined ocean front with cool water on the left side and warm water on the right. As the scan spot moves from left to right across the front, the abrupt change in signal level is accentuated and, on successive scans, the front is outlined in white on the picture. On the other hand, if the aircraft were to reverse direction and travel along the front such that the warm water were on the left and the cool water were on the right, the effect of differentiation would be to outline the front in black. These effects are illustrated in Figures 7 and 8.

Because these infrared imaging sets do not provide dc response or dc restoration, an apparent temperature depicted at a given point in the imagery represents only the effective temperature at that point relative to the effective temperatures of other nearby points along the same scan line. For this reason, gradual variations in scene temperature along the direction of flight are not revealed on the imagery.

Typically, the scan rate of the infrared imaging equipments was significantly greater than that required to produce contiguous scans as the aircraft advanced. Therefore, the radiation from the scene was sampled a number of times during successive scans. Because the photographic film used as a recording medium was capable of integrating the signals over successive scans, the signals would build up in proportion to the number of independent looks at any given target point, whereas the noise would build up only in proportion to the square root of the number of looks. Accordingly, the recorded signal-to-noise ratio was improved relative to what the (single-look) noise equivalent temperature difference should imply, by a factor of the square root of the overlap ratio. As an example, consider the AN/AAD-2 operating with a 2.5- by 2.5-mm detector at an aircraft altitude of 2000 feet and a speed of 180 knots. A detector of such dimensions in an optical system of 153-mm focal length provides an instantaneous field of view of 16.3 mrad which, when projected to the water surface beneath the

aircraft, defines a square area 32.6 feet on a side. During the interval between each successive scan (0.01 second), though, the aircraft advances only about three feet. Thus, for this set of conditions, the scanner will acquire more than ten looks at each point in the scene and an attendant improvement in sensitivity of the square root of ten.

Because of the nature of the equipment, the infrared pictures obtained are cylindrical projections of the scene under surveillance. The horizontal dimension of each picture is a time axis, which can be treated as a measure of the distance for the general case where the aircraft velocity is held constant for the length of the picture. The vertical dimension is angular, but the displacement of the scanning spot from a point directly below the aircraft is proportional to the tangent of the scanning angle with respect to the normal. This causes information at large viewing angles to appear compressed on the imagery in the direction of scan. This distortion can be seen near the edges of Figure 8.

Numerical values of sea state accompany some of the infrared pictures as an additional aid to interpretation of the imagery. The sea state is a description of the ocean surface with regard to wave action. According to the U.S. Navy Oceanographic Office scale, low values of sea state (0-1) indicate relatively calm seas; larger numbers correspond to progressively rougher surfaces, and high values (8-9) describe a confused ocean with mountainous, foaming waves.

Large temperature variations across the surface of the water may overload the highly sensitive equipment and produce signal overshoots of the opposite polarity. These overshoots, which appear beyond the patterns in the direction of scan, should be disregarded.

Two parallel dark lines run along the length of some of the pictures; these are the result of partial film desensitization caused by crimping of the recording film in the compact film magazine and should be ignored.

The infrared imagery presented here is not necessarily centered directly below the line of flight of the aircraft since most of the figures were cropped before being printed. For the same reason, the vertical dimension of each figure may be less than the lateral field of view of the equipment employed. One may assume, for instance, a vertical scale of approximately 110^{o} (rather than the total field-of-view value of 120^{o}) for scenes recorded with the AN/AAD-2.

INFRARED IMAGERY

This section contains 192 thermal pictures taken from aircraft over bodies of water during the period May 1959 to May 1972. Surface expressions of eddies, convection cells, currents, and thermal fronts in addition to sea ice, wind streaks, whitecaps, and waves are pictured. Portions of National Ocean Survey charts corresponding to the imagery are included in some cases.

The figures are grouped in the following manner:

Subject Matter	Figure Number
Shoreline Scenes	3-6
Natural Surface Patterns	7-30
Manasquan Inlet Recorded with Different Equipment	31-33
Barnegat Inlet: Effects of Varying the Roll-Off Setting	34-37
Natural Surface Patterns	38-78
St. Andrew Bay	79-84
Chesapeake Bay Bridge	85-86
Islands and Reefs	87-96
Natural Surface Patterns	97-154
Persistence of Thermal Pattern	155-159
Gulf Stream	160-161
Bute Inlet	162-179
Oil Slicks	180-181
Pollutants in the Delaware and Schuylkill Rivers	182-186
Ice	187-194

Figure captions for most of the thermal pictures in this atlas adhere to the following format:

Figure number. Title.
Date; time (local civil time); aircraft altitude; latitude; longitude; equipment; size of detector and detector type; aircraft.

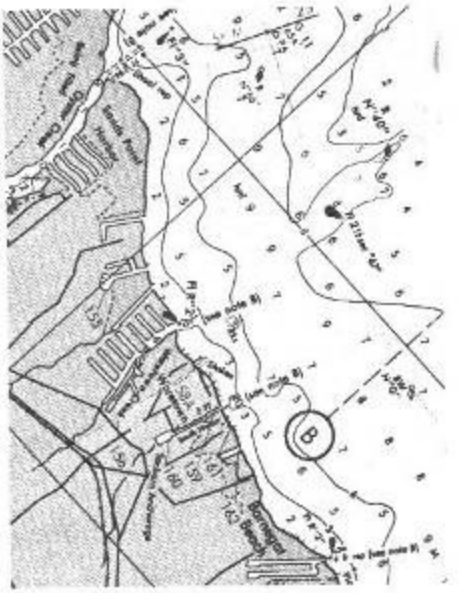

Figure 3. Shoal Water in the Vicinity of Waretown, New Jersey.
20 May 1959; 2200; 5000 ft; 39°48'N; 74°10'W; Reconofax Camera; 3.2 mm^2 (circular) p-type Ge:Au; HRB-Singer, Inc.; Cessna 310-B aircraft.
Compare with portion of NOAA Nautical Chart 12324 shown (soundings are in feet).

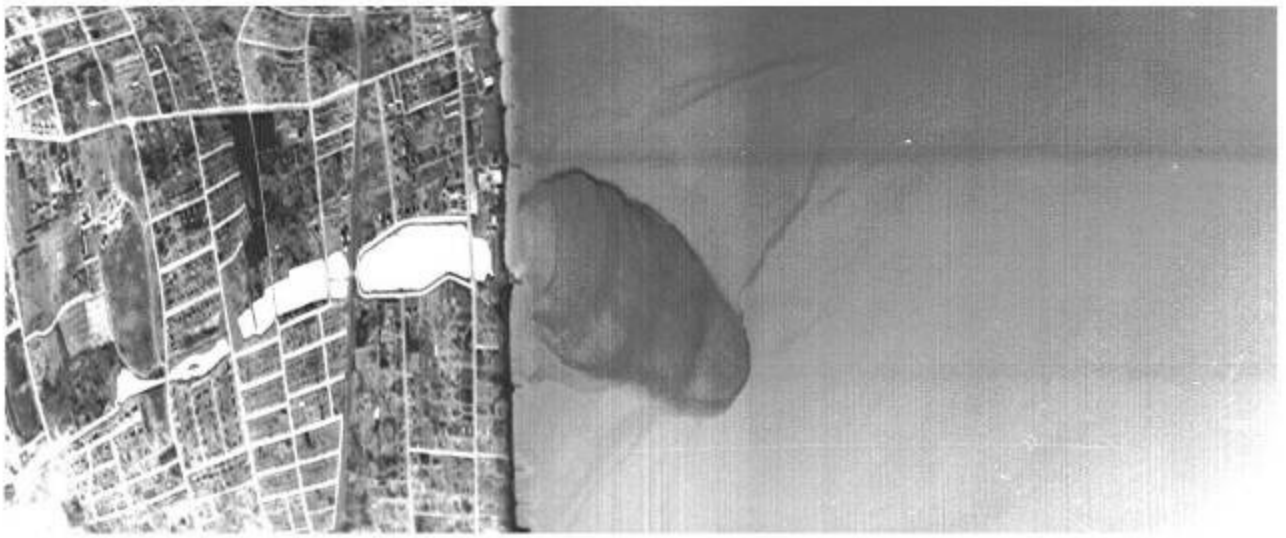

Figure 4. Overflow of Water from Takanassee Lake Reservoir. 3 April 1961; 2306; 2200 ft; $40^{o}17'N$; $74^{o}00'W$; AN/AAD-2; 3 mm^2 (circular) p-type Ge:Au; HRB-Singer, Inc.; Cessna 310-B aircraft.

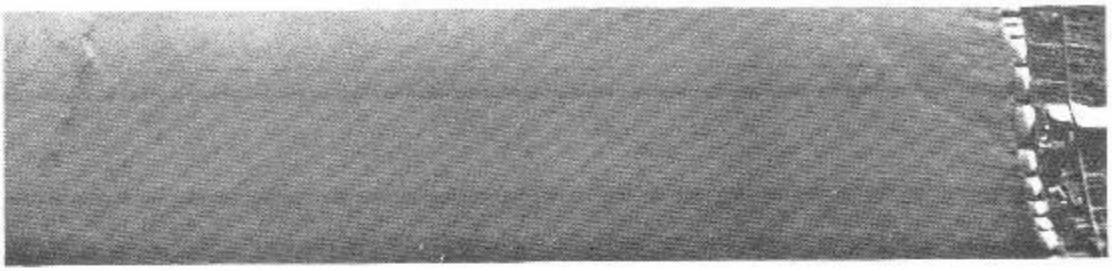

Figure 5. Shoreline, Piers, and Sea Surface Patterns.
8 November 1961; 2330; 2500 ft; 40°17'N; 74°02'W; AN/AAD-2;
2.5 X 2.5 mm InSb; P2V-5F aircraft Bu. No. 131403.
Notice the thermal discontinuity offshore.

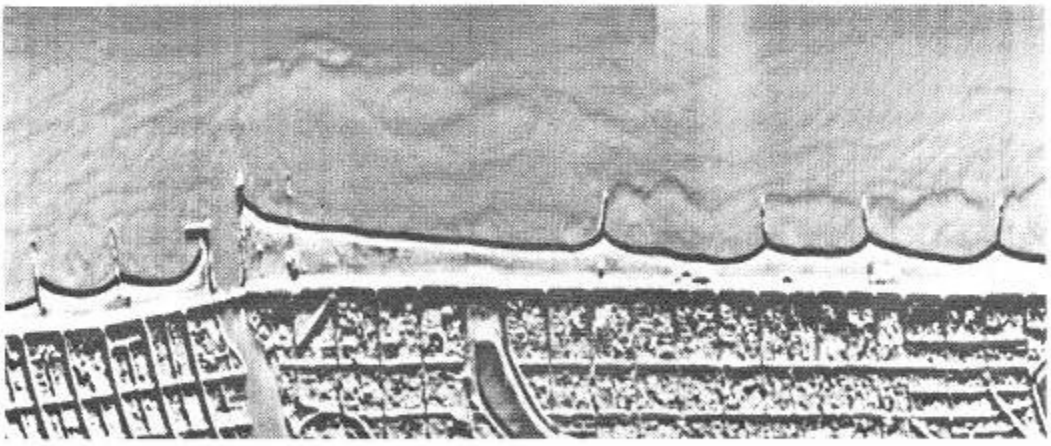

Figure 6. Shark River Inlet.
20 May 1964; 2151; 1400 ft; 40°11'N; 74°01'W; Reconofax IV
Mark II; 2.5 X 2.5 mm Ge:Hg; SP-2H aircraft Bu. No. 135616.

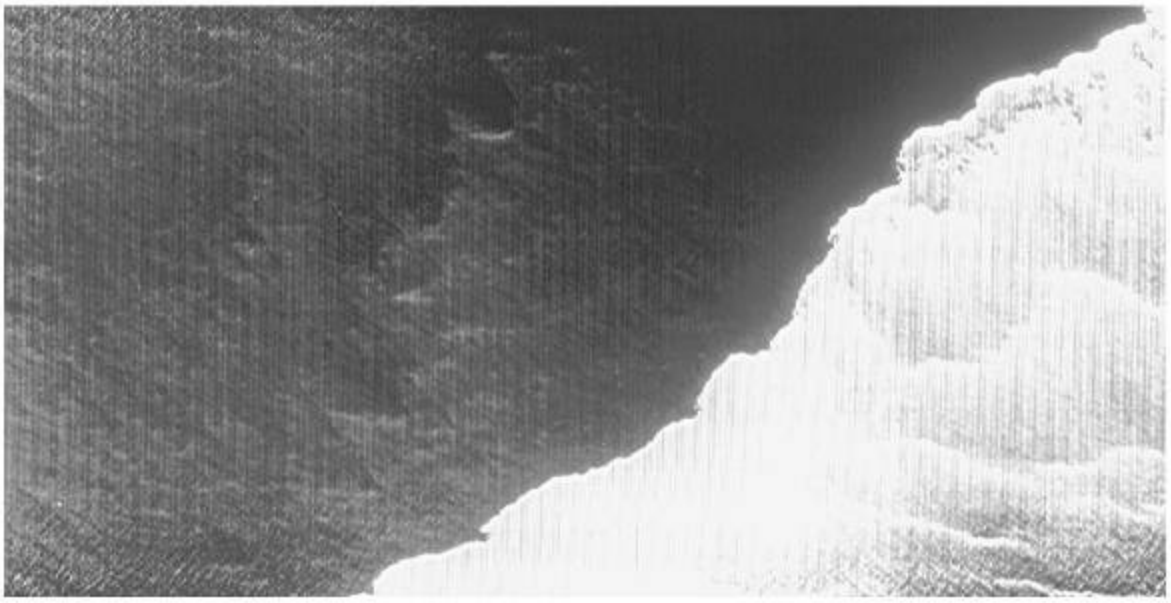

Figure 7. Thermal Front.
1 June 1967; 2011; 450 ft; AN/AAR-30; 6.25 mm^2 (circular) Ge:Cu; NP-2E aircraft Bu. No. 131403.

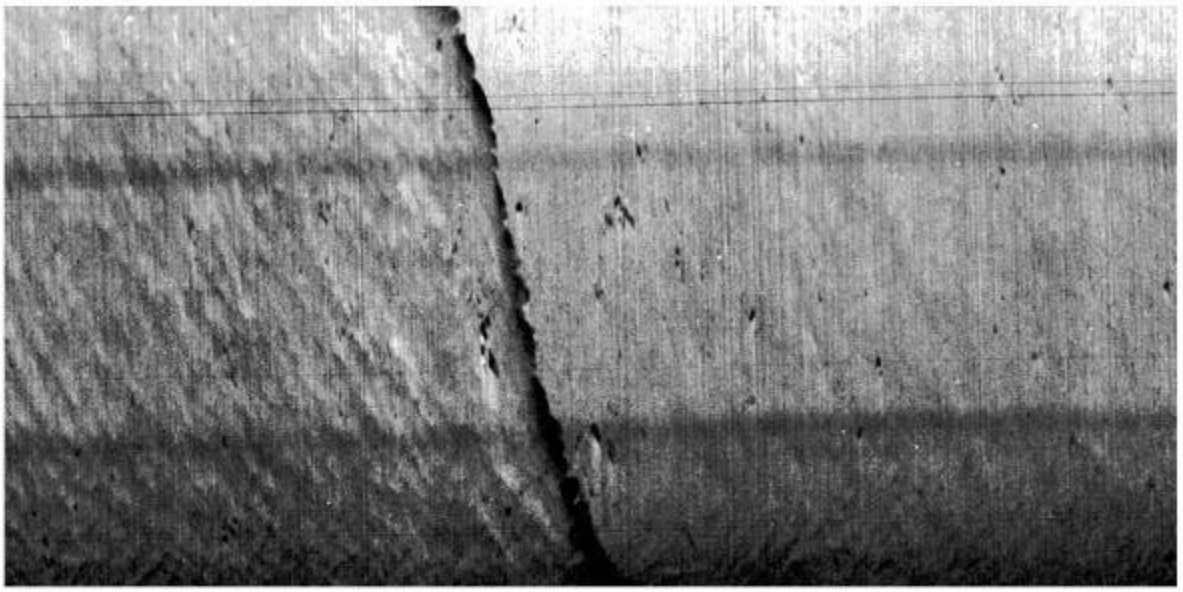

Figure 8. Natural Sea Surface Patterns.
21 November 1961; 1909; 2000 ft; 39°20'N; 71°55'W; AN/AAD-2; 2.5 X 2.5 mm InSb; P2V-5F aircraft Bu. No. 131403.
Note the whitecaps and the change in thermal "texture" across the front.

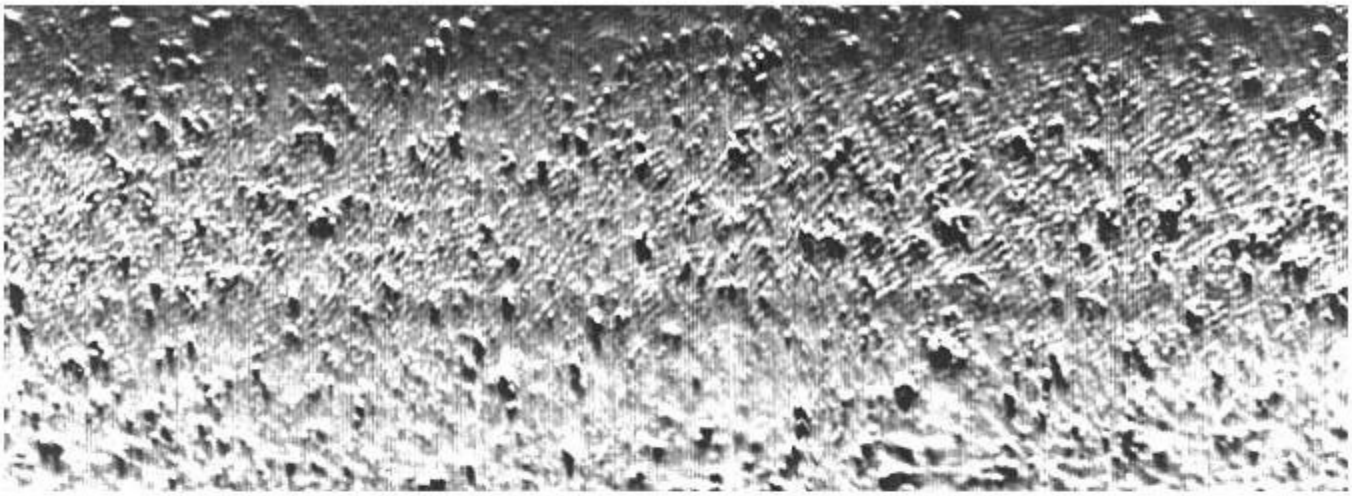

Figure 9. Whitecaps.
20 February 1962; 1507; 2600 ft; 39°34'N; 74°08'W; AN/AAD-2;
6.25 mm^2 (circular) Ge:Cu; P2V-5F aircraft Bu. No. 131403.
Sea state: 3.

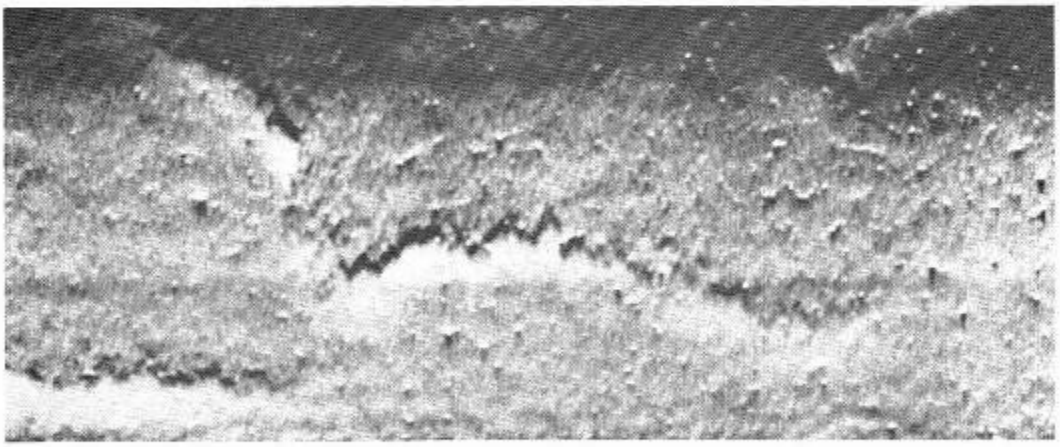

Figure 10. Whitecaps and Background Surface Patterns.
20 February 1962; 1548; 2600 ft; 39°23'N; 73°49'W; AN/AAD-2;
6.25 mm^2 (circular) Ge:Cu; P2V-5F aircraft Bu. No. 131403.
Sea state: 3.

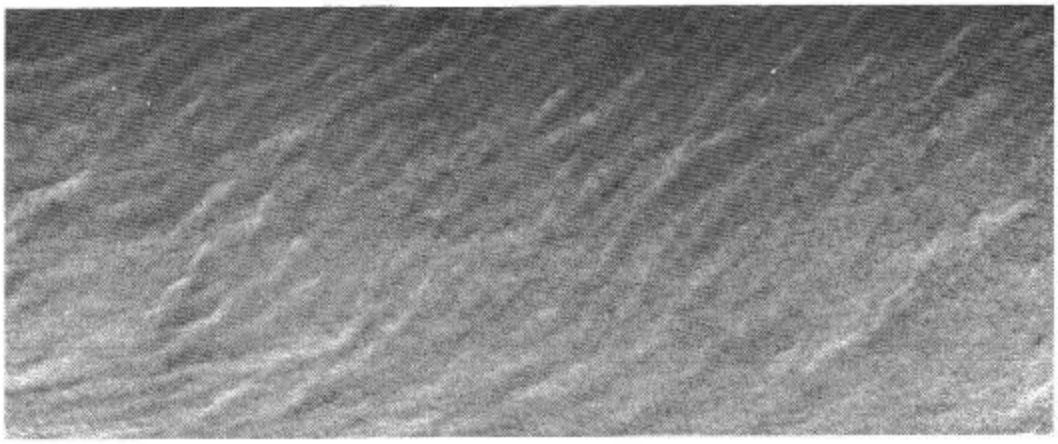

Figure 11. Natural Sea Surface Patterns.
15 March 1962; 1850; 1200 ft; 24°38'N; 83°02'W; AN/AAD-2;
6.25 mm^2 (circular) Ge:Cu; P2V-5F aircraft Bu. No. 131403.
Sea state: 2.

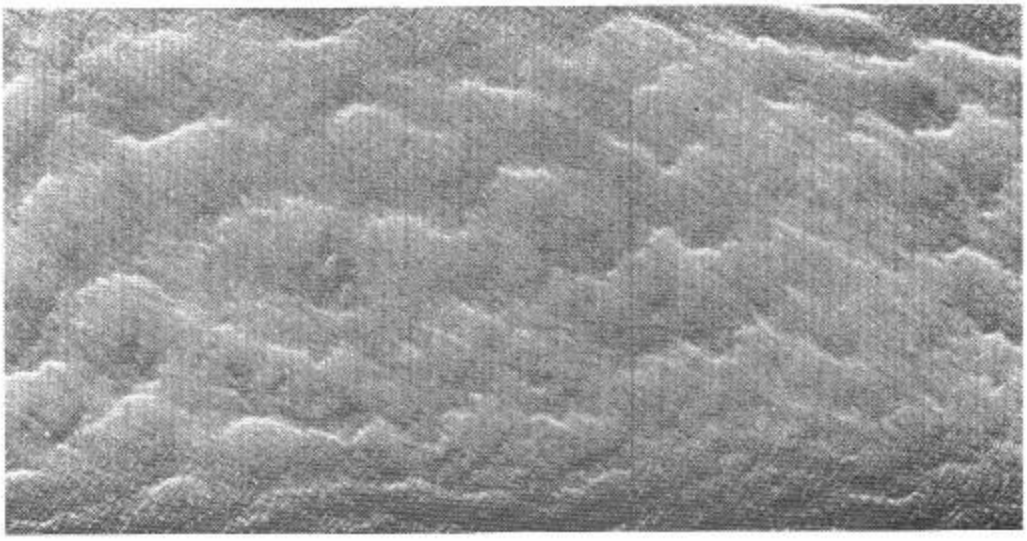

Figure 12. Natural Surface Patterns.
1 June 1967; 2012; 450 ft; AN/AAR-30; 6.25 mm^2 (circular) Ge:Cu;
NP-2E aircraft Bu. No. 131403.

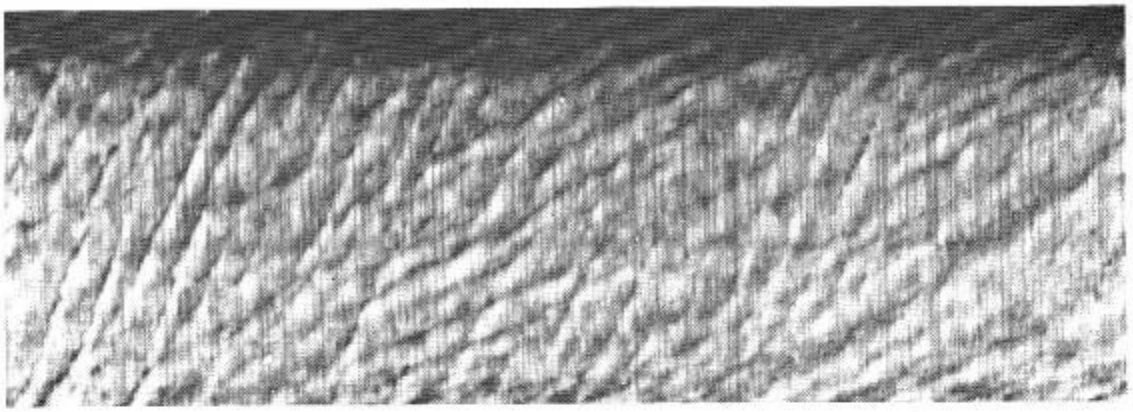

Figure 13. Wave Patterns.
5 March 1964; 2029; 1000 ft; 30°05'N; 85°43'W; Reconofax IV Mark II; 4 mm^2 (circular) Ge:Hg; NP-2E aircraft Bu. No. 131403.
Notice the propagation of waves in two different directions.

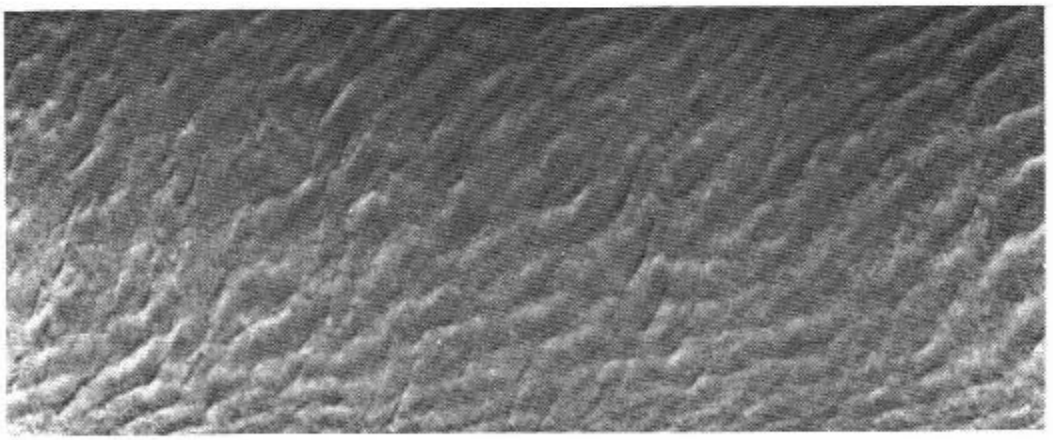

Figure 14. Natural Sea Surface Patterns.
15 March 1962; 1853; 1200 ft; 24°37'N; 83°03'W; AN/AAD-2; 6.25 mm^2 (circular) Ge:Cu; P2V-5F aircraft Bu. No. 131403.
Sea state: 2.

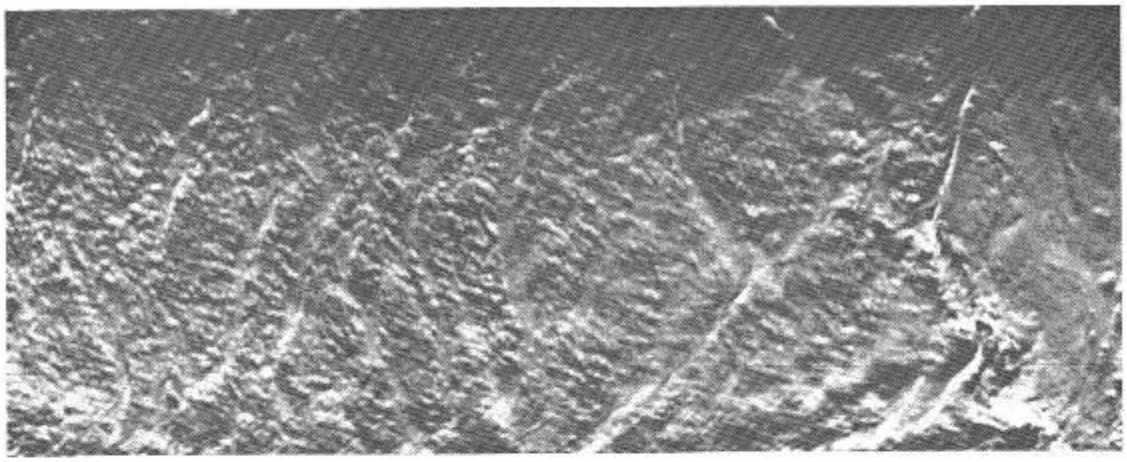

Figure 15. Natural Sea Surface Patterns.
19 April 1962; 2213; 2400 ft; 39°56'N; 71°16'W; AN/AAD-2;
6.25 mm^2 (circular) Ge:Cu; P2V-5F aircraft Bu. No. 131403.

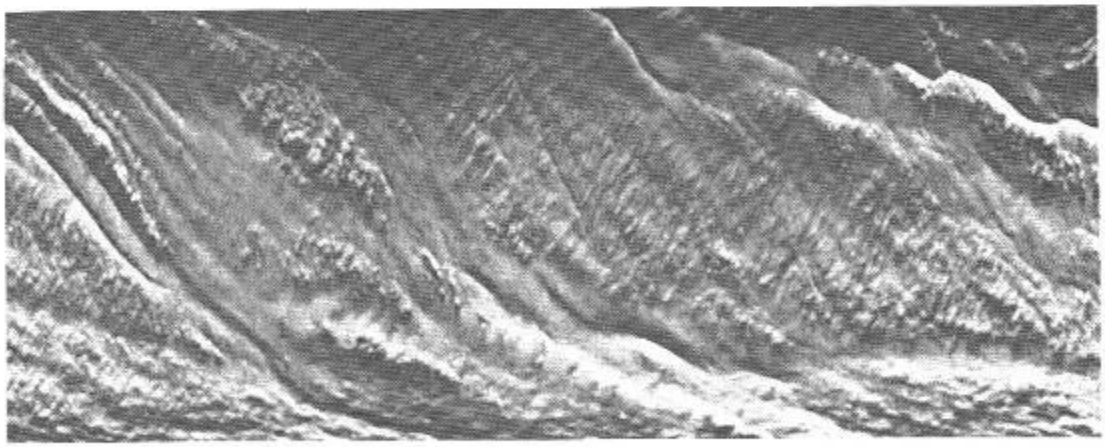

Figure 16. Natural Sea Surface Patterns.
19 April 1962; 2329; 2000 ft; 40°02'N; 71°19'W; AN/AAD-2;
6.25 mm^2 (circular) Ge:Cu; P2V-5F aircraft Bu. No. 131403.

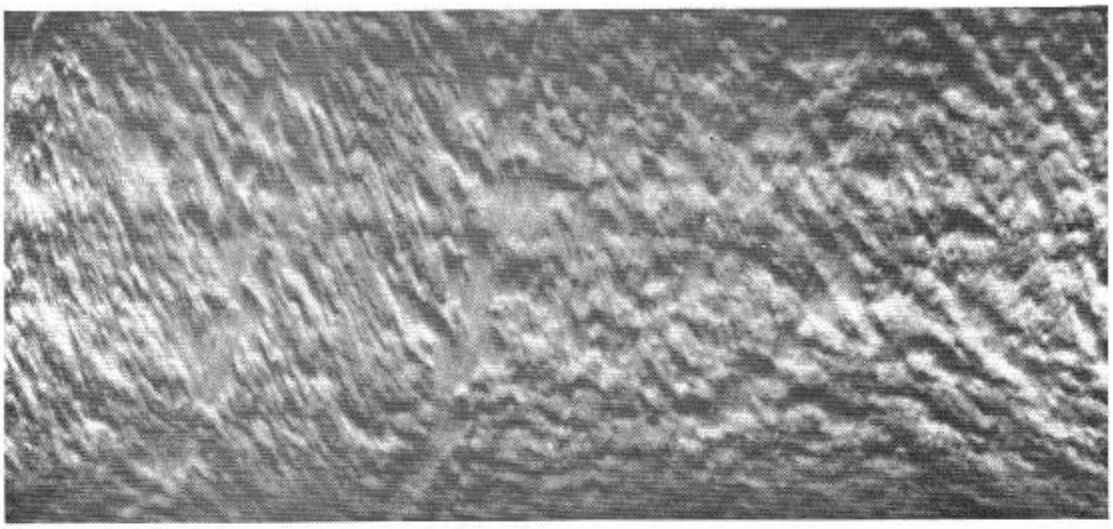

Figure 17. Natural Sea Surface Patterns.
1 September 1967; 2355; 450 ft; 24°17'N; 82°17'W; AN/AAR-32;
0.5 mm (diameter) Ge:Hg; NP-2E aircraft Bu. No. 131403.
Sea state: 0-1.

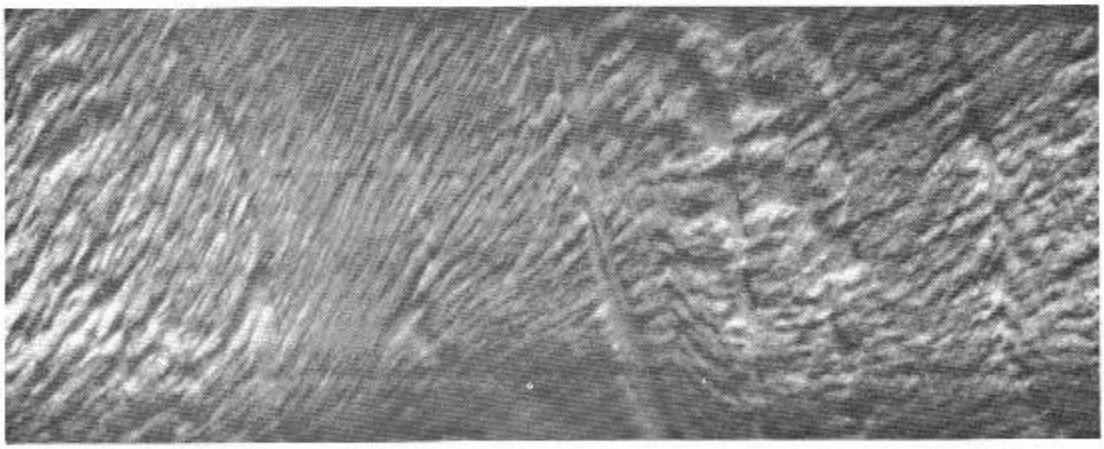

Figure 18. Natural Sea Surface Patterns.
1 September 1967; 2300; 325 ft; 24°16'N; 82°14'W; AN/AAR-32;
0.5 mm (diameter) Ge:Hg; NP-2E aircraft Bu. No. 131403.
Sea state: 0-1.

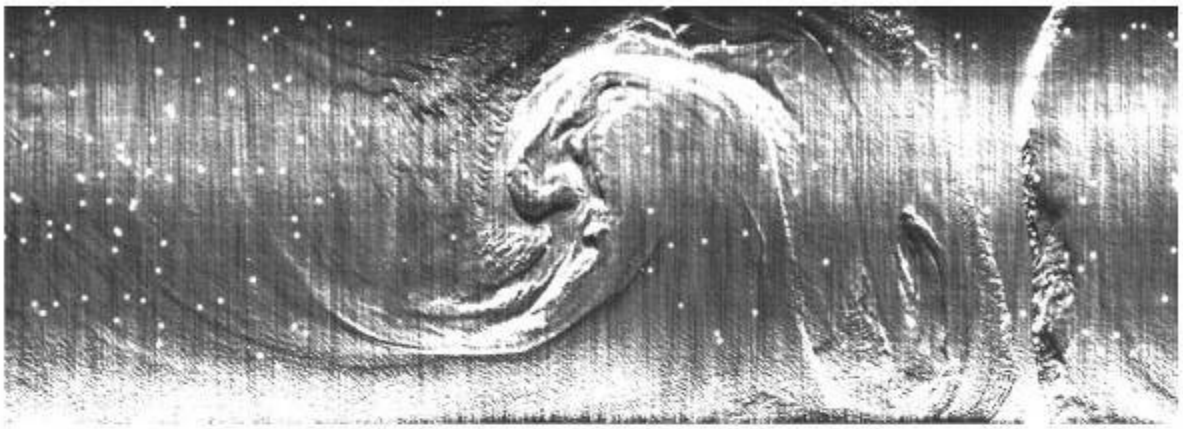

Figure 19. Eddy in the North Atlantic Ocean.
26 April 1963; 2230; 6700 ft; 41°40'N; 64°40'W; AN/AAR-30;
6.25 mm^2 (circular) Ge:Cu; SP-2E aircraft Bu. No. 131403.
The white dots are an electronic artifact and should be disregarded.

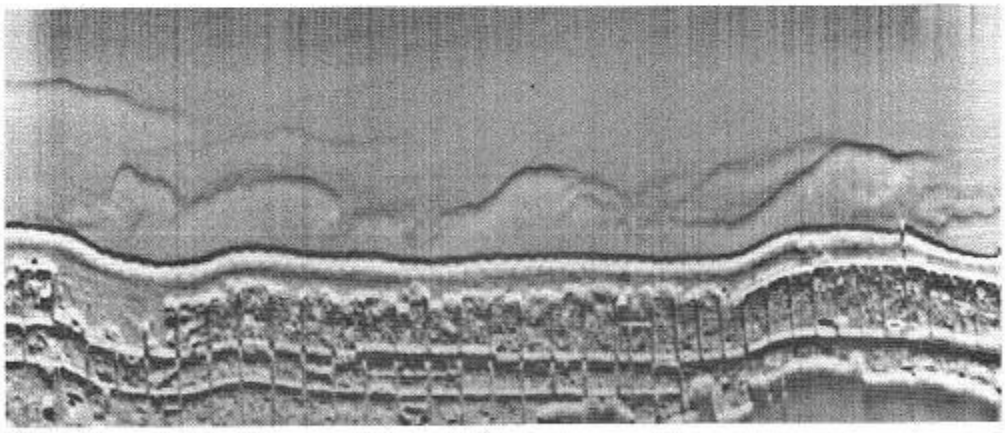

Figure 20. Coastline and Natural Sea Surface Patterns.
20 May 1964; 2314; 1400 ft; 39°39'N; 74°10'W; Reconofax IV
Mark II; 2.5 X 2.5 mm Ge:Hg;SP-2H aircraft Bu. No. 135616.

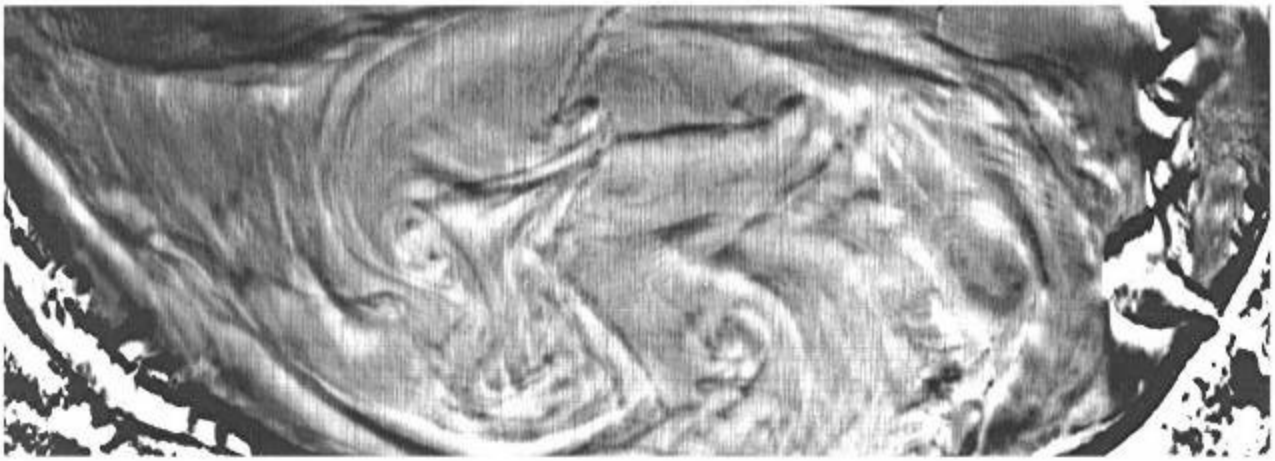

Figure 21. Eddy Resulting from the Converging of Waters from the East and West Branches of St. Andrew Bay.
5 March 1964; 2234; 2500 ft; 30°09'N; 85°40'W; Reconofax IV Mark II; 4 mm^2 (circular) Ge:Hg; NP-2E aircraft Bu. No. 131403.

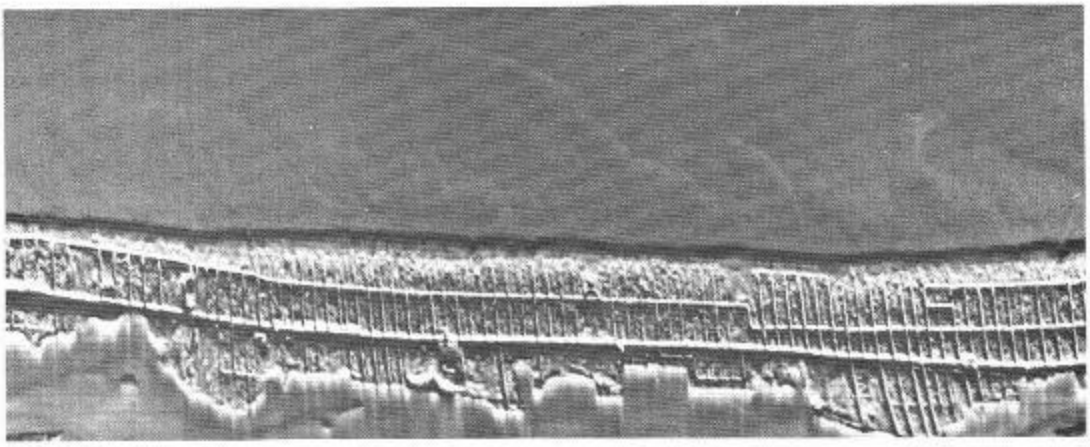

Figure 22. Coastline and Natural Ocean Surface Patterns.
3 October 1963; 1958; 2500 ft; 39°25'N; 74°22'W; Reconofax IV Mark II; Ge:Cu; NP-2E aircraft Bu. No. 131403.

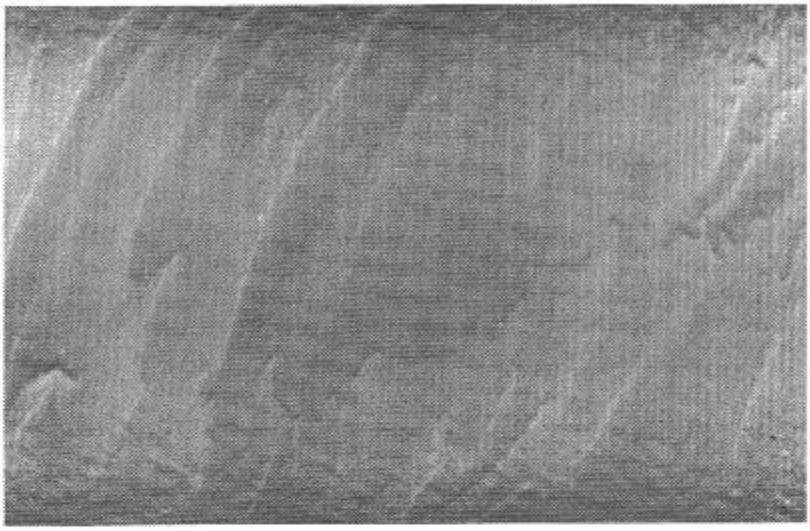

Figure 23. Natural Sea Surface Patterns.
3 May 1967; 1419; 600 ft; 39°28'N; 73°47'W; AN/AAR-30;
6.25 mm^2 (circular) Ge:Cu; NP-2E aircraft Bu. No. 131403.

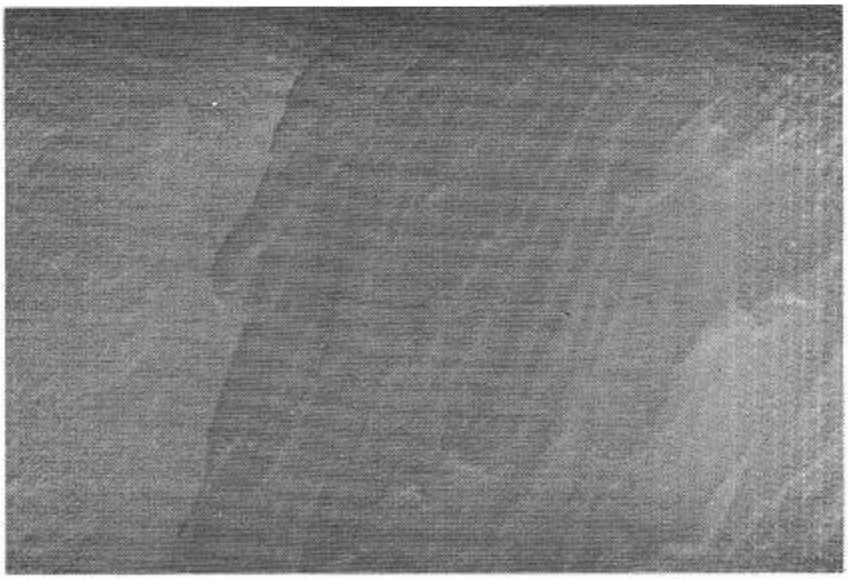

Figure 24. Natural Sea Surface Patterns.
3 May 1967; 1353; 1000 ft; 39°39'N; 74°02'W; AN/AAR-30;
6.25 mm^2 (circular) Ge:Cu; NP-2E aircraft Bu. No. 131403.

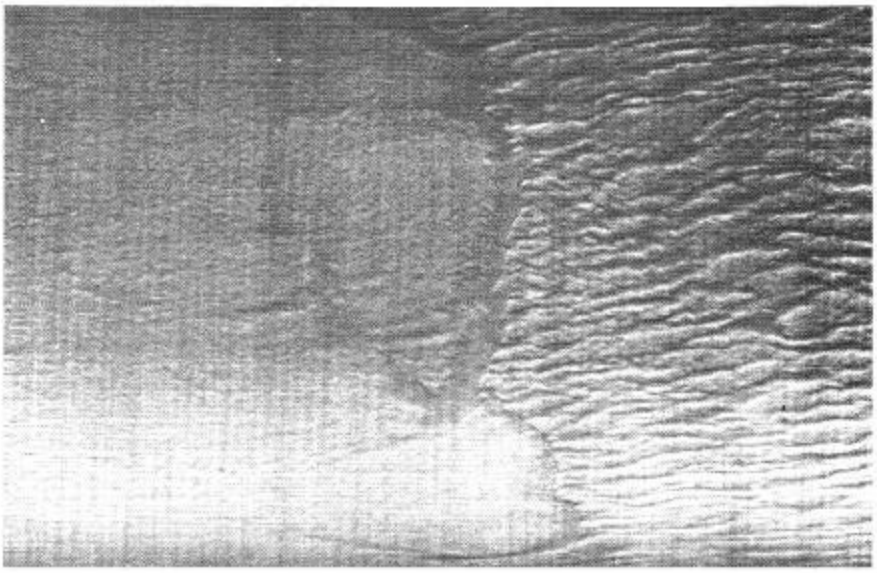

Figure 25. Natural Sea Surface Patterns.
23 May 1968; 2039; 25°30'N; 76°00'W; AN/AAR-30;
2.5 X 2.5 mm Ge:Hg; NP-2E aircraft Bu. No. 131403.

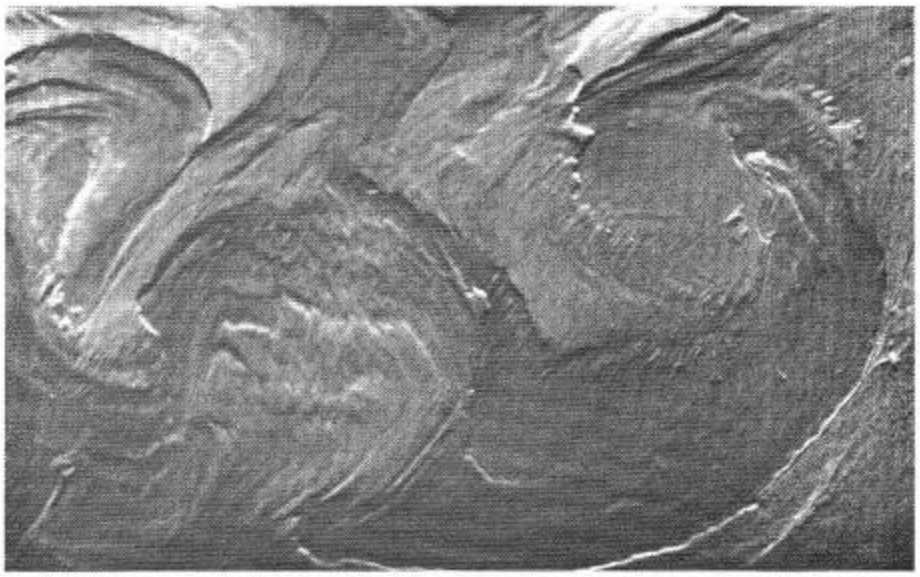

Figure 26. Natural Surface Patterns.
9 December 1965; 2050; 2200 ft; 37°08'N; 76°00'W; AN/AAR-30;
0.45 X 0.43 mm HgCdTe; NP-2E aircraft Bu. No. 131403.

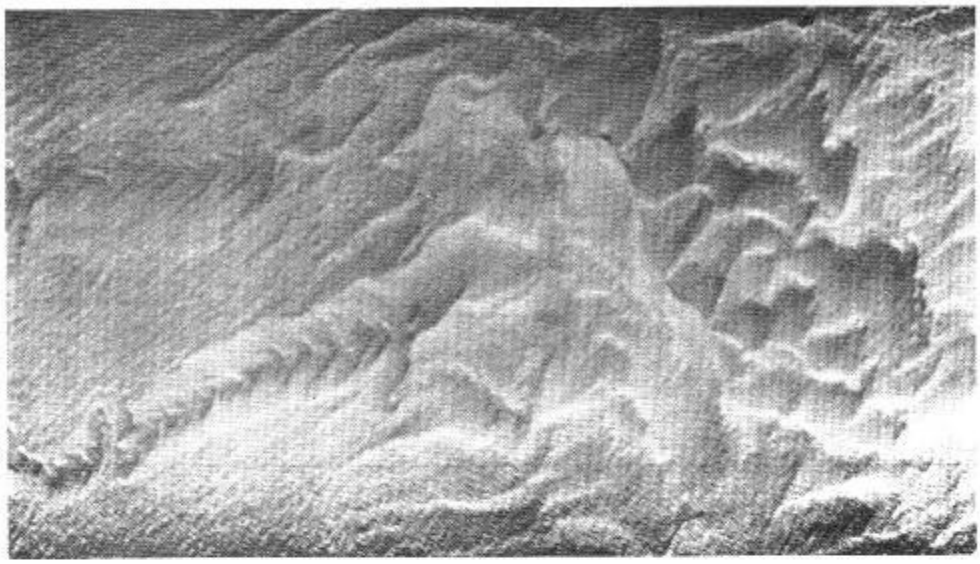

Figure 27. Natural Sea Surface Patterns.
3 May 1967; 1355; 1000 ft; 39°40'N; 74°06'W; AN/AAR-30;
6.25 mm^2 (circular) Ge:Cu; NP-2E aircraft Bu. No. 131403.

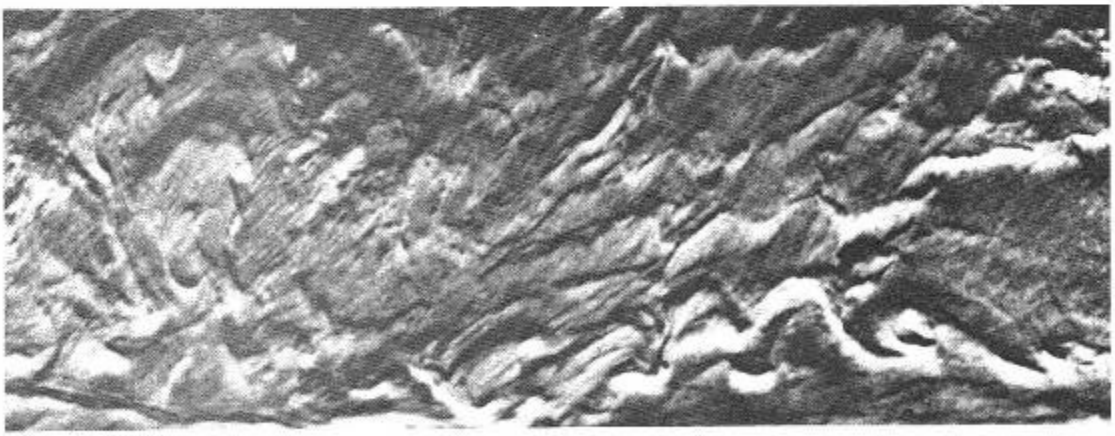

Figure 28. Surface Patterns in Chesapeake Bay.
26 June 1962; 2123; 2000 ft; 38°59'N; 76°23'W; AN/AAD-2;
6.25 mm^2 (circular) Ge:Cu; P2V-7 aircraft Bu. No. 140985.

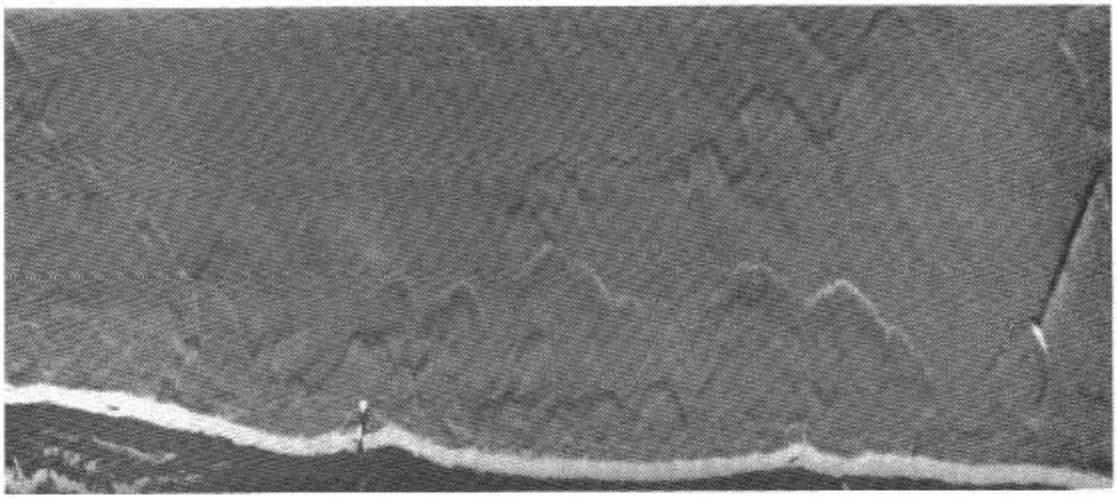

Figure 29. Coast and Natural Surface Patterns.
30 March 1967; 1429; 3400 ft; AN/AAR-32; 0.5 mm (diameter) Ge:Hg; NP-2E aircraft Bu. No. 131403.

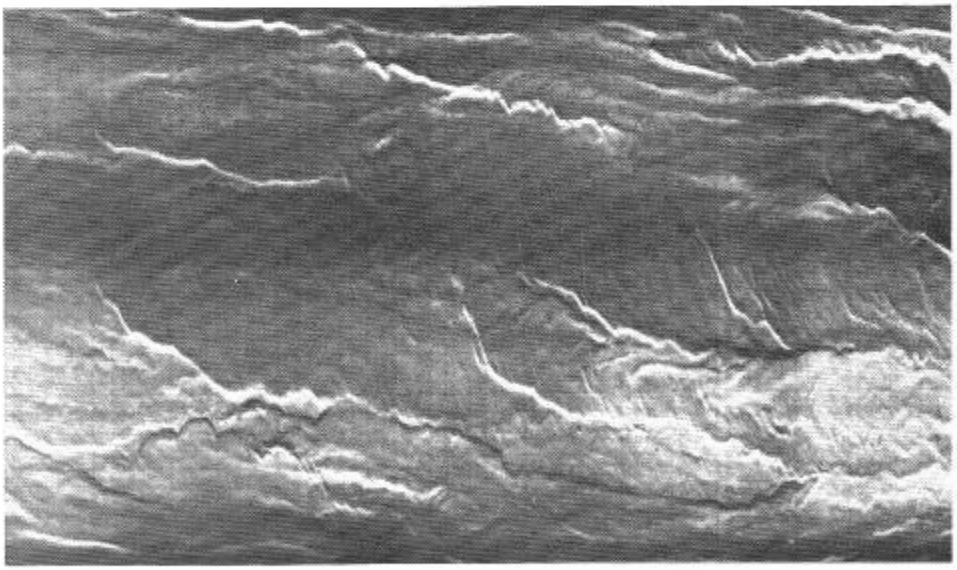

Figure 30. Surface Patterns in Delaware Bay.
1 October 1963; 2336; 12,000 ft; 39°08'N; 75°13'W; AN/AAR-30; 0.5 mm (diameter) Ge:Cu; NP-2E aircraft Bu. No. 131403.

Figures 31 - 33 show three scenes of Manasquan Inlet. They are presented together to facilitate comparison of the photographic results of different pieces of equipment and detectors.

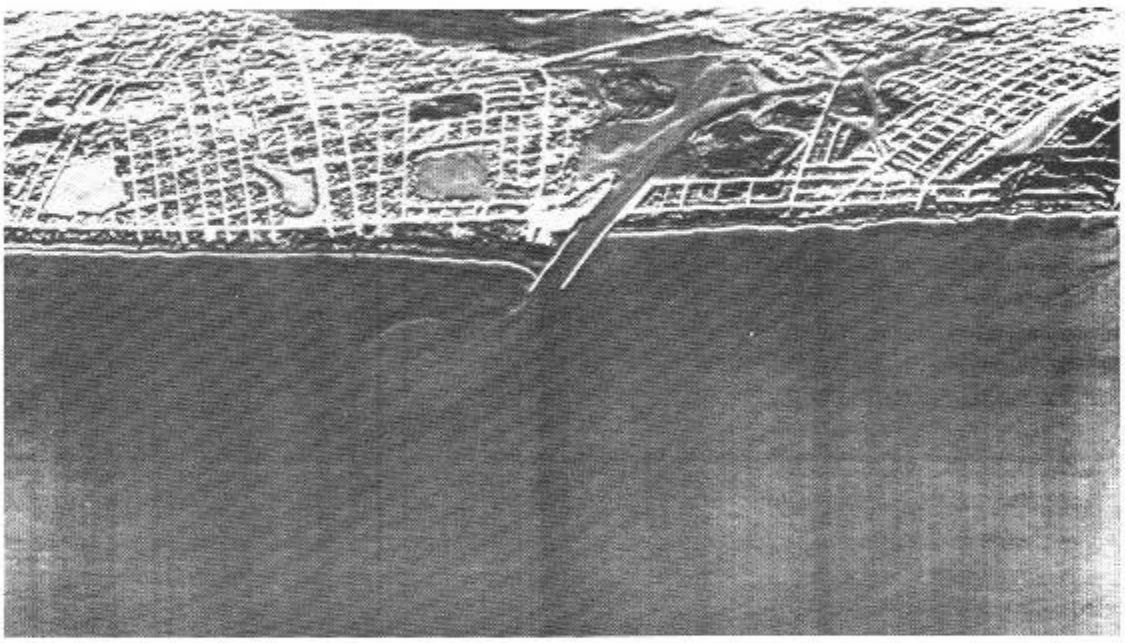

Figure 31. 11 October 1962; 2042; 4000 ft; $40^{\circ}07'$N; $74^{\circ}02'$W; AN/AAR-30; 7 X 7 mm InSb; HRB-Singer's D-18 aircraft.

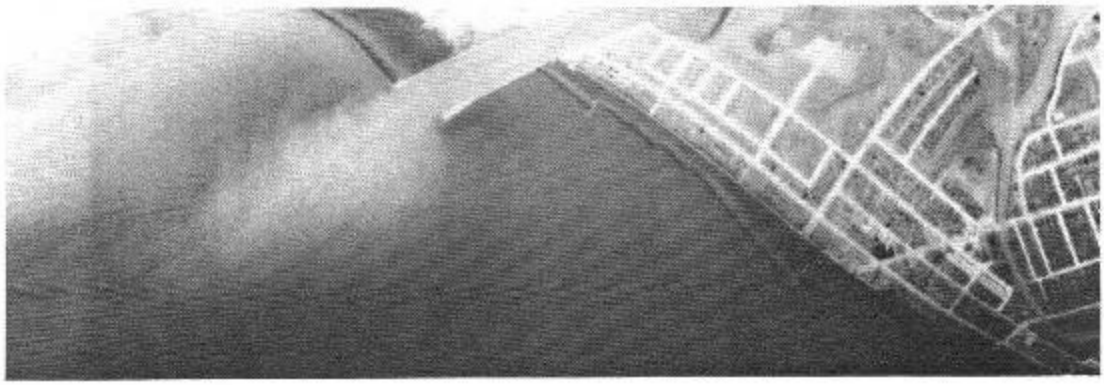

Figure 32. 27 July 1970; 2145; 500 ft; 40°07'N; 74°02'W; Reconofax XIIIA; 0.1 X 0.1 mm HgCdTe; P-3A aircraft Bu. No. 149677.

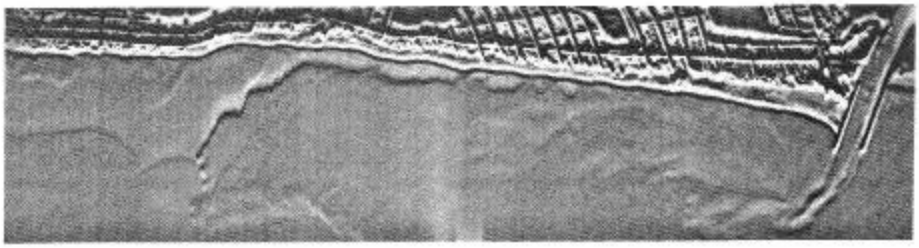

Figure 33. 20 May 1964; 2153; 1500 ft; 40°05'N; 74°02'W; Reconofax IV Mark II; 2.5 X 2.5 mm Ge:Hg; SP-2H aircraft Bu. No. 135616.

Figures 34-37 were recorded during passes over Barnegat Inlet on 30 January 1964 while the AN/AAR-30 operated with a copper doped germanium detector of 0.5-mm diameter. The pictures illustrate the effects of varying the roll-off setting on the equipment. At high roll-off settings, surface patterns can be easily distinguished; however, apparent temperature variations occurring at low frequencies are suppressed. Low values of roll-off permit greater sensitivity to thermal differences but provide poor resolution of small-area details.

To give some indication of actual temperature changes along the flight path, sections of the strip-chart recording of radiometric data are juxtaposed to their respective infrared pictures. Temperature variations displayed on the strip charts correspond to readings on a horizontal line, which passes roughly through the center of each picture. It can be seen that the changes in temperature across the inlet are nearly equal (about 0.27 K) for the two passes over the area.

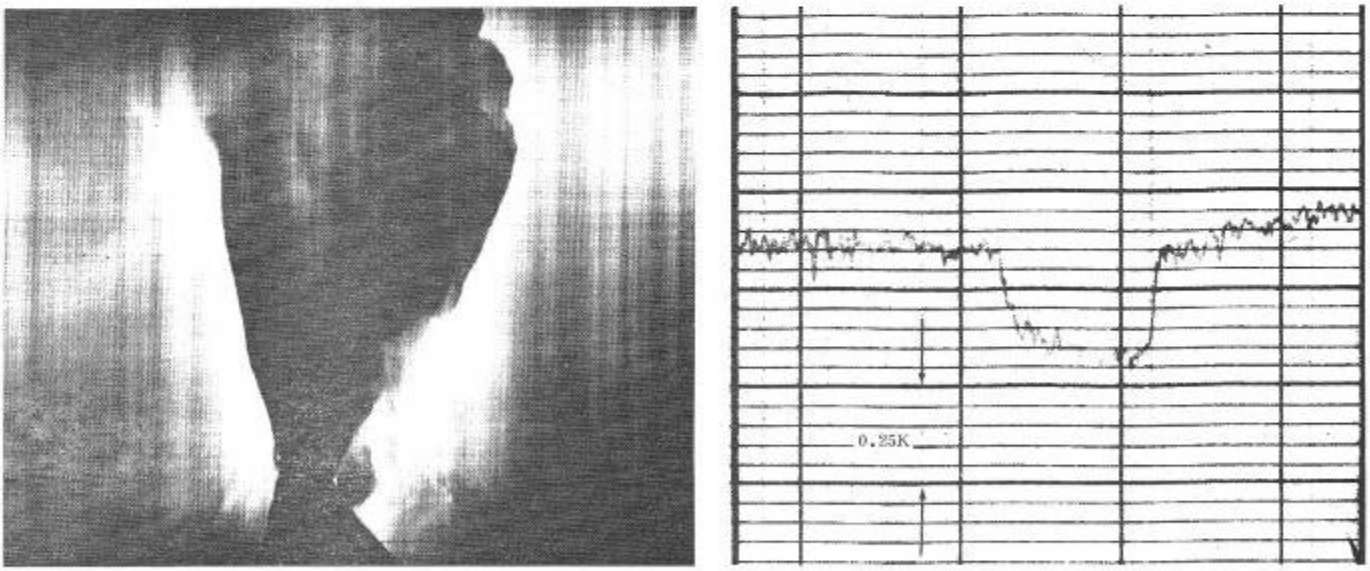

Figure 34. Time: 1827
Roll-off: 1.0.

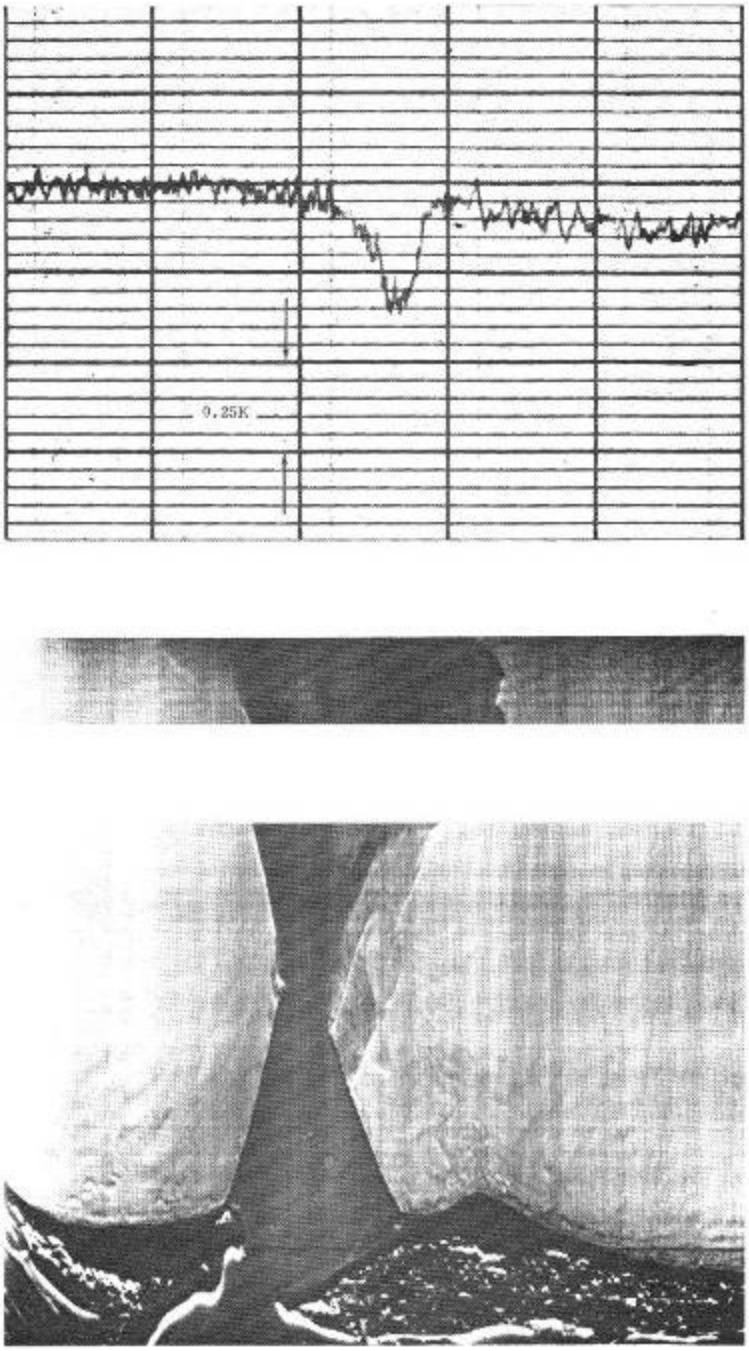

Figure 35. Time: 1808
Roll-off: 2.0.

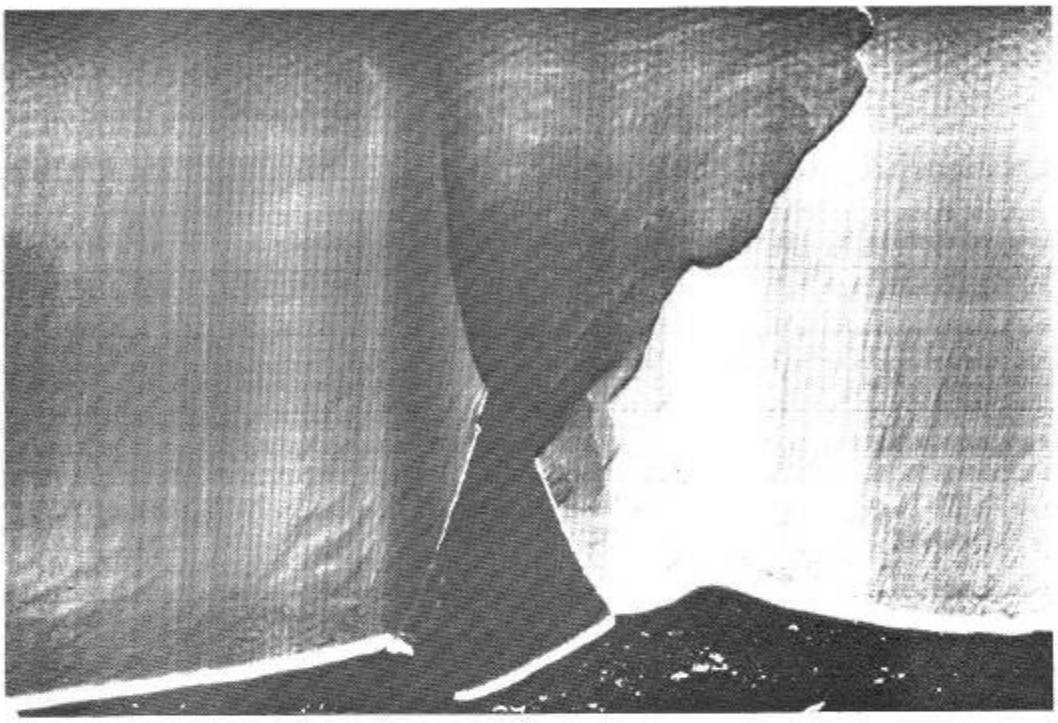

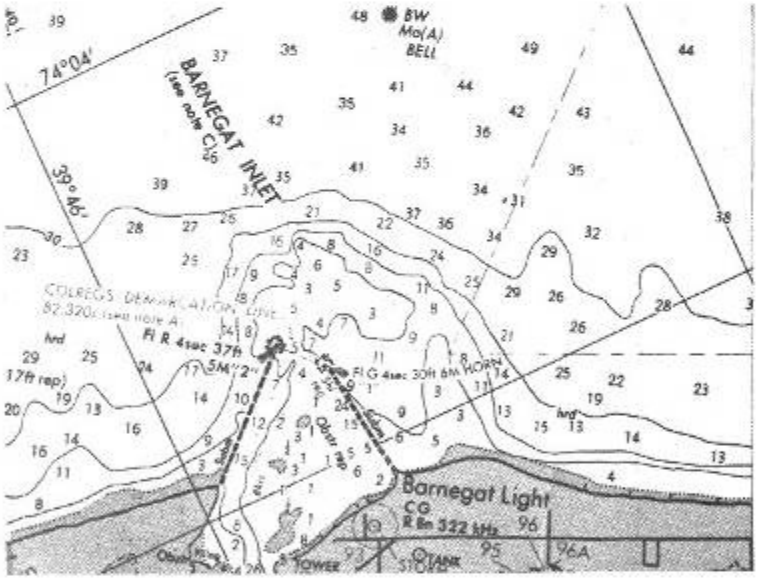

Figure 36. Time: 1850
Roll-off: 3.0.
A portion of NOAA Nautical Chart 12324 is also pictured (soundings are in feet).

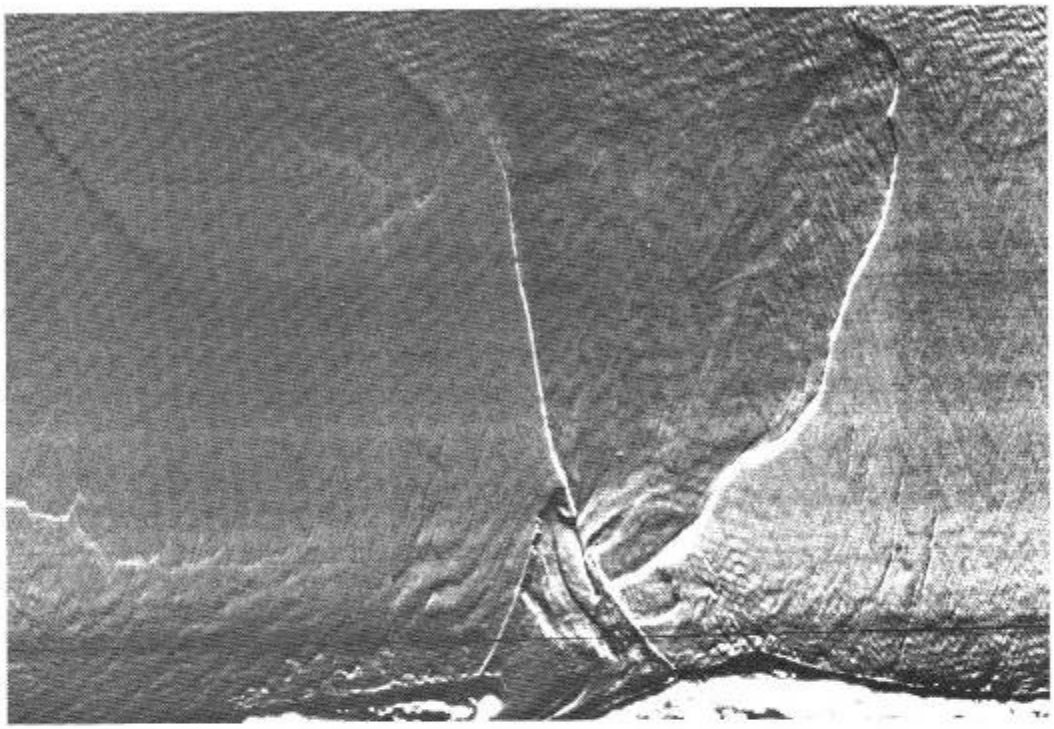

Figure 37. Time: 1922
Roll-off: 5.0.

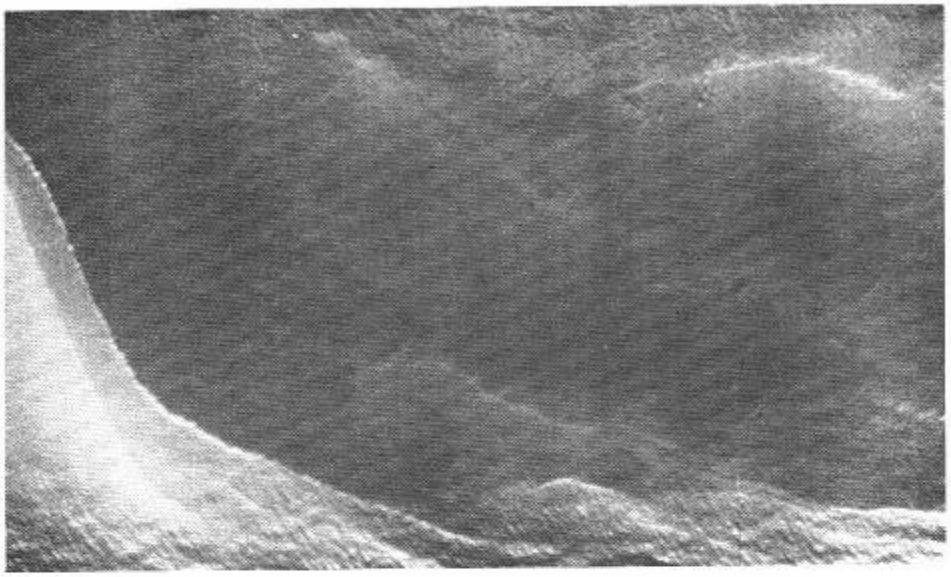

Figure 38. Natural Sea Surface Patterns.
5 May 1970; 2019; AN/AAR-30; 2.5 X 2.5 mm Ge:Hg.

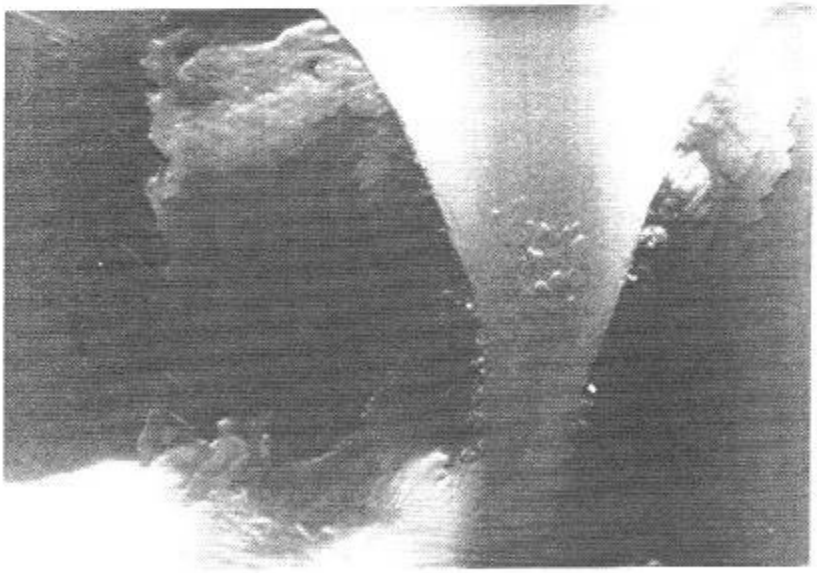

Figure 39. Natural Sea Surface Patterns.
19 May 1970; 1409; 1300 ft; 33°27'N; 78°53'W; AN/AAR-30;
2.5 X 2.5 mm Ge:Hg.

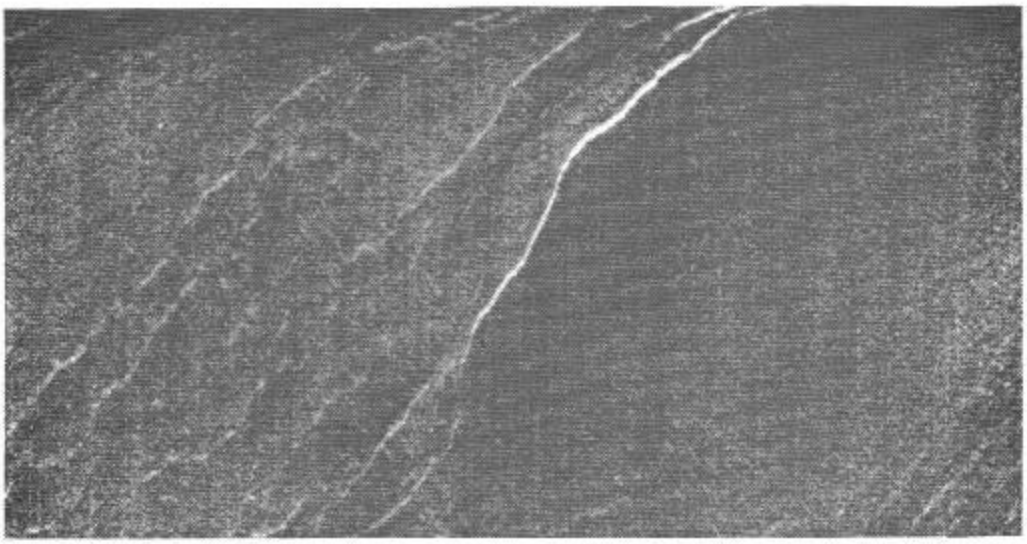

Figure 40. Natural Sea Surface Patterns.
27 May 1968; 2117; 1100 ft; 25°34'N; 76°01'W; AN/AAR-30;
2.5 X 2.5 mm Ge:Hg; NP-2E aircraft Bu. No. 131403.

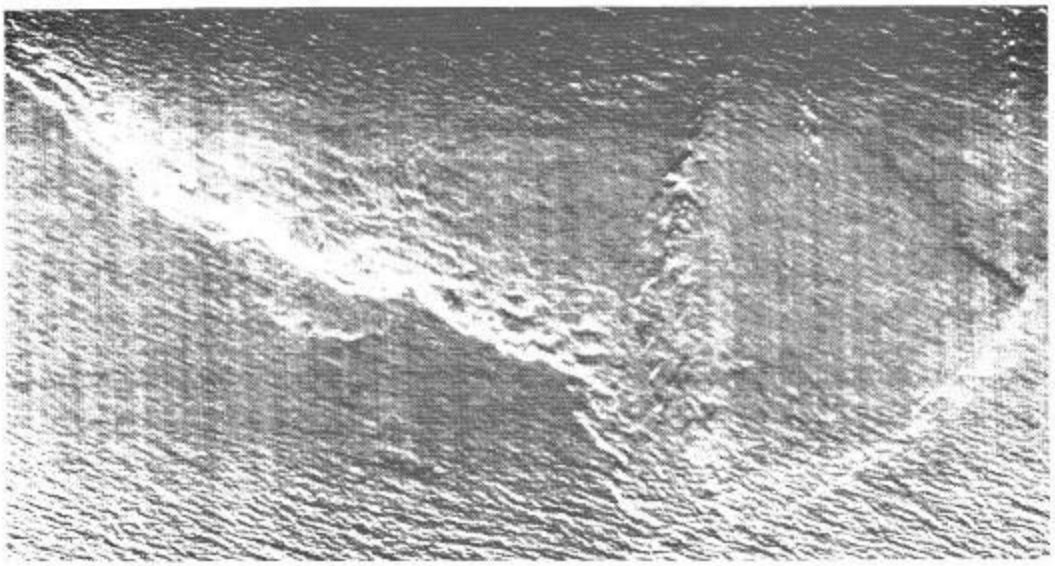

Figure 41. Natural Sea Surface Patterns.
25 April 1963; 0007; 41°50'N; 64°26'W; AN/AAR-30; 6.25 mm^2
(circular) Ge:Cu; SP-2E aircraft Bu. No. 131403.
Note the enhancement of waves along the upper and lower edges.

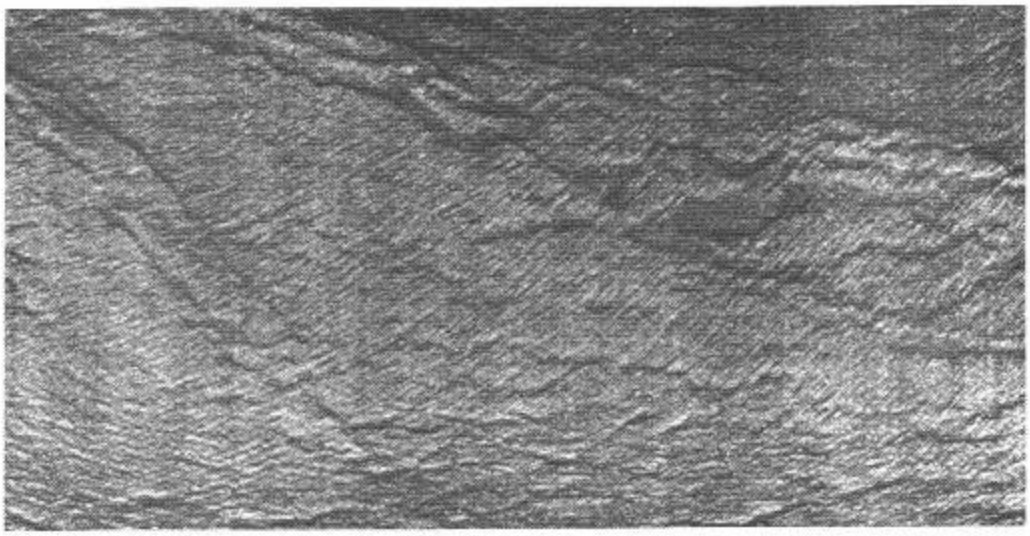

Figure 42. Natural Sea Surface Patterns.
27 May 1968; 2120; 1100 ft; 25°32'N; 76°00'W; AN/AAR-30;
2.5 X 2.5 mm Ge:Hg; NP-2E aircraft Bu. No. 131403.

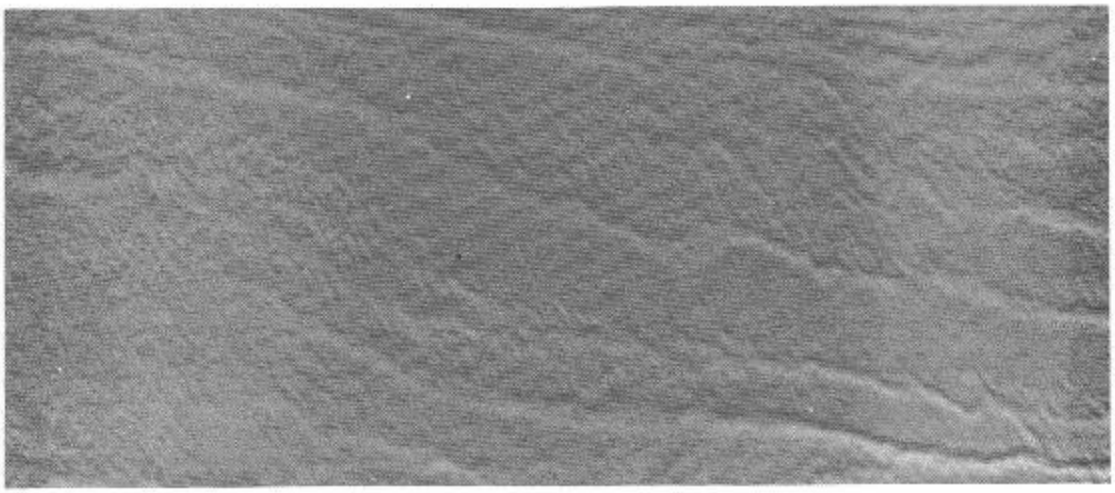

Figure 43. Natural Sea Surface Patterns.
14 May 1966; 23°31'N; 77°14'W; AN/AAR-32; 2.5 X 2.5 mm
Ge:Hg; P-3A aircraft Bu. No. 148883.

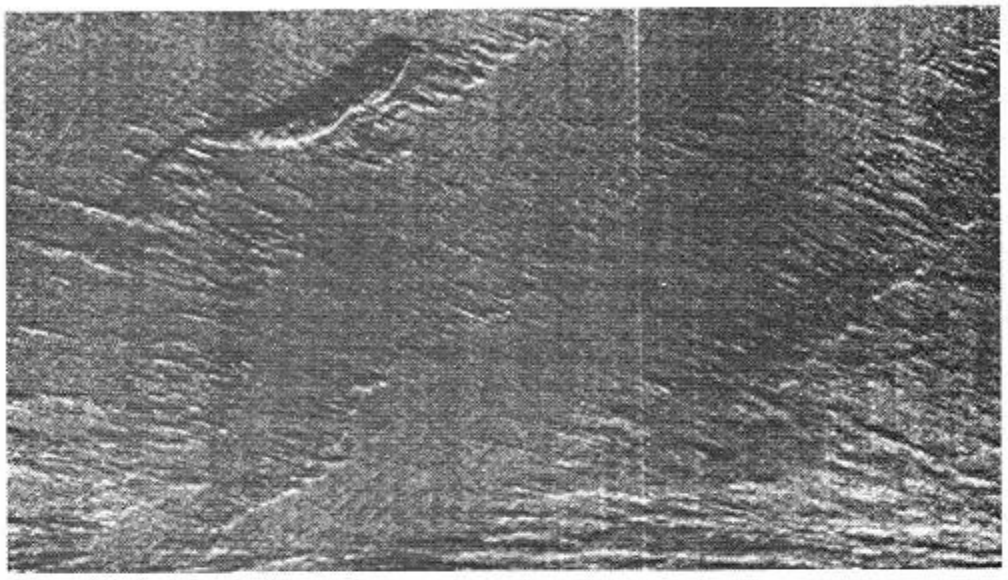

Figure 44. Natural Sea Surface Patterns.
23 May 1968; 2232; 800 ft; 25°30'N; 73°14'W; AN/AAR-30;
2.5 X 2.5 mm Ge:Hg; NP=2E aircraft Bu. No. 131403.

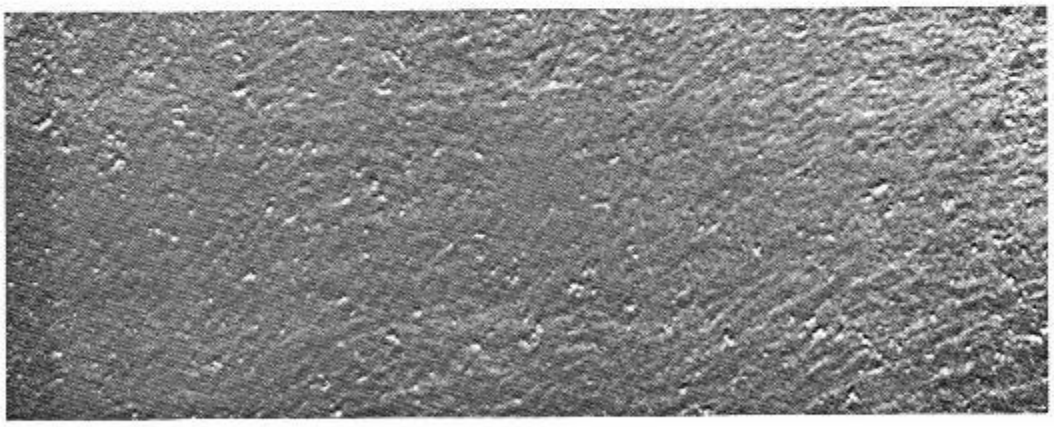

Figure 45. Whitecaps.
20 December 1962; 2240; 4000 ft; AN/AAR-30; 3 X 3 mm
Ge:Hg; HRB-Singer's Beechcraft D-18 aircraft.

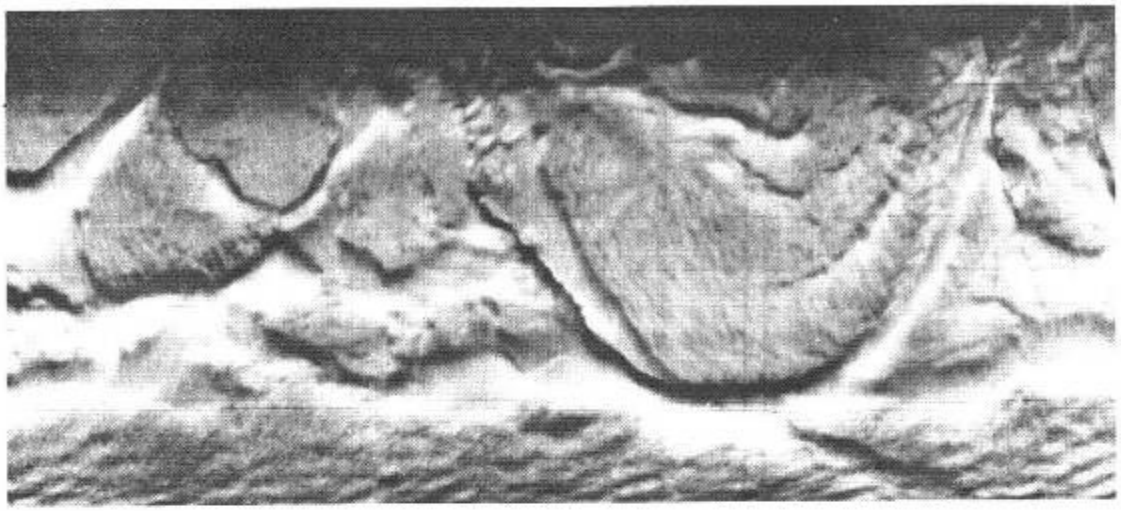

Figure 46. Coastline (Along Upper Edge) and Natural Surface Patterns. 9 April 1963; 1922; 1400 ft; 39°56'N; 74°04'W; AN/AAD-2; 6.25 mm^2 (circular) Ge:Cu; SP-2E aircraft Bu. No. 131403.

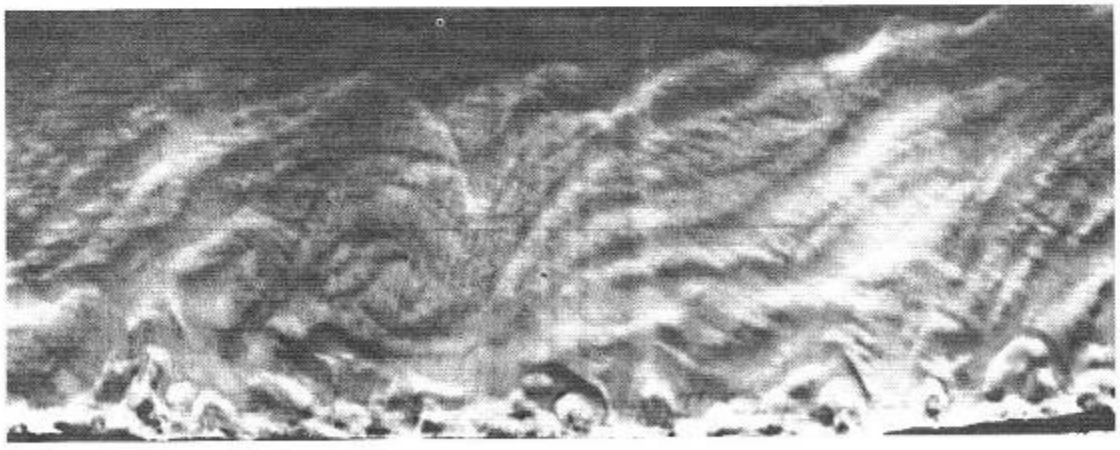

Figure 47. Coastline (Along Lower Edge) and Natural Surface Patterns. 9 April 1963; 1938; 1500 ft; 40°01'N; 74°03'W; AN/AAD-2; 6.25 mm^2 (circular) Ge:Cu; SP-2E aircraft Bu. No. 131403.

Figure 48. Natural Sea Surface Patterns.
10 May 1962; 2035; 5000 ft; 39°40'N; 71°40'W; AN/AAD-2;
6.25 mm^2 (circular) Ge:Cu; P2V-7 aircraft Bu. Nc. 140985.

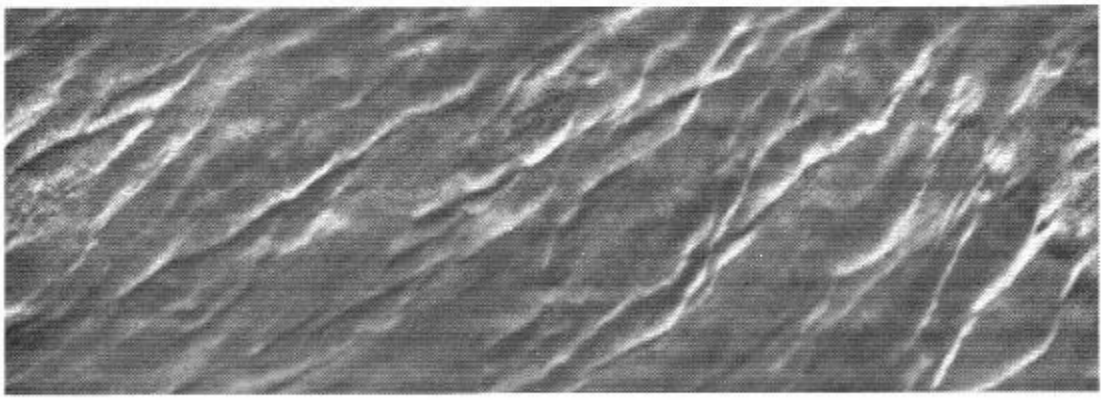

Figure 49. Natural Surface Patterns.
6 September 1967; 2053; 700 ft; 24°19'N; 82°18'W; AN/AAR-32;
0.5 mm (diameter) Ge:Hg; NP-2E aircraft Bu. No. 131403.
Sea state: 1-2.

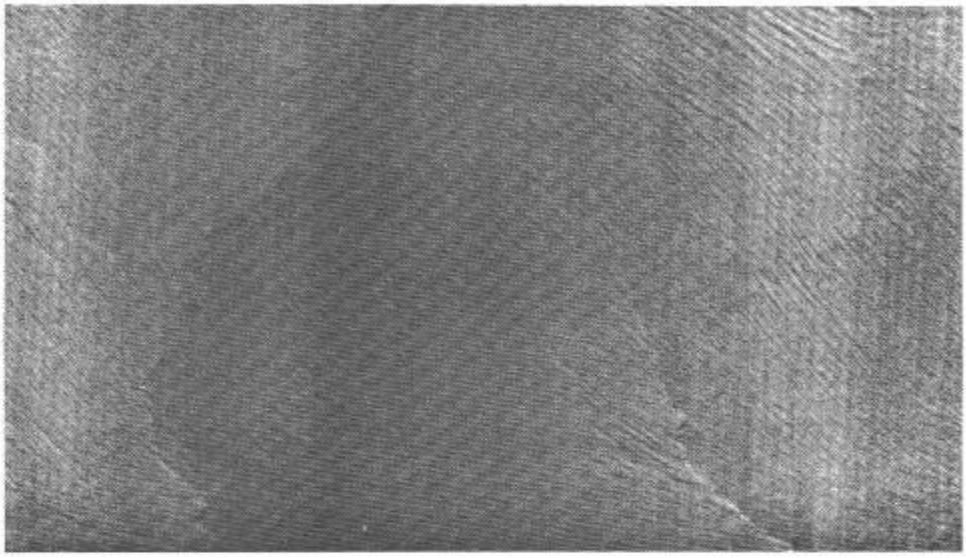

Figure 50. Natural Sea Surface Patterns.
22 May 1968; 2315; 1200 ft; 25°32'N; 75°58'W; AN/AAR-30;
2.5 X 2.5 mm Ge:Hg; NP-2E aircraft Bu. No. 131403.

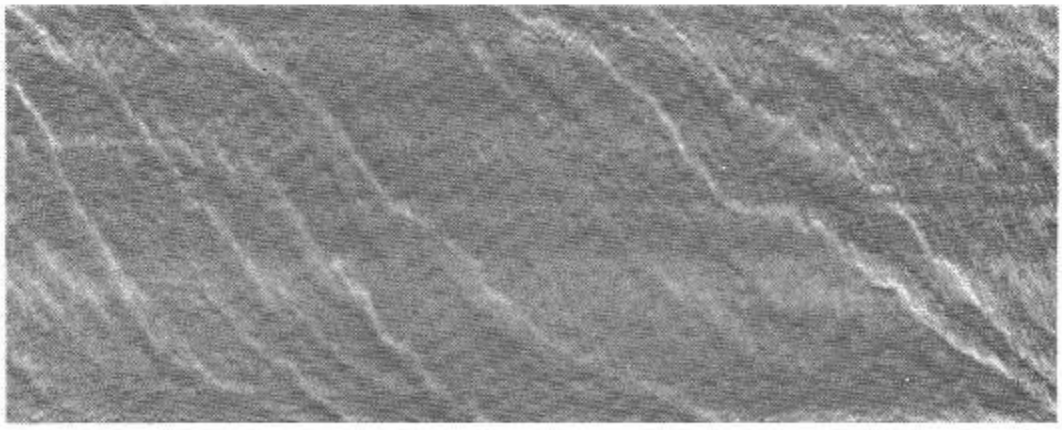

Figure 51. Natural Sea Surface Patterns.
21 June 1967; 2234; 1200 ft; 25°52'N; 76°11'W; AN/AAR-32;
0.5 mm (diameter) Ge:Hg; NP-2E aircraft Bu. No. 131403.
Sea state: 0.

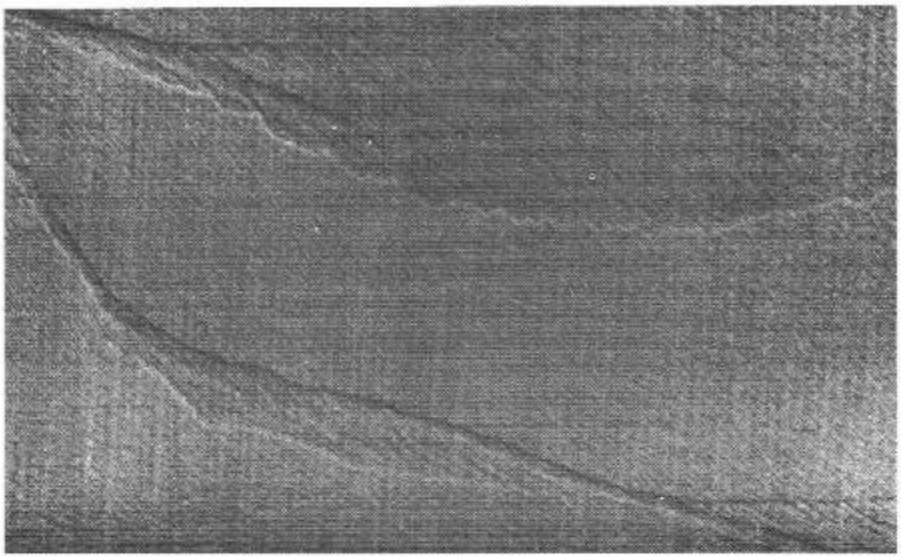

Figure 52. Natural Sea Surface Patterns.
22 May 1968; 2314; 1200 ft; 25°31'N; 75°59'W; AN/AAR-30;
2.5 X 2.5 mm Ge:Hg; NP-2E aircraft Bu. No. 131403.

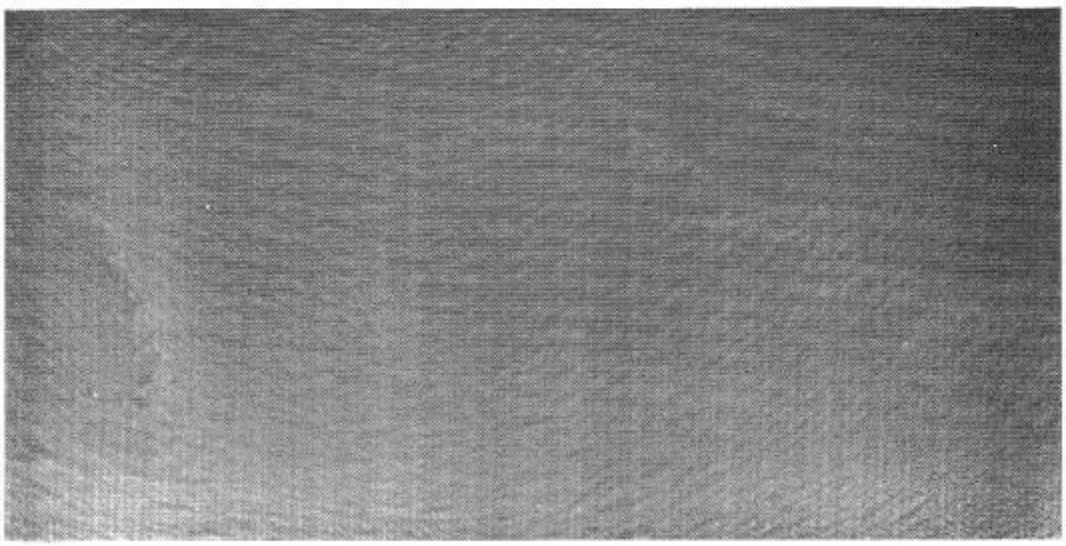

Figure 53. Natural Sea Surface Patterns.
3 May 1967; 1415; 600 ft; 39°26'N; 73°40'W; AN/AAR-30;
6.25 mm^2 (circular) Ge:Cu; NP-2E aircraft Bu. No. 131403.

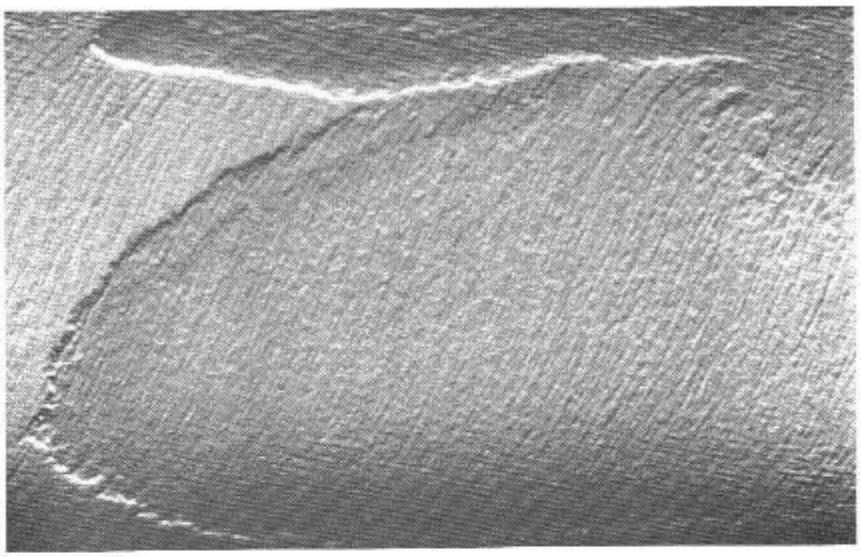

Figure 54. Thermal Front.
9 December 1965; 2049; 2200 ft; 37°08'N; 75°57'W; AN/AAR-30;
0.45 X 0.43 mm HgCdTe; NP-2E aircraft Bu. No. 131403.

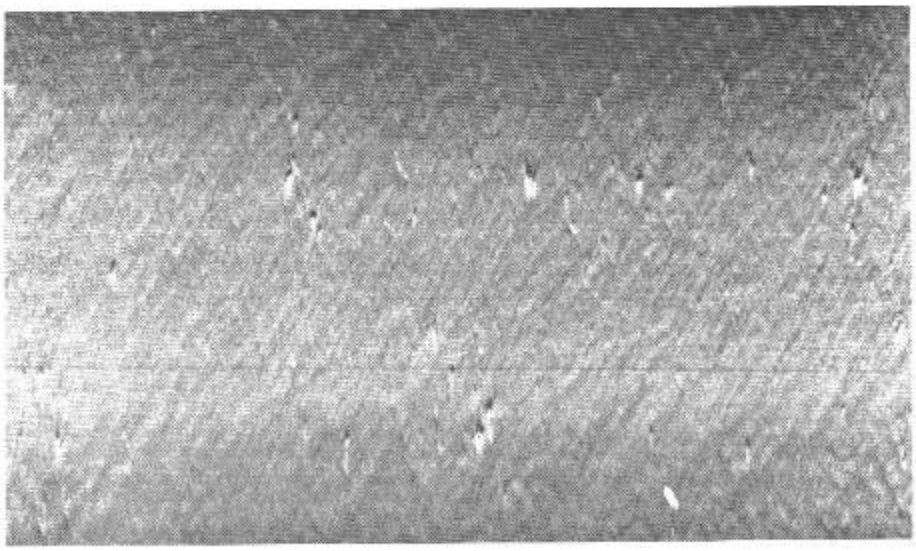

Figure 55. Whitecaps and Natural Background Patterns.
17 November 1963; 2003; 2300 ft; 24°32'N; 81°51'W; AN/AAR-30;
0.5 mm (diameter) Ge:Cu; NP-2E aircraft Bu. No. 131403.

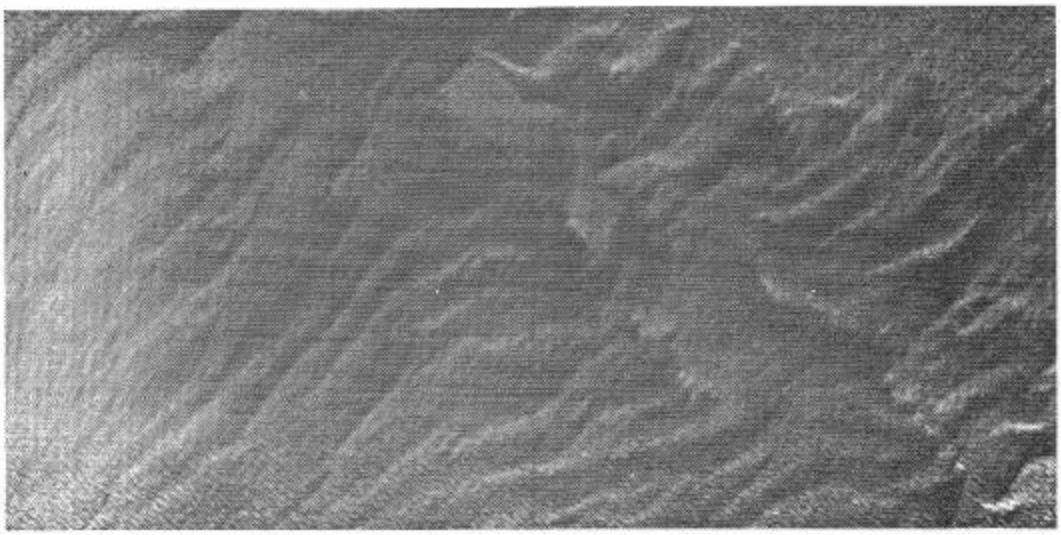

Figure 56. Natural Sea Surface Patterns.
3 May 1967; 1409; 650 ft; 39°31'N; 73°34'W; AN/AAR-30;
6.25 mm^2 (circular) Ge:Cu; NP-2E aircraft Bu. No. 131403.

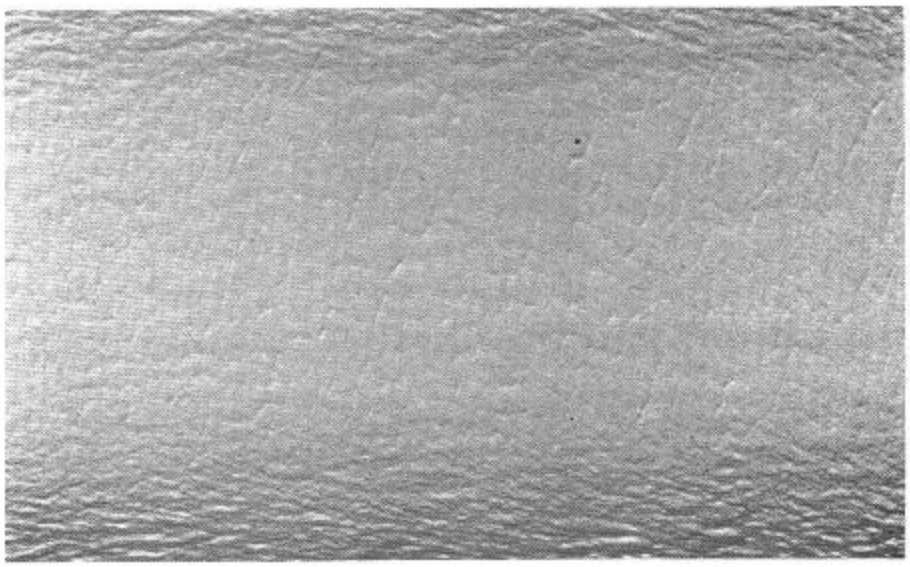

Figure 57. Natural Surface Patterns.
5 March 1964; 2040; 1000 ft; 30°06'N; 85°44'W; AN/AAR-30;
4 mm^2 (circular) Ge:Cu; NP-2E aircraft Bu. No. 131403.
Note the waves at the edges of the picture.

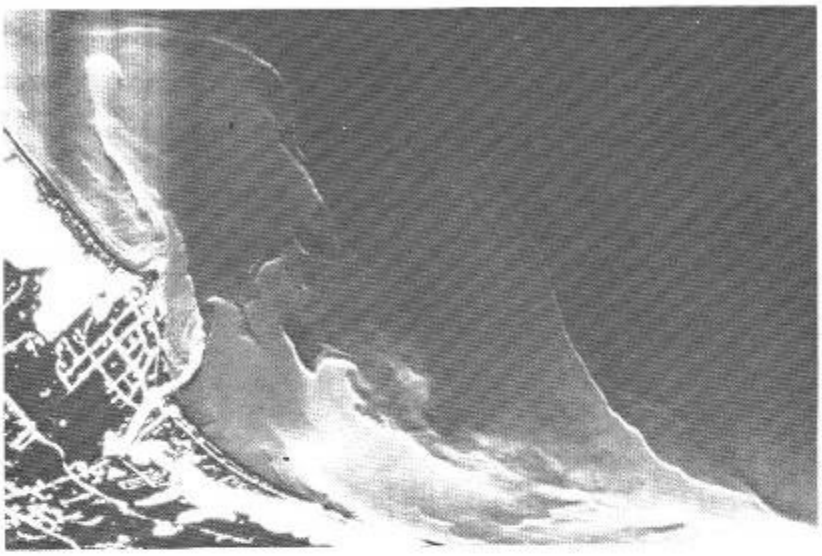

Figure 58. Coast and Adjacent Surface Patterns.
24 May 1972; 0058; 4500 ft; AN/AAR-30; 2.5 X 2.5 mm Ge:Hg.

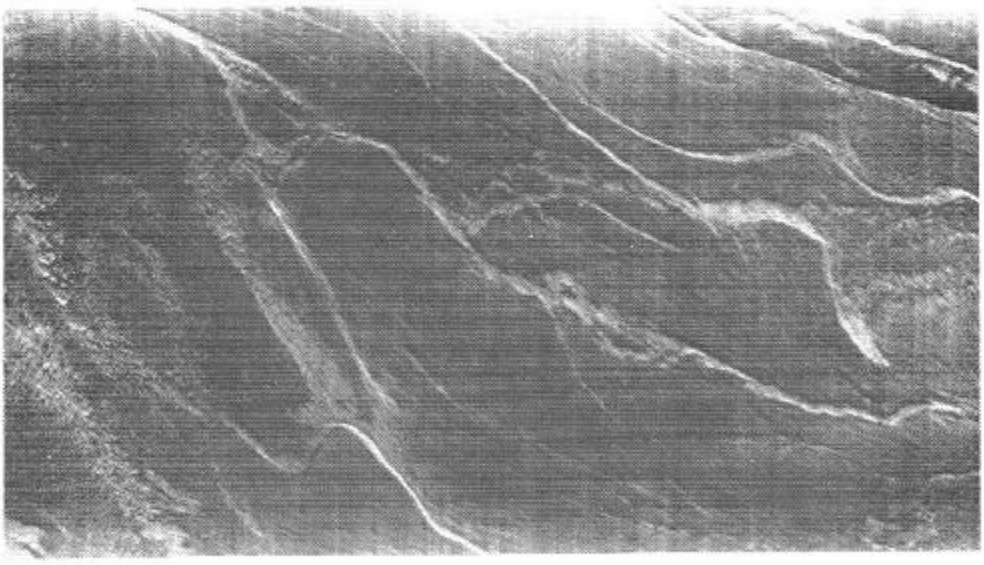

Figure 59. Natural Sea Surface Patterns.
1 September 1964; 2038; 3500 ft; AN/AAR-30; 6.25 mm^2 (circular)
Ge:Hg; NP-2E aircraft Bu. No. 131403.

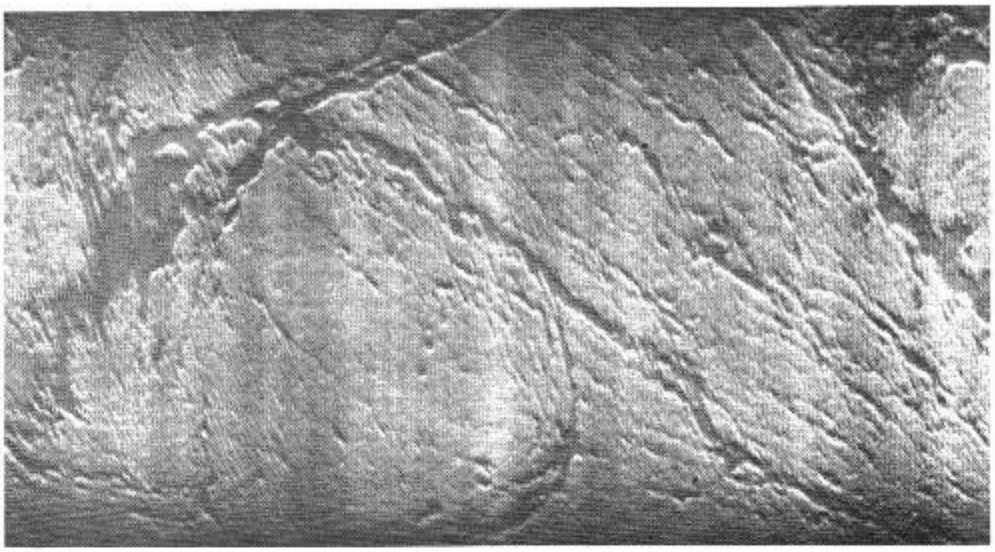

Figure 60. Natural Sea Surface Patterns.
9 April 1970; 1942; 3000 ft; 28°23'N; 80°01'W; AN/AAR-30;
2.5 X 2.5 mm Ge:Hg.

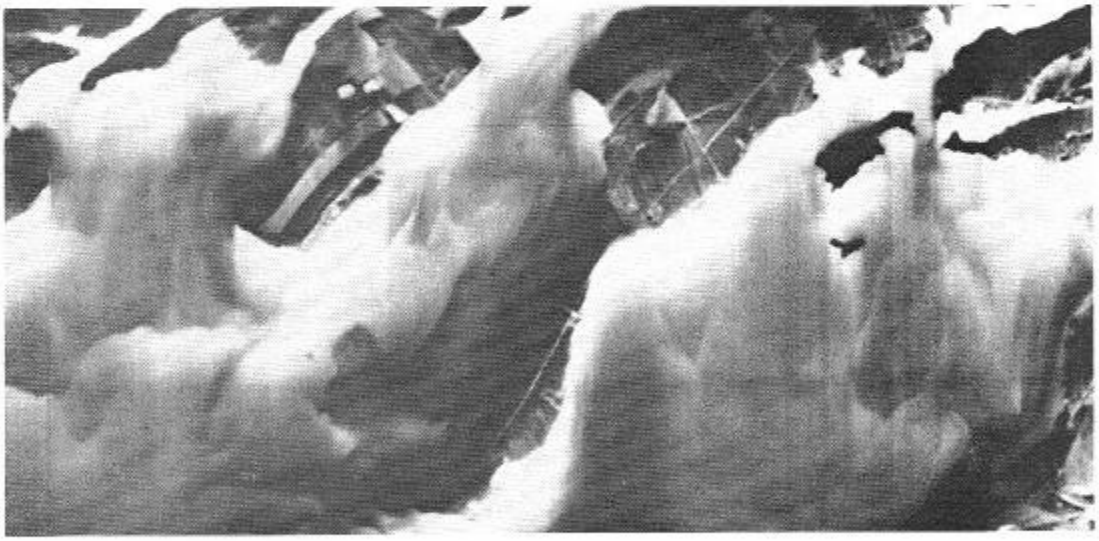

Figure 61. Outcroppings of Land and Neighboring Water Patterns in Chesapeake Bay.
9 November 1961; 2138; 5000 ft; 39°20'N; 76°18'W; AN/AAD-2;
2.5 X 2.5 mm InSb; P2V-5F aircraft Bu. No. 131403.

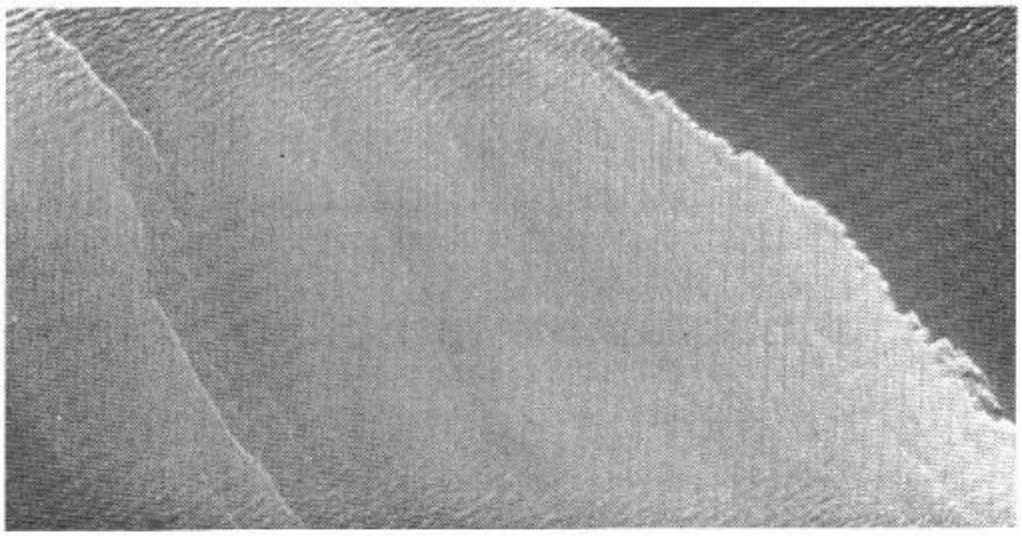

Figure 62. Thermal Front.
1 June 1967; 2007; 450 ft; AN/AAR-30; 6.25 mm^2 (circular) Ge:Cu; NP-2E aircraft Bu. No. 131403.
Note the waves at the edges of the picture.

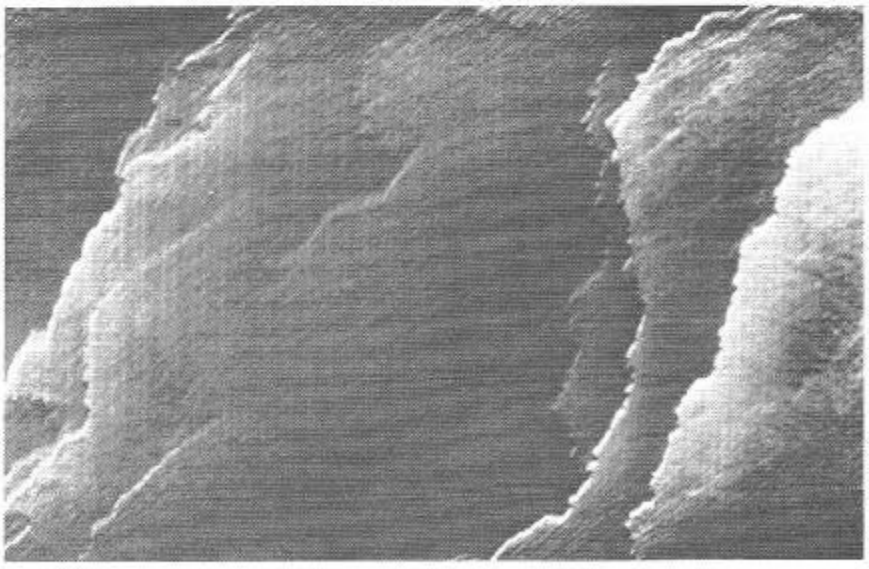

Figure 63. Successive Thermal Fronts.
3 May 1967; 1406; 650 ft; 39°33'N; 73°39'W; AN/AAR-30; 6.25 mm^2 (circular) Ge:Cu; NP-2E aircraft Bu. No. 131403.

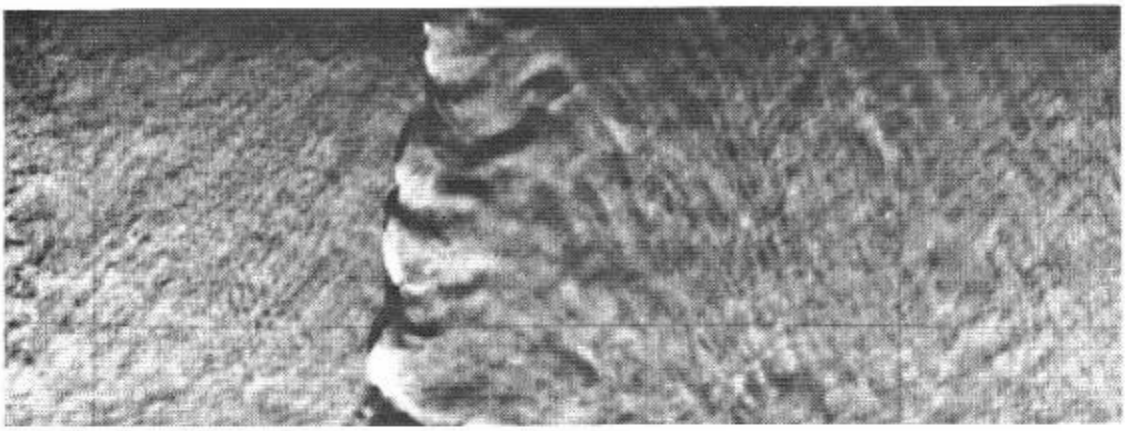

Figure 64. Natural Sea Surface Patterns.
15 August 1962; 2121; 2600 ft; 39°50'N; 71°29'W; AN/AAD-2;
6.25 mm^2 (circular) Ge:Cu; P2V-5FS aircraft
Bu. No. 131403.
Note change in thermal "texture" across front. Sea state: 1/2.

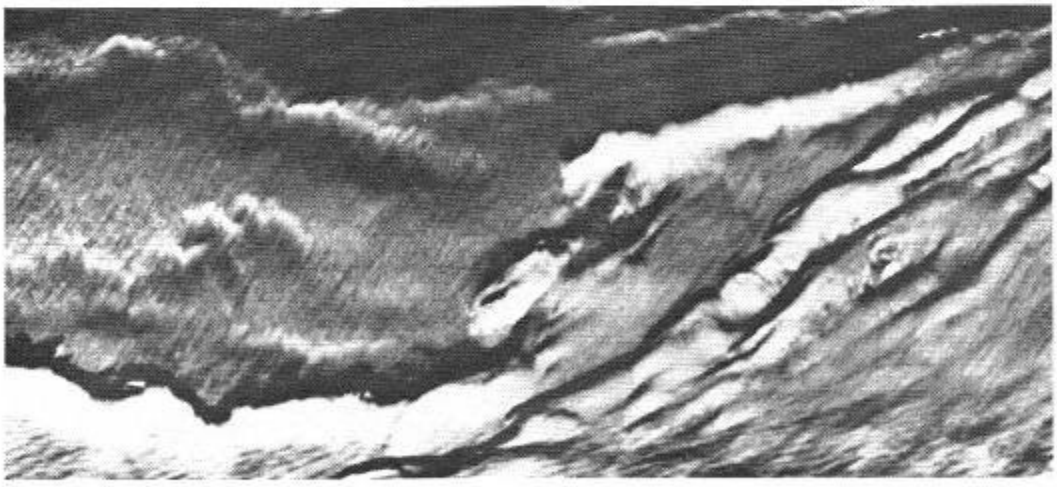

Figure 65. Natural Sea Surface Patterns.
19 April 1962; 2115; 2500 ft; 40°06'N; 71°18'W; AN/AAD-2;
6.25 mm^2 (circular) Ge:Cu; P2V-5F aircraft Bu. No. 131403.

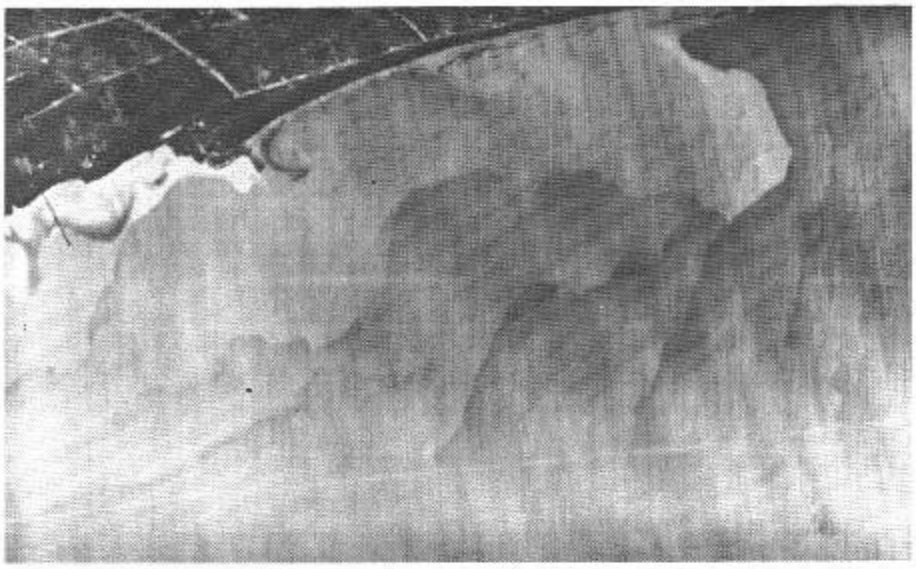

Figure 66. Coastline and Adjacent Water Surface Patterns.
28 October 1964; 2004; 500 ft; 30°10'N; 85°41'W; AN/AAR-30;
6.25 mm^2 (circular) Ge:Hg; NP-2E aircraft Bu. No. 131403.

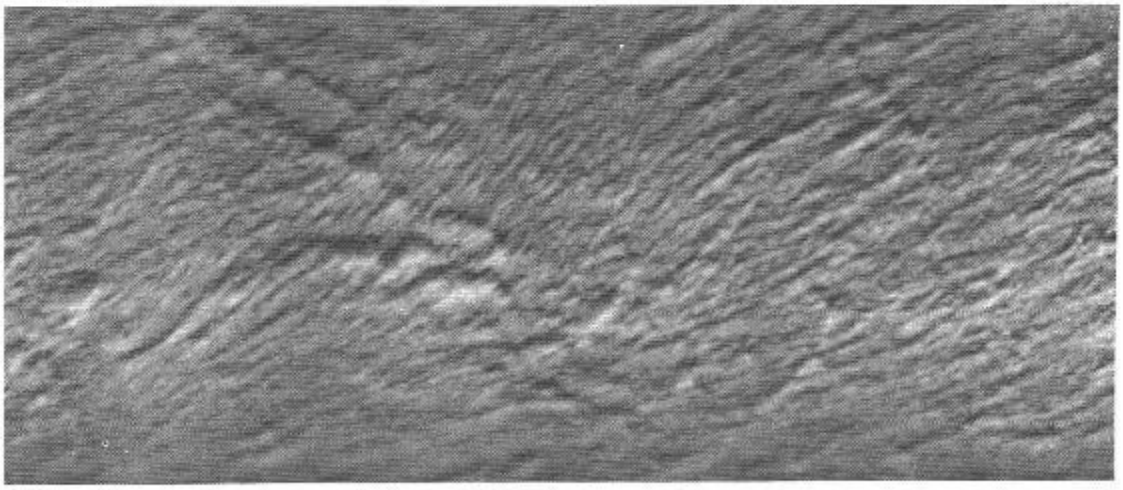

Figure 67. Natural Sea Surface Patterns.
1 September 1967; 2142; 700 ft; 24°20'N; 82°18'W; AN/AAR-32;
0.5 mm (diameter) Ge:Hg; NP-2E aircraft Bu. No. 131403.
Sea state: 0-1.

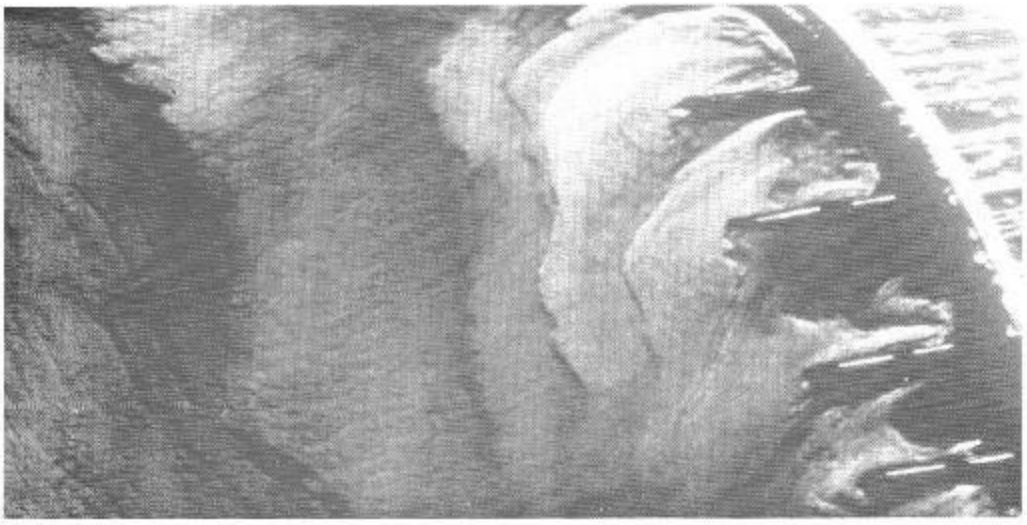

Figure 68. Shoreline, Jetties, and Sea Surface Patterns.
1 June 1967; 2018; 500 ft; AN/AAR-30; 6.25 mm^2 (circular)
Ge:Cu; NP-2E aircraft Bu. No. 131403.

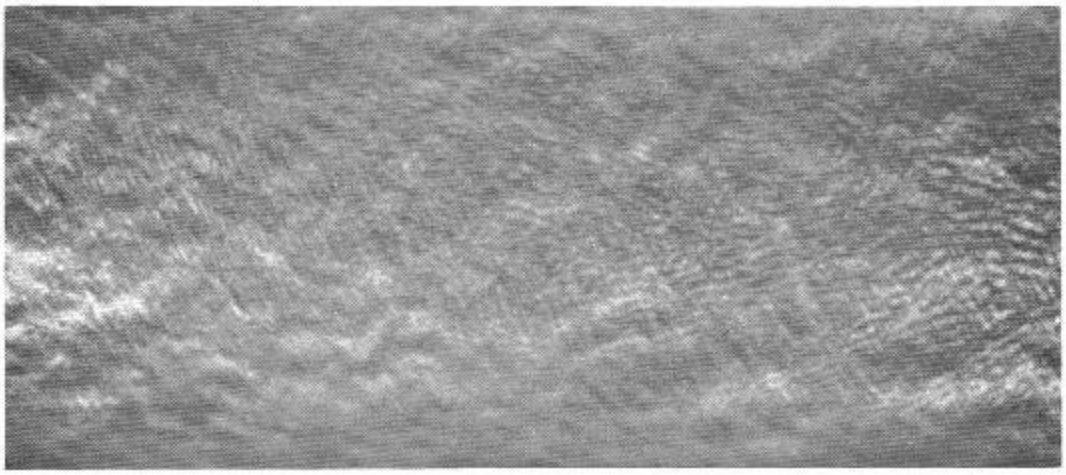

Figure 69. Natural Sea Surface Patterns.
2 September 1967; 2144; 800 ft; 24°20'N; 82°15'W; AN/AAR-32;
0.5 mm (diameter) Ge:Hg; NP-2E aircraft Bu. No. 131403.
Sea state: 1-2.

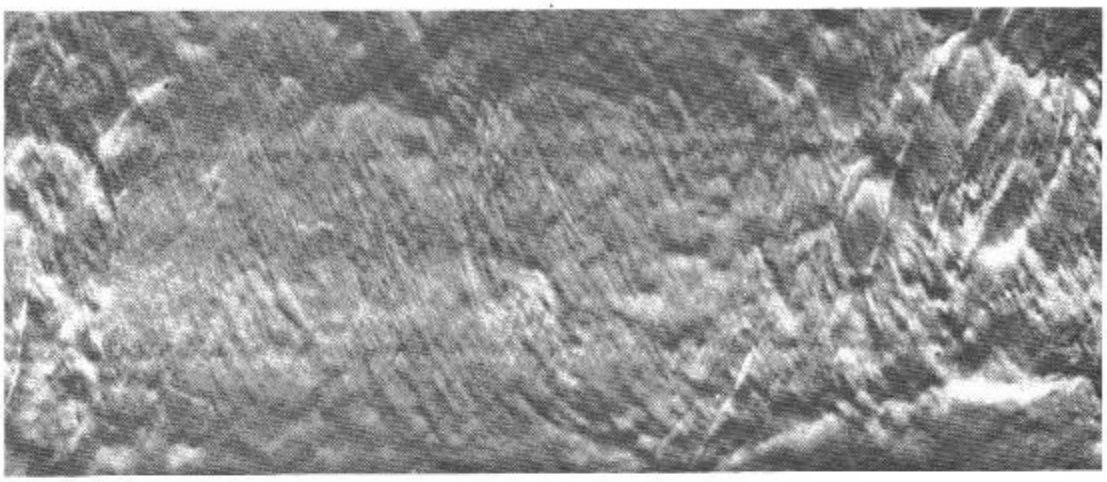

Figure 70. Natural Sea Surface Patterns.
4 September 1967; 1949; 500 ft; 24°19'N; 82°14'W; AN/AAR-32;
0.5 mm (diameter) Ge:Hg; NP-2E aircraft Bu. No. 131403.
Sea state: 0.

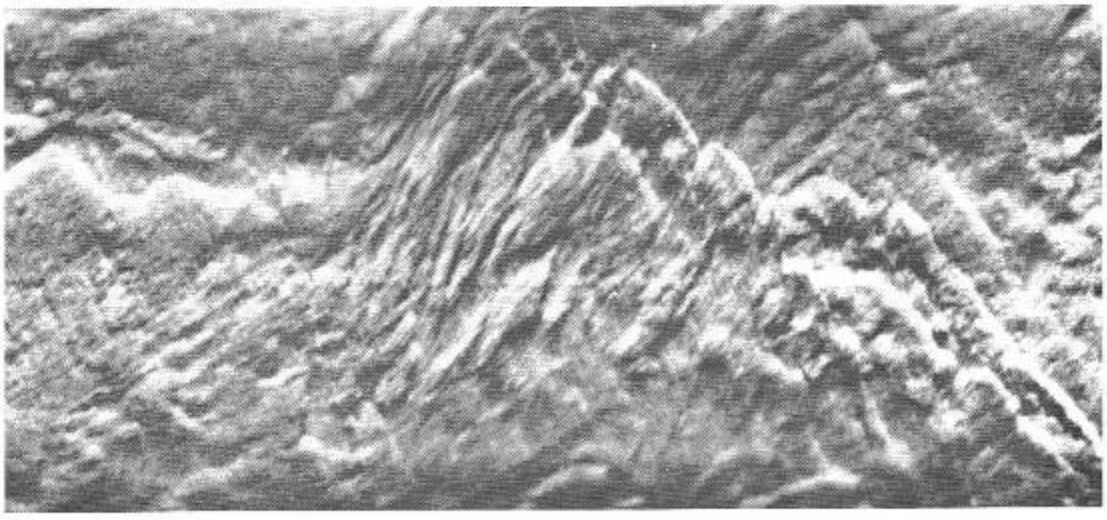

Figure 71. Natural Sea Surface Patterns.
4 September 1967; 2136; 500 ft; 24°09'N; 82°16'W; AN/AAR-32;
0.5 mm (diameter) Ge:Hg; NP-2E aircraft Bu. No. 131403.
Sea state: 0.

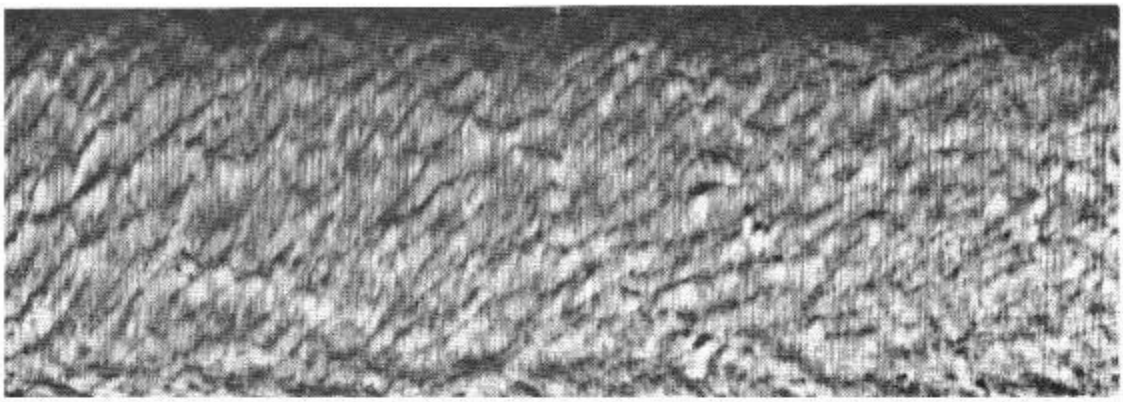

Figure 72. Natural Surface Patterns.
5 March 1964, 2042; 1000 ft; 30°07'N; 85°45'W; Reconofax IV Mark II; 4 mm^2 (circular) Ge:Hg; NP-2E aircraft Bu. No. 131403.
Note the whitecaps to the right of center. Sea state: 2.

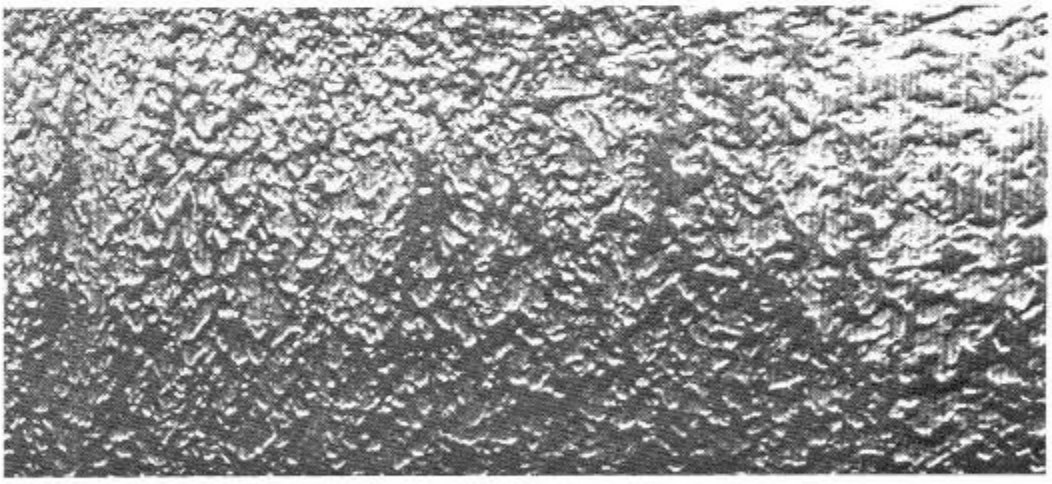

Figure 73. Natural Sea Surface Patterns.
26 April 1963; 1841; 41°39'N; 68°40'W; AN/AAR-30; 6.25 mm^2 (circular) Ge:Cu; SP-2E aircraft Bu. No. 131403.

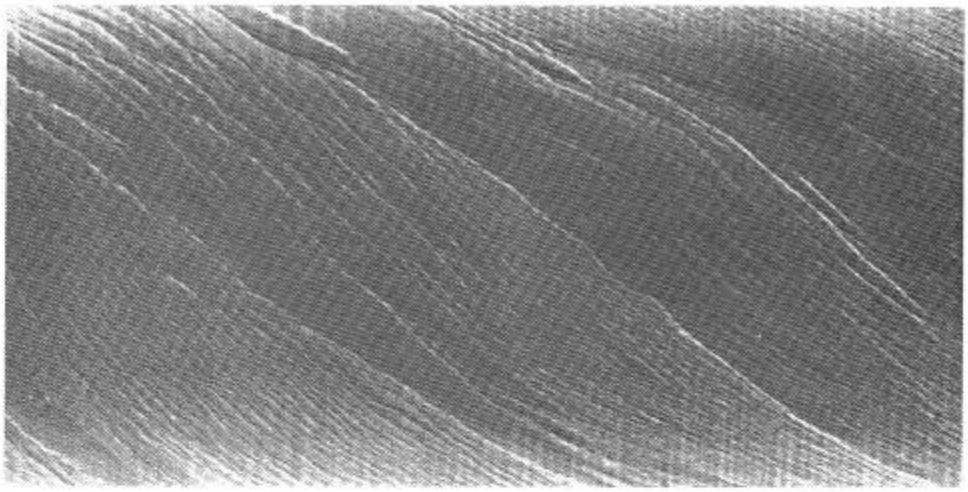

Figure 74. Wind Streaks.
1 September 1964; 2102; 3500 ft; AN/AAR-30; 6.25 mm^2 (circular)
Ge:Hg; NP-2E aircraft Bu. No. 131403.

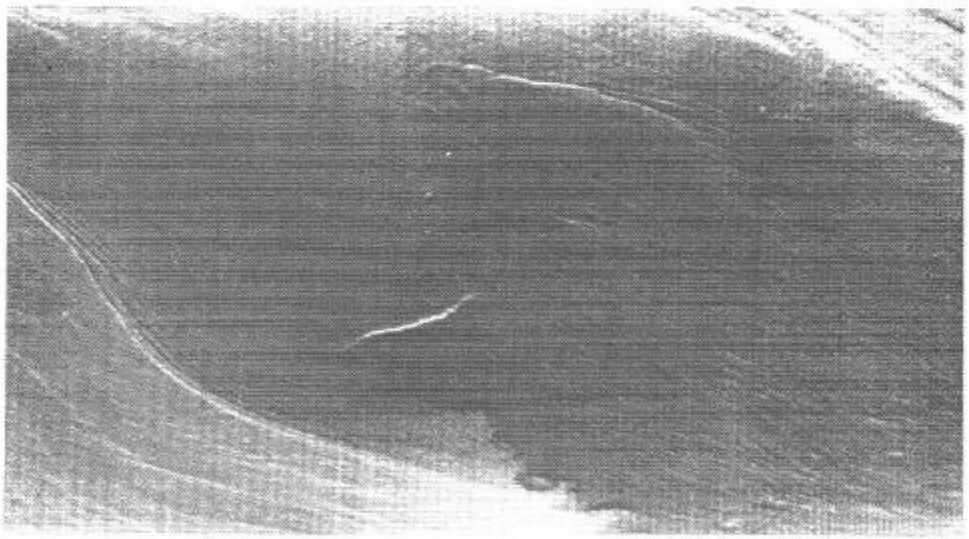

Figure 75. Natural Sea Surface Patterns.
1 September 1964; 2101; 3500 ft; AN/AAR-30; 6.25 mm^2 (circular)
Ge:Hg; NP-2E aircraft Bu. No. 131403.

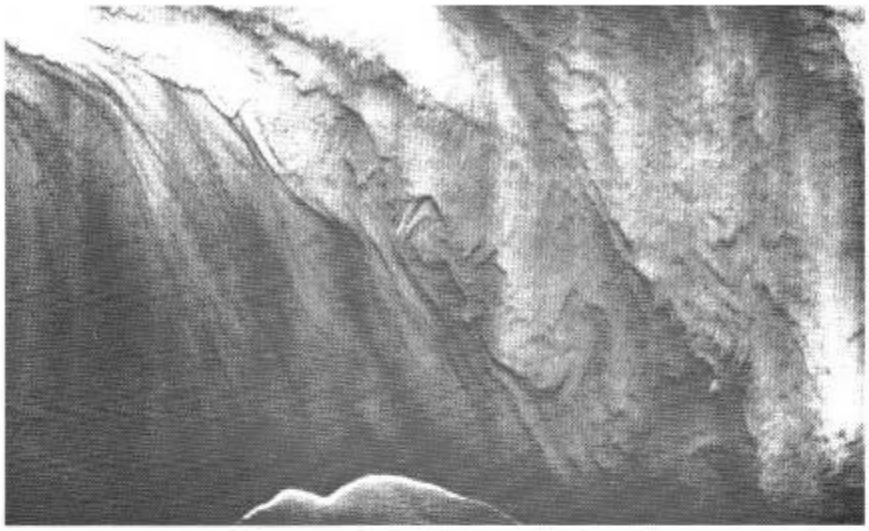

Figure 76. Natural Sea Surface Patterns.
8 April 1970; 1254; 3000 ft; 32°35'N; 79°40'W; AN/AAR-30;
2.5 X 2.5 mm Ge:Hg.

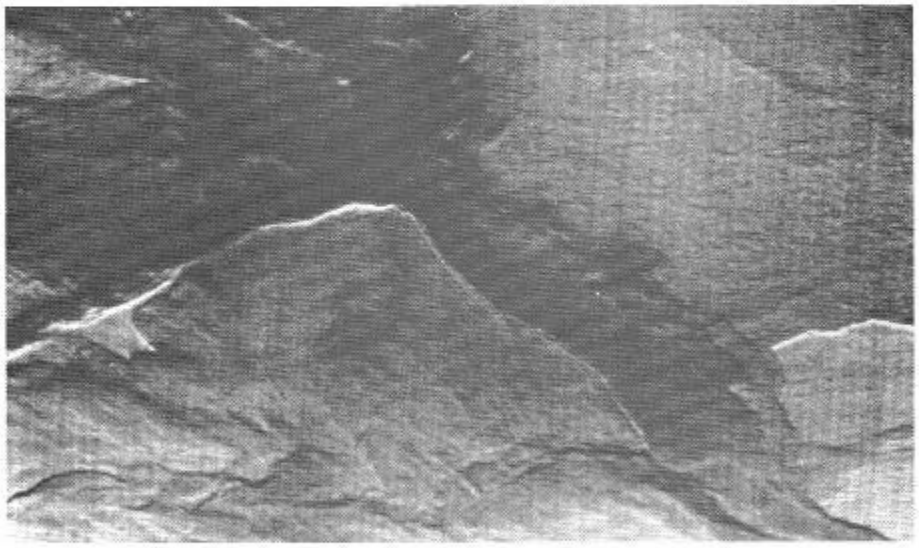

Figure 77. Natural Sea Surface Patterns.
23 May 1968; 2041; 25°32'N; 75°59'W; AN/AAR-30; 2.5 X 2.5 mm
Ge:Hg; NP-2E aircraft Bu. No. 131403.

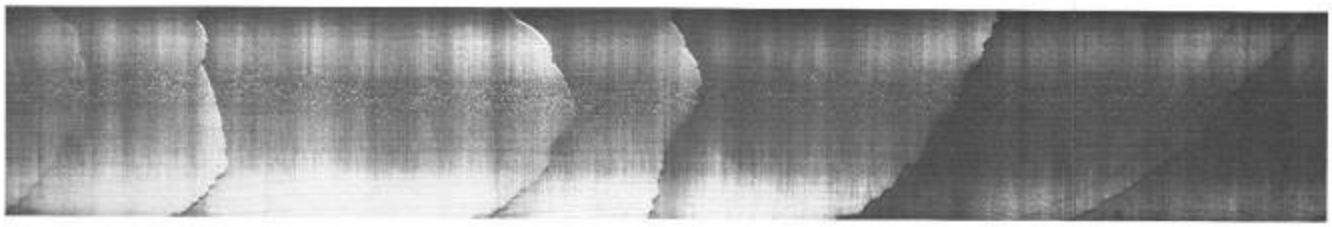

Figure 78. Successive Thermal Fronts.
7 May 1970; 2052; AN/AAR-30; 2.5 X 2.5 mm Ge:Hg.
The white dots running down the length of the picture are an instrumental artifact.

Figure 79. Mouth of St. Andrew Bay.
27 October 1964; 1711; 1000 ft; 30°07'N; 85°44'W; AN/AAR-30; 6.25 mm^2 (circular) Ge:Hg; NP-2E aircraft Bu. No. 131403.
Also pictured is a portion of U.S. Coast and Geodetic Survey Chart 489 (soundings are in feet).

Successively recorded infrared pictures from the flight of 5 March 1964 reveal the advance of a thin fan-shaped sheet of warmer, less saline water from St. Andrew Bay over the more dense water of the Gulf of Mexico. Figures 80-84 show portions of the interface between these two water masses.

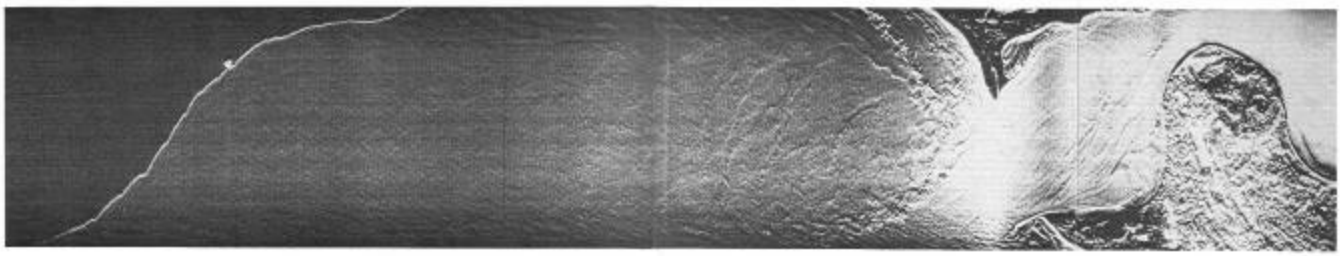

Figure 80. 5 March 1964; 2102; 100 ft; 30°07'N; 85°45'W; AN/AAR-30; 4 mm^2 (circular) Ge:Cu; NP-2E aircraft Bu. No. 131403.

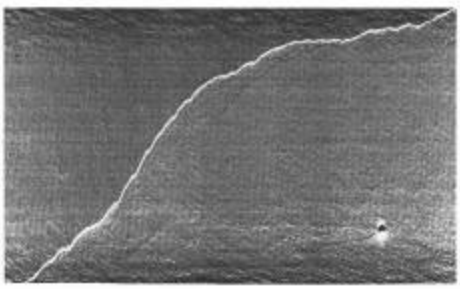

Figure 81. 5 March 1964; 2213; 960 ft; 30°07'N; 85°45'W; AN/AAR-30; 4 mm^2 (circular) Ge:Cu; NP-2E aircraft Bu. No. 131403.

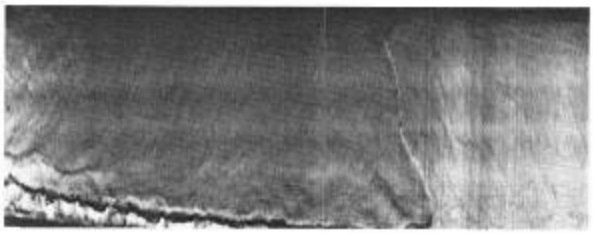

Figure 82. 5 March 1964; 2246; 2350 ft; 30°08'N; 85°45'W; Reconofax IV Mark II; 4 mm^2 (circular) Ge:Hg; NP-2E aircraft Bu. No. 131403.
The mouth of St. Andrew Bay is just off the left side of the picture. Note the breakers near the coast along the lower edge.

Figure 83. 5 March 1964; 1547; 1060 ft; $30^{o}07'N$; $85^{o}45'W$; Reconofax IV Mark II; 4 mm^2 (circular) Ge:Hg; NP-2E aircraft Bu. No. 131403.
Notice the whitecaps in the left half of the picture. Sea state: 2.

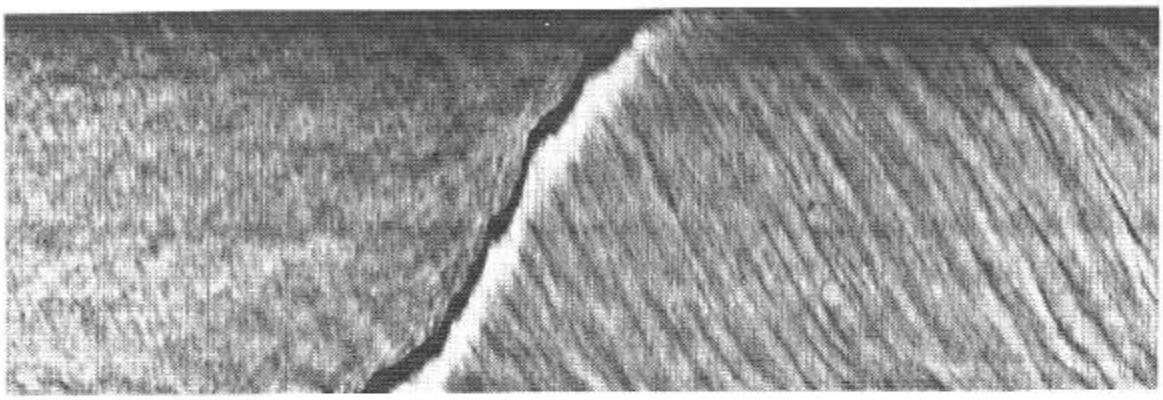

Figure 84. 5 March 1964; 2055; 1000 ft; 30°07'N; 85°45'W; Reconofax IV Mark II; 4 mm^2 (circular) Ge:Hg; NP-2E aircraft Bu. No. 131403.

Figure 85. Wakes from Piers of Chesapeake Bay Bridge.
10 July 1962; 2201; 1000 ft; 38°59'N; 76°23'W; AN/AAD-2;
6.25 mm^2 (circular) Ge:Cu; P2V-7 aircraft
Bu. No. 140985.

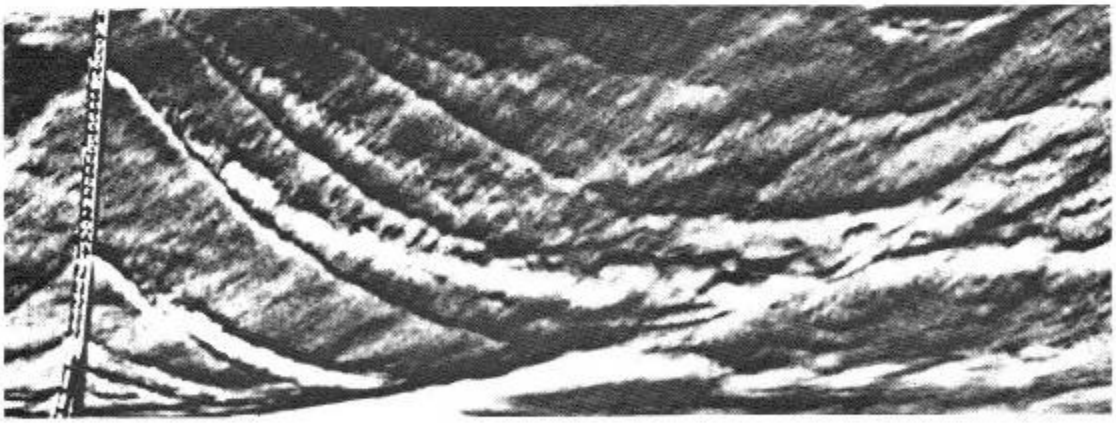

Figure 86. Wakes from Piers of Chesapeake Bay Bridge.
26 June 1962; 2138; 1000 ft; 38°59'N; 76°23'W; AN/AAD-2;
6.25 mm^2 (circular) Ge:Cu; P2V-7 aircraft
Bu. No. 140985.

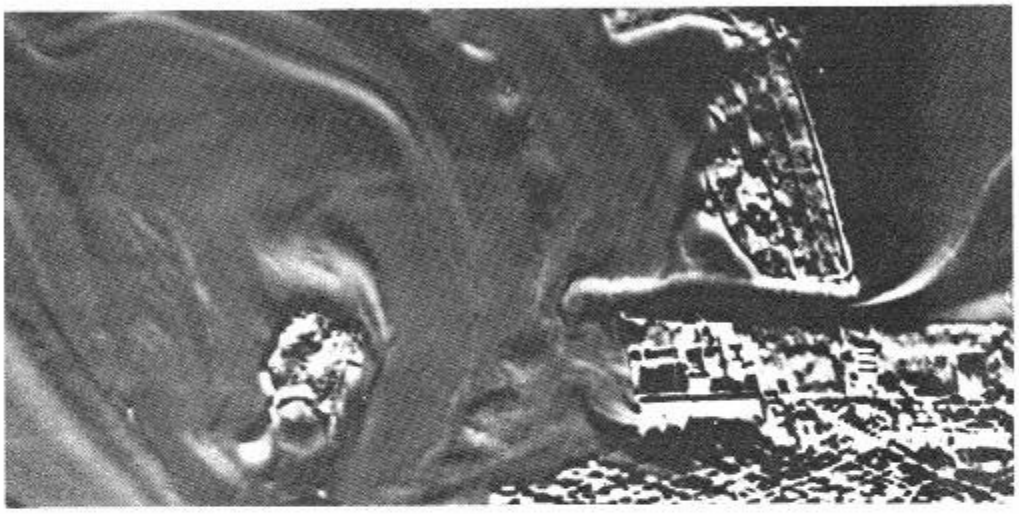

Figure 87. Natural Surface Patterns in the Vicinity of Key West.
14 March 1962; 2244; 2300 ft; $24^{o}34'$N; $81^{o}48'$W; AN/AAD-2;
6.25 mm^2 (circular) Ge:Cu; P2V-5F aircraft
Bu. No. 131403.

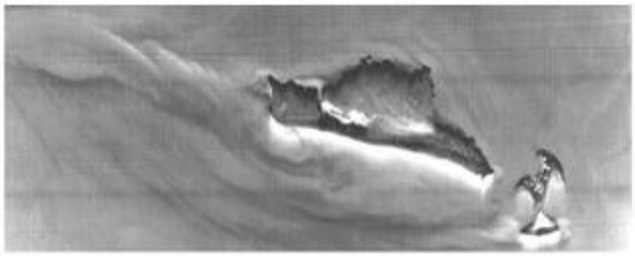

Figure 88. Woman Key and Ballast Key.
12 March 1962; 2152; 2000 ft; 24°31'N; 81°58'W; AN/AAD-2;
6.25 mm^2 (circular) Ge:Cu; P2V-5F aircraft Bu. No. 131403.
A portion of NOAA Nautical Chart 11441 is also presented
(soundings are in feet).

Figure 89. Key West and Neighboring Surface Patterns.
12 March 1962; 2230; 2500 ft;24°33'N; 81°49'W; AN/AAD-2;
6.25 mm^2 (circular) Ge:Cu; P2V-5F aircraft Bu. No. 131403.
Compare with portion of NOAA Nautical Chart 11441 shown
(soundings are in feet).

Figure 90. Boca Grande Key, Woman Key, and Ballast Key.
15 March 1962; 2222; 1900 ft; 24°32'N;
81°59'W; AN/AAD-2; 6.25 mm^2 (circular)
Ge:Cu; P2V-5F aircraft Bu. No. 131403.

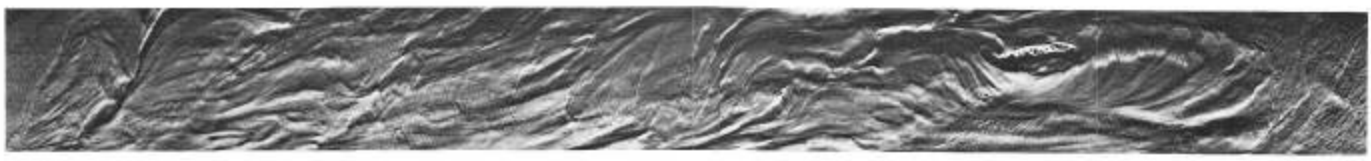

Figure 91. Loggerhead Key and Surrounding Surface Patterns.
15 March 1962; 1831; 4500 ft; 24°38'N;
82°56'W; AN/AAD-2; 6.25 mm^2
(circular) Ge:Cu; P2V-5F aircraft
Bu. No. 131403.

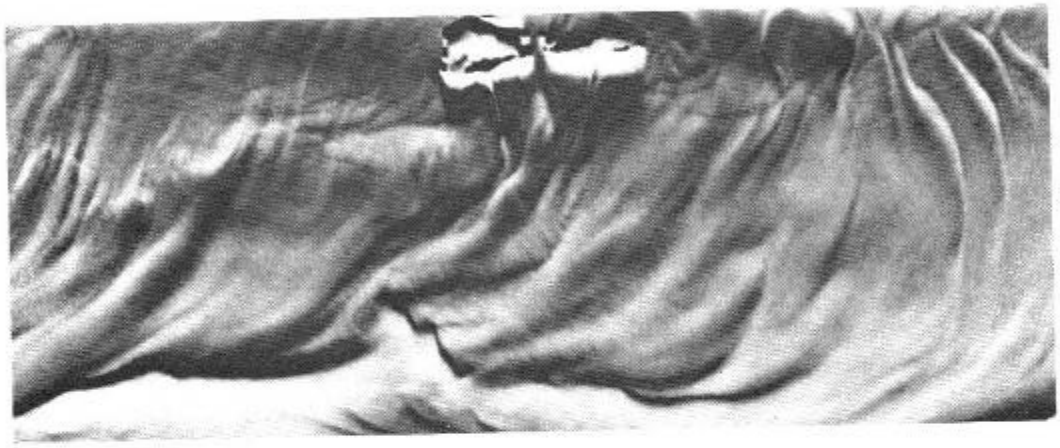

Figure 92. Small Islands Near Florida and Surrounding Surface Patterns. 12 March 1962; 1947; 3000 ft; AN/AAD-2; 6.25 mm^2 (circular) Ge:Cu; P2V-5F aircraft Bu. No. 131403.

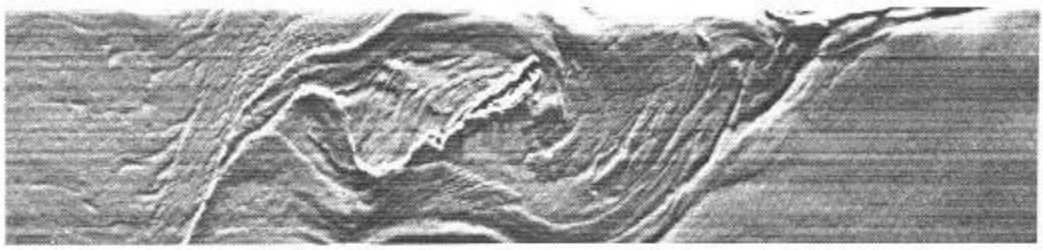

Figure 93. Small Island in the Tongue of the Ocean.
13 May 1966; 2008; 24°19'N; 77°46'W; AN/AAR-32;
2.5 X 2.5 mm Ge:Hg; P-3A aircraft Bu. No. 148883.

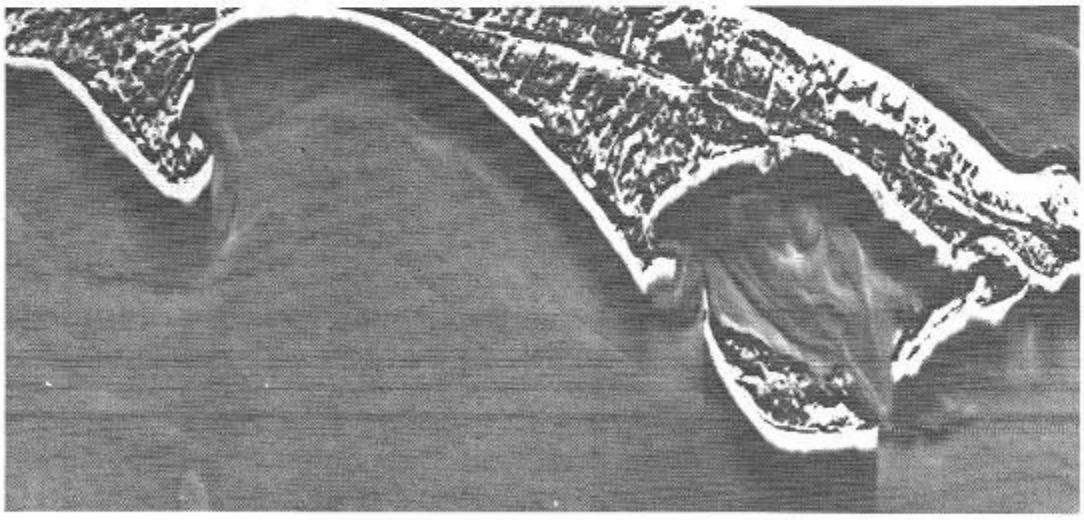

Figure 94. Sandy Hook, New Jersey, and Nearby Water Patterns.
1 October 1963; 2050; 2500 ft; 40°26'N; 74°00'W; Reconofax IV
Mark II; 0.5 mm (diameter) Ge:Cu; NP-2E aircraft
Bu. No. 131403.

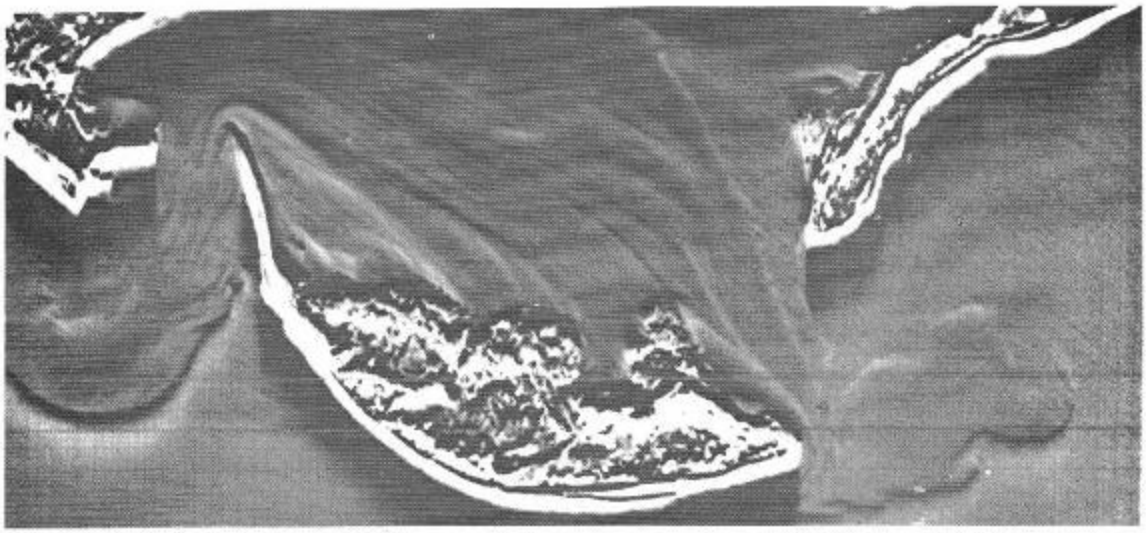

Figure 95. Spermaceti Cove.
1 October 1963; 2126; 1000 ft; 40°25'N; 73°59'W; Reconofax IV Mark II; 0.5 mm (diameter) Ge:Cu; NP-2E aircraft Bu. No. 131403.

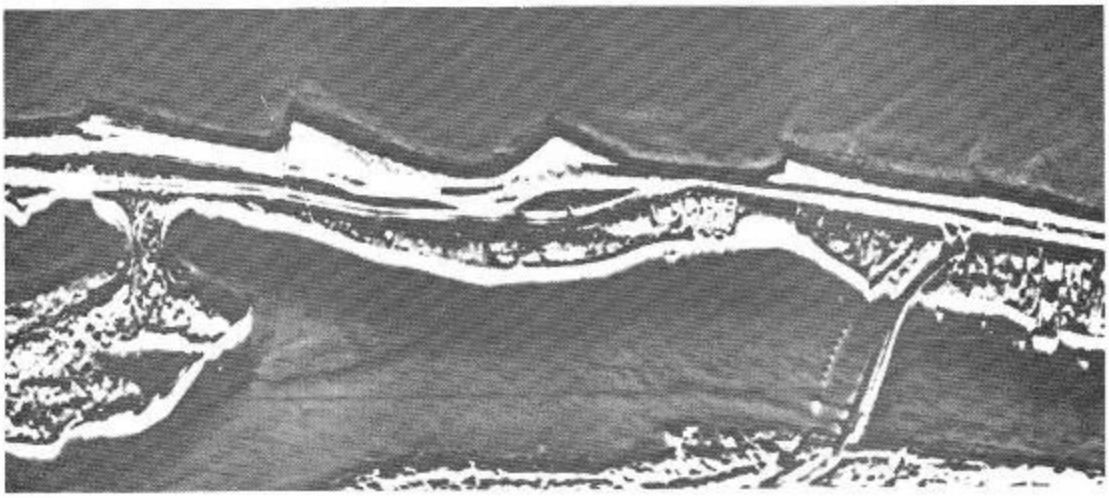

Figure 96. Shoreline and Adjacent Surface Patterns.
1 October 1963; 2115; 1000 ft; 40°24'N; 73°59'W; Reconofax IV Mark II; 0.5 mm (diameter) Ge:Cu; NP-2E aircraft Bu. No. 131403.

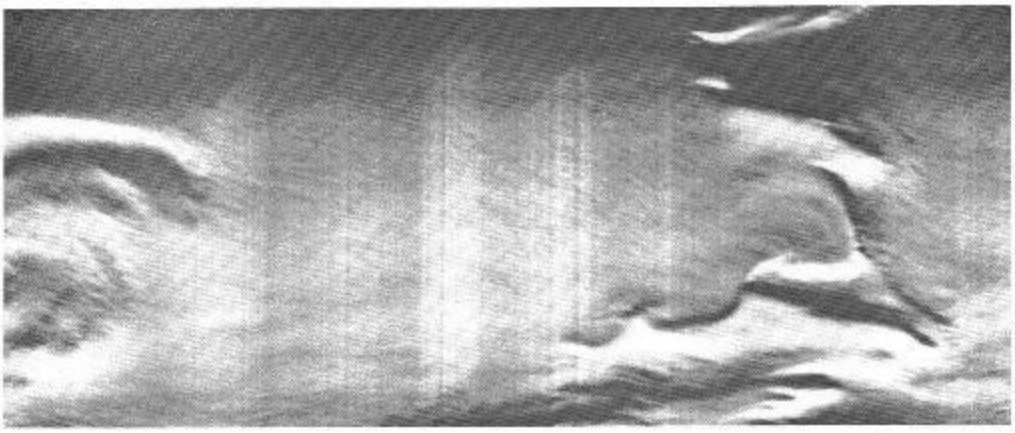

Figure 97. Natural Sea Surface Patterns.
10 May 1962; 2341; 8000 ft; 39°37'N; 71°34'W; AN/AAD-2;
6.25 mm^2 (circular) Ge:Cu; P2V-7 aircraft Bu. No. 140985.

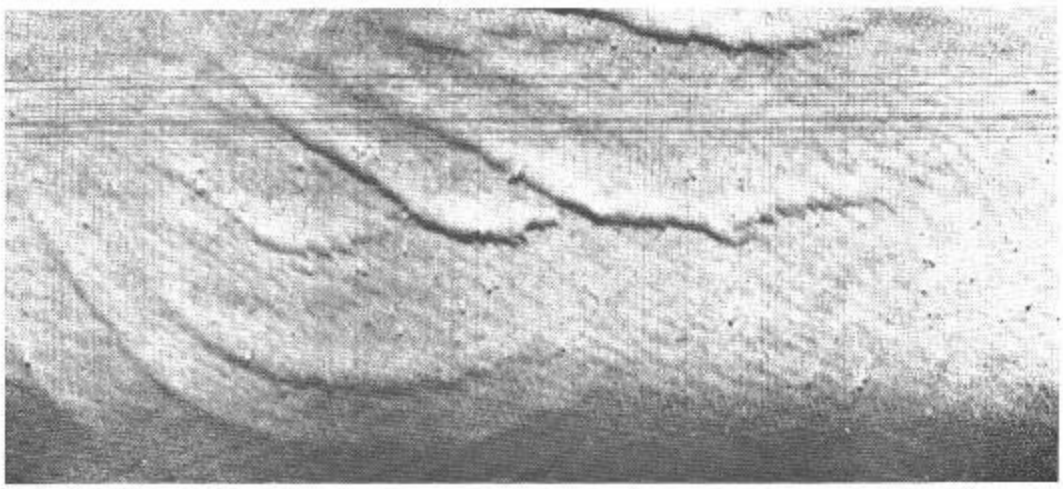

Figure 98. Whitecaps and Natural Sea Background Patterns.
15 January 1964; 1726; 3600 ft; 41°00'N; 70°31'W; Reconofax IV
Mark II; 4 mm^2 (circular) Ge:Hg; NP-2E aircraft Bu. No. 131403.
Sea state: 3.

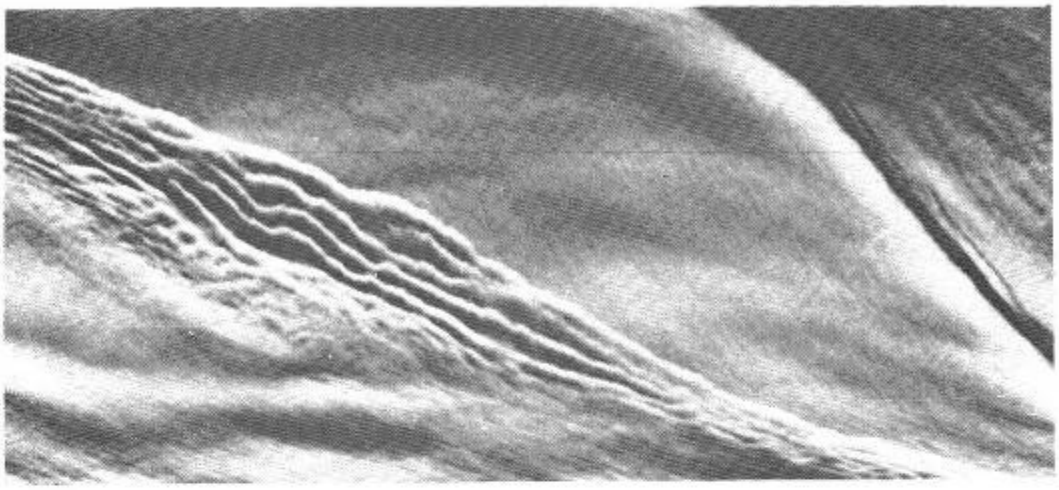

Figure 99. Natural Sea Surface Patterns.
28 March 1962; 2128; 2700 ft; 40°30'N; 71°58'W; AN/AAD-2;
6.25 mm^2 (circular) Ge:Cu; P2V-5F aircraft Bu. No. 131403.

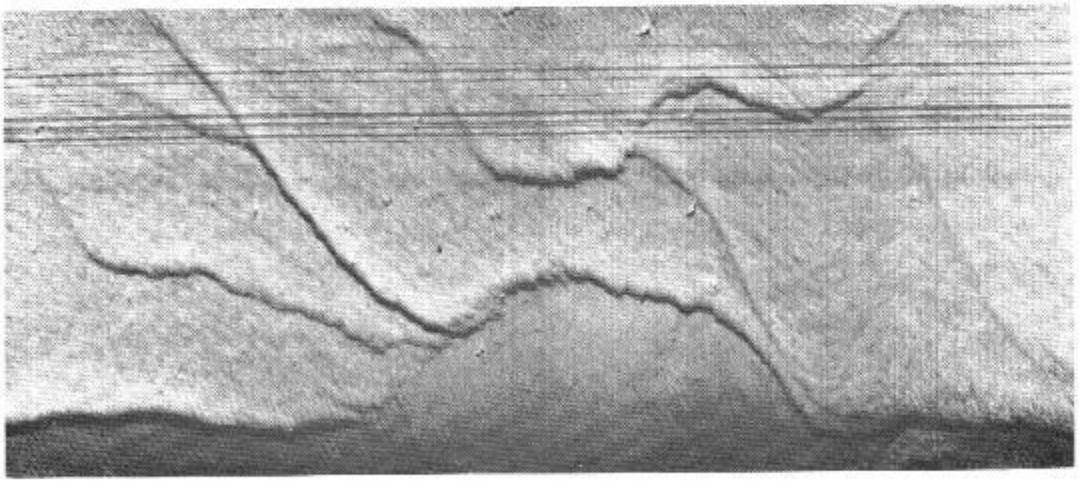

Figure 100. Whitecaps and Natural Sea Background Patterns.
15 January 1964; 1730; 3600 ft; 41°00'N; 70°42'W; Reconofax IV
Mark II; 4 mm^2 (circular) Ge:Hg; NP-2E aircraft Bu. No. 131403.
Sea state: 3.

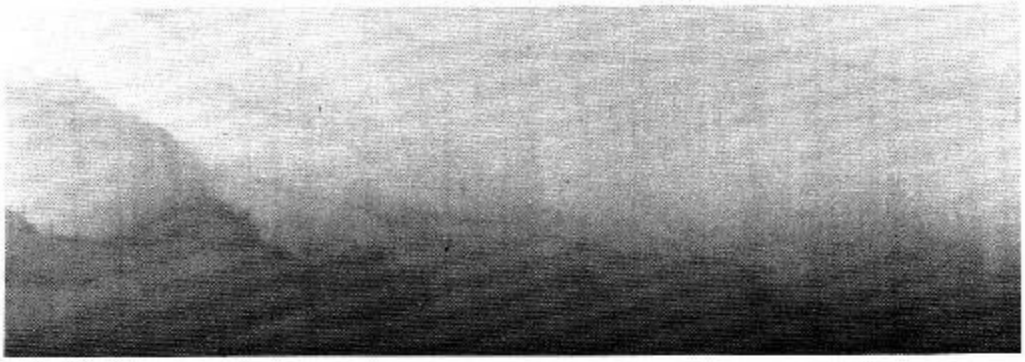

Figure 101. Natural Sea Surface Patterns.
27 July 1970; 2019; 1000 ft; 39°05'N; 73°54'W; Reconofax XIIIA;
0.1 X 0.1 mm HgCdTe; P-3A aircraft Bu. No. 149677.

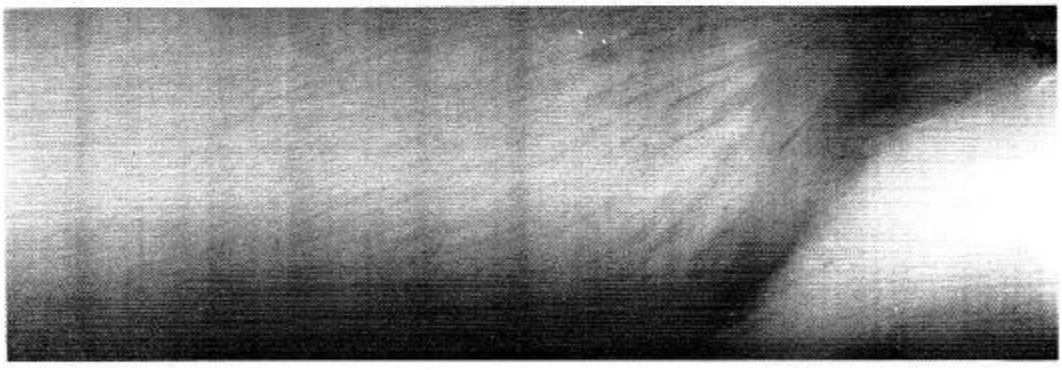

Figure 102. Natural Sea Surface Patterns.
4 August 1970; 0630; 1500 ft; 37°56'N; 75°01'W; Reconofax XIIIA;
0.2 X 0.2 mm HgCdTe; P-3A aircraft Bu. No. 150499.

Figure 103. Natural Surface Patterns.
24 May 1972; 1901; 7000 ft; AN/AAR-30; 2.5 X 2.5 mm Ge:Hg.

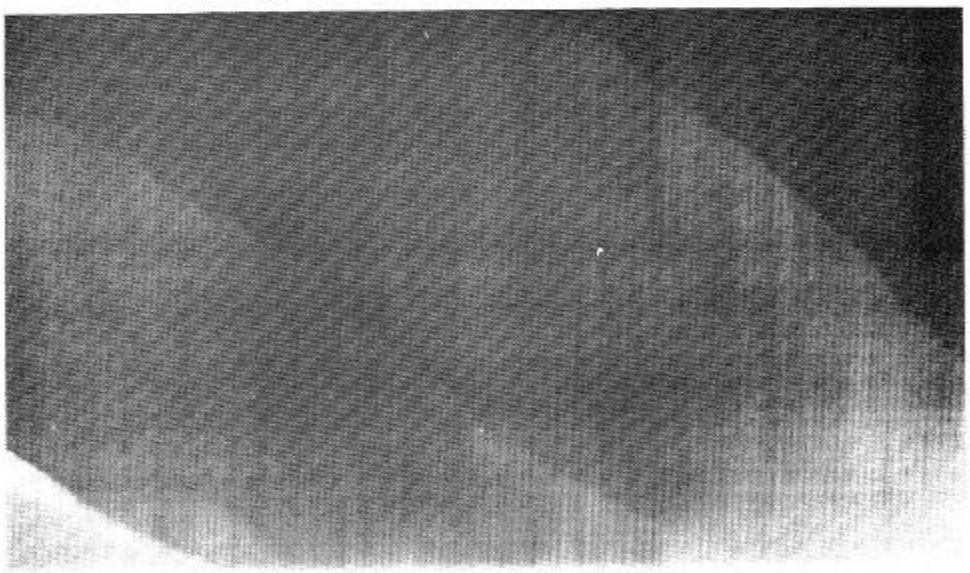

Figure 104. A Succession of Thermal Fronts.
3 October 1963; 1920; 2500 ft; 39°41'N; 73°57'W; AN/AAR-30;
0.5 mm (diameter) Ge:Cu; NP-2E aircraft Bu. No. 131403.

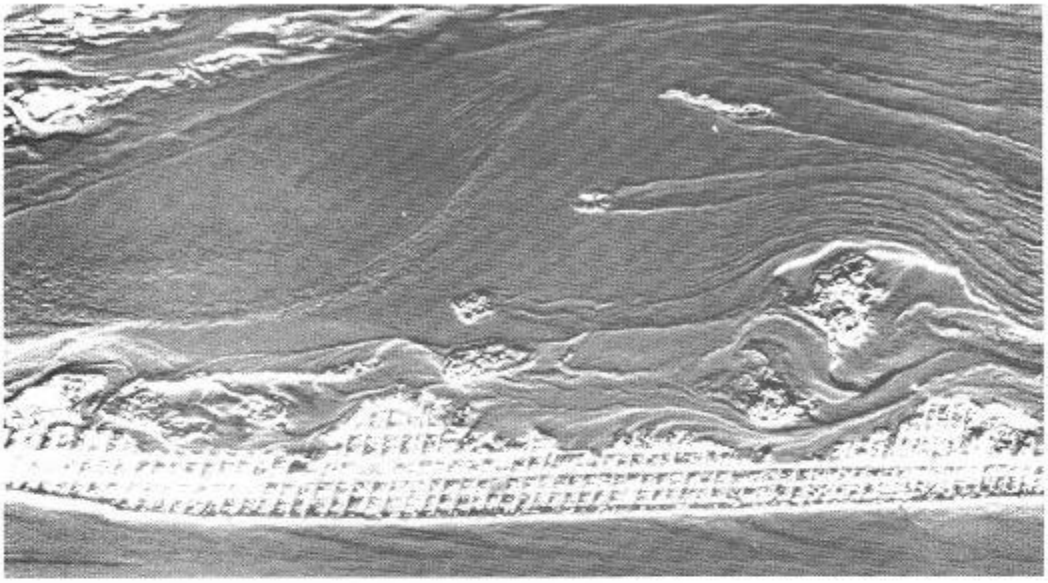

Figure 105. Beach Haven, New Jersey, and Neighboring Surface Patterns. 11 October 1962; 2028; 4000 ft; 39°33'N; 74°14'W; AN/AAR-30; 7 X 7 mm InSb; HRB-Singer's D-18 aircraft.

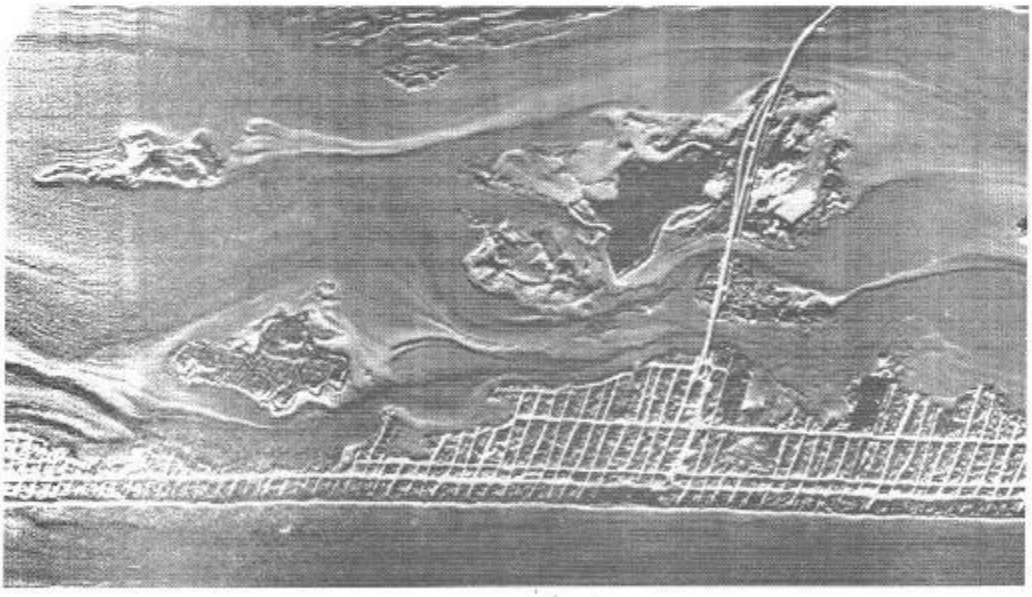

Figure 106. Ship Bottom, New Jersey, and Area Surface Patterns. 11 October 1962; 2030; 4000 ft; 39°38'N; 74°11'W; AN/AAR-30; 7 X 7 mm InSb; HRB-Singer's D-18 aircraft.

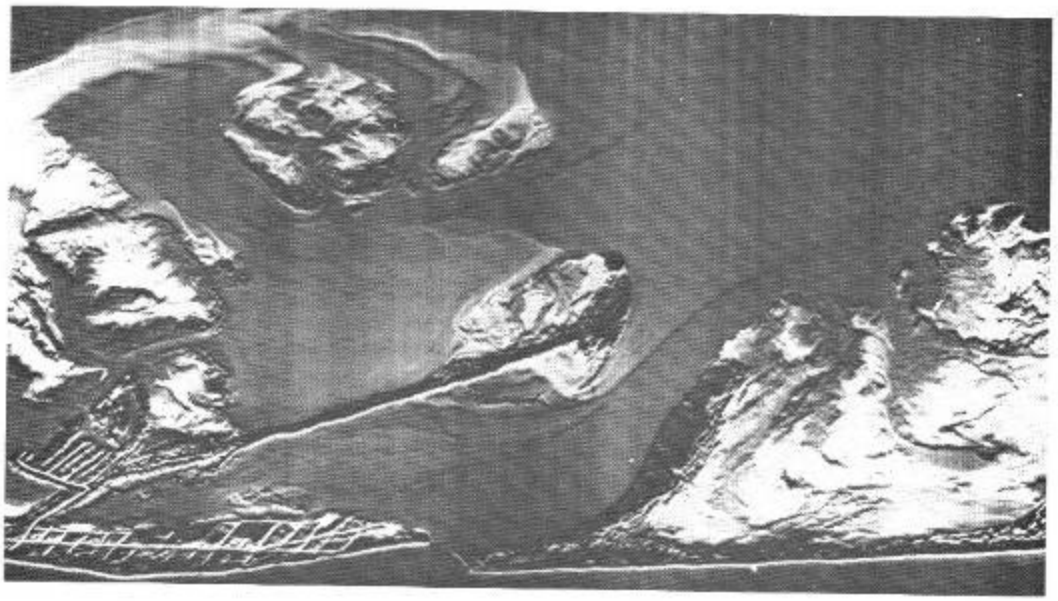

Figure 107. Barnegat Inlet and Bay.
11 October 1962; 2033; 4000 ft; 39°45'N; 74°06'W; AN/AAR-30;
7 X 7 mm InSb; HRB-Singer's D-18 aircraft.

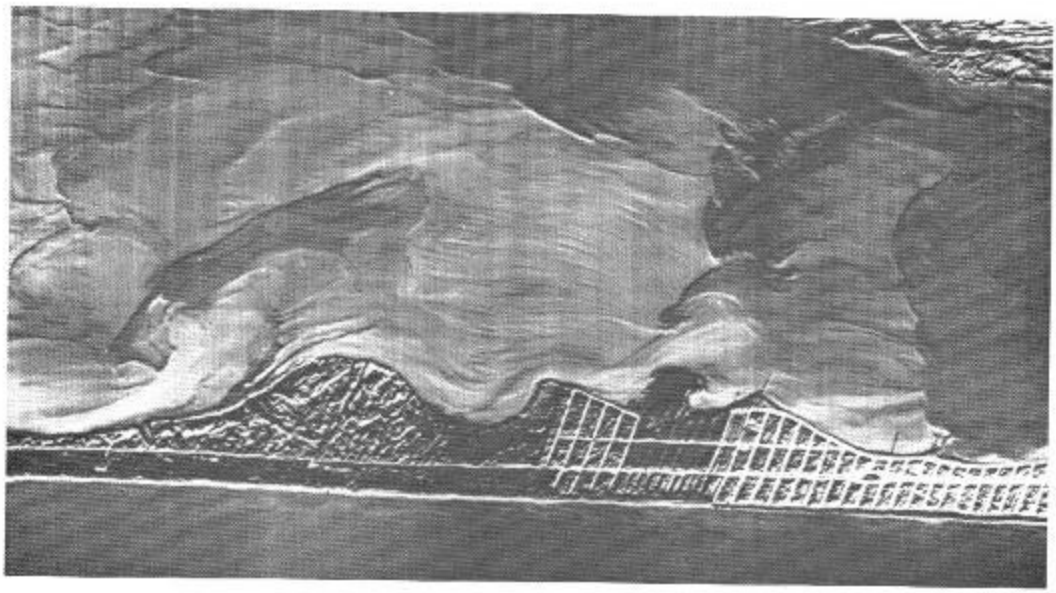

Figure 108. Barnegat Bay.
11 October 1962; 2037; 4000 ft; 39°56'N; 74°05'W; AN/AAR-30;
7 X 7 mm InSb; HRB-Singer's D-18 aircraft.

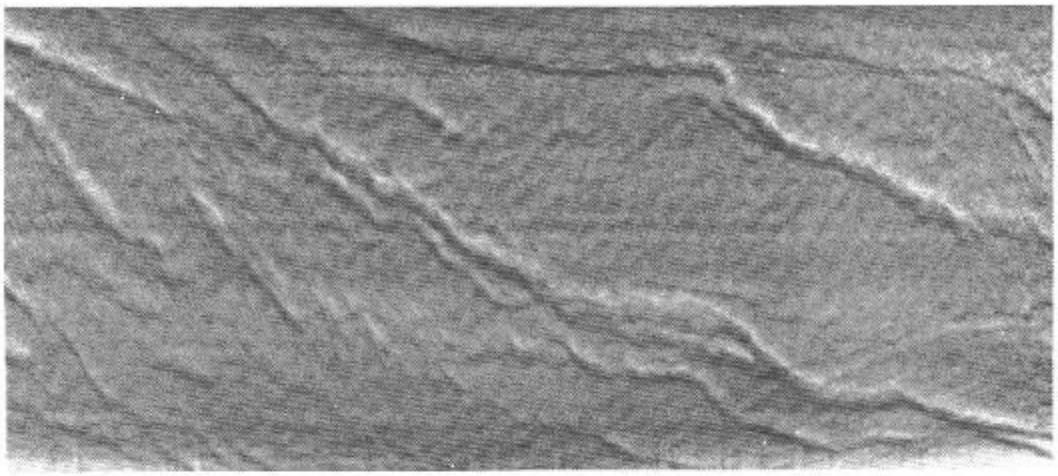

Figure 109. Natural Sea Surface Patterns.
21 June 1967; 2147; 1200 ft; 25°43'N; 76°05'W; AN/AAR-32;
0.5 mm (diameter) Ge:Hg; NP-2E aircraft Bu. No. 131403.
Sea state: 0.

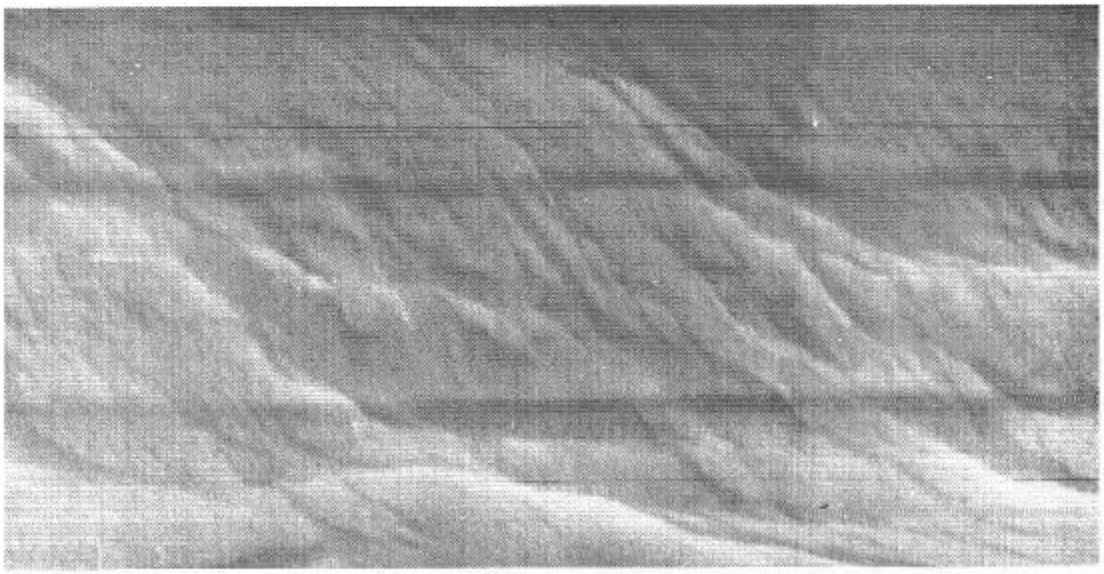

Figure 110. Natural Surface Patterns in Chesapeake Bay.
15 November 1961; 1935; 1000 ft; 37°42'N, 76°12'W; AN/AAD-2;
2.5 X 2.5 mm InSb; P2V-5F aircraft Bu. No. 131403.

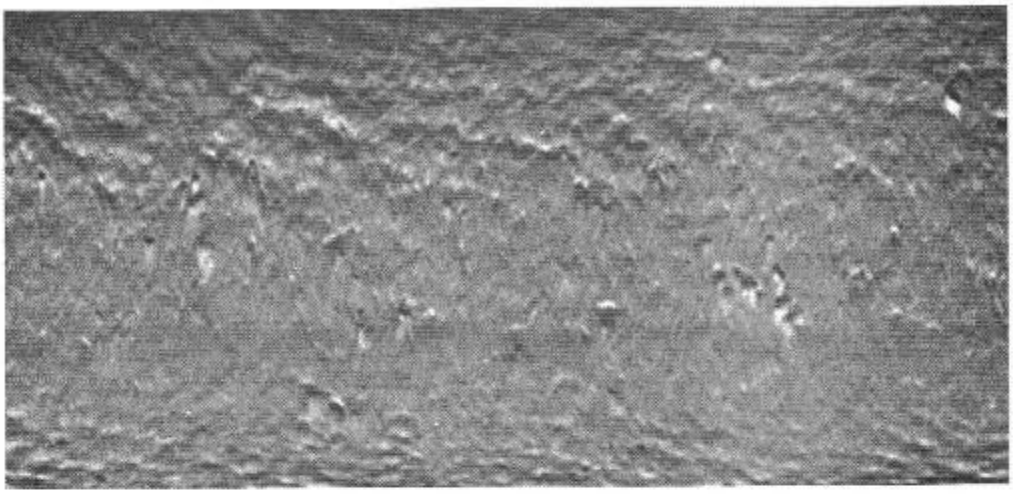

Figure 111. Whitecaps and Natural Background Patterns.
15 May 1962; 2033; 1000 ft; 23°53'N; 81°26'W; AN/AAD-2;
6.25 mm^2 (circular) Ge:Cu; P2V-7 aircraft Bu. No. 140985.
Sea state: 4.

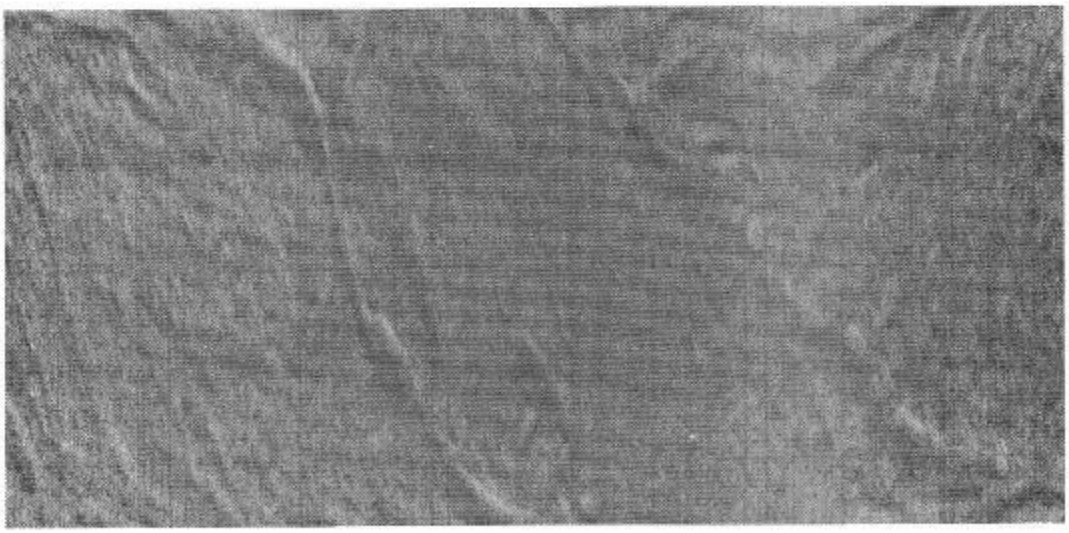

Figure 112. Natural Sea Surface Patterns.
8 July 1965; 1221; 1700 ft; 38°43'N; 74°52'W; AN/AAD-2;
0.5 mm (diameter) Ge:Cu; NP-2F aircraft Bu. No. 131403.

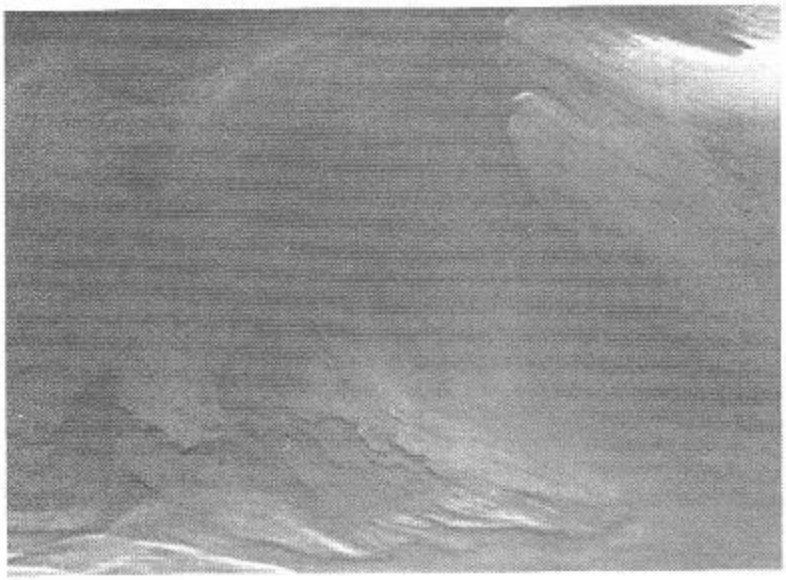

Figure 113. Natural Surface Patterns.
24 May 1972; 0101; 4600 ft; AN/AAR-30; 2.5 X 2.5 mm Ge:Hg.

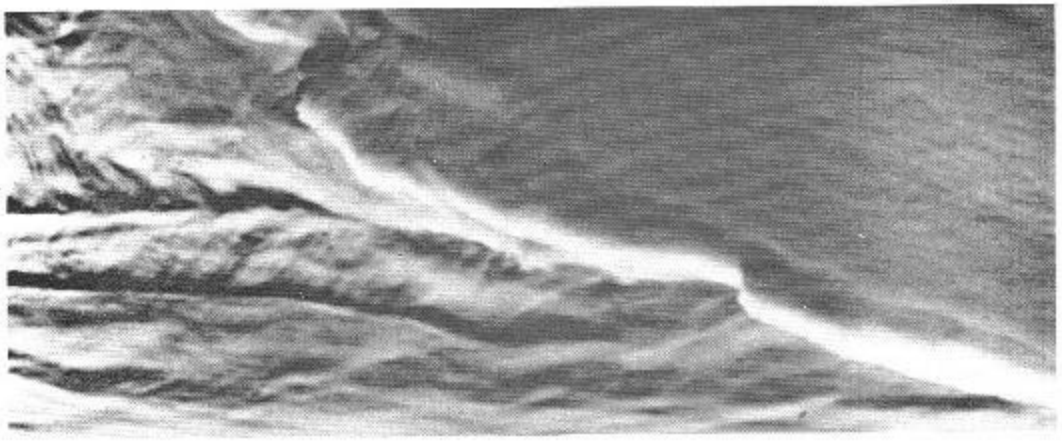

Figure 114. Natural Surface Patterns in the Strait of Georgia.
21 July 1969; 1557; 1500 ft; Reconofax IV Mark II; 2.5 X 2.5 mm Ge:Hg; S-2D aircraft.

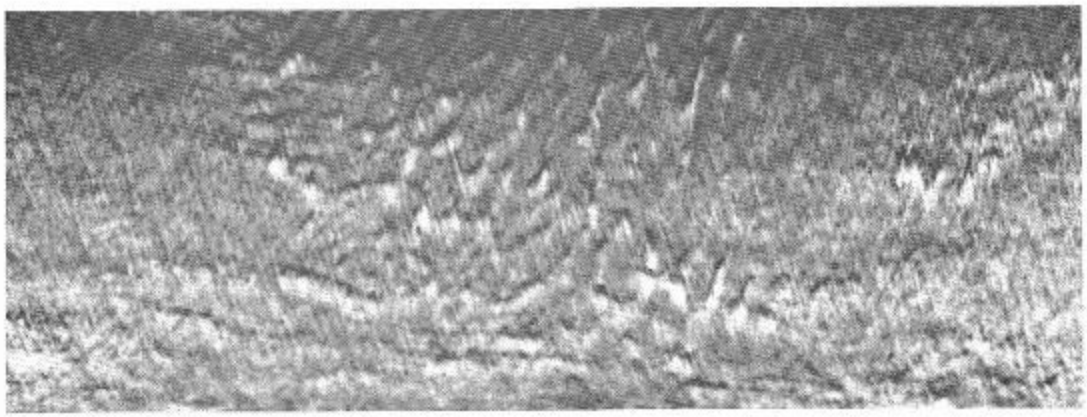

Figure 115. Natural Sea Surface Patterns.
13 June 1962; 1858; 1000 ft; 24°31'N; 81°50'W; AN/AAD-2;
6.25 mm^2 (circular) Ge:Cu; P2V-7 aircraft Bu. No. 140985.
Sea state: 1/2.

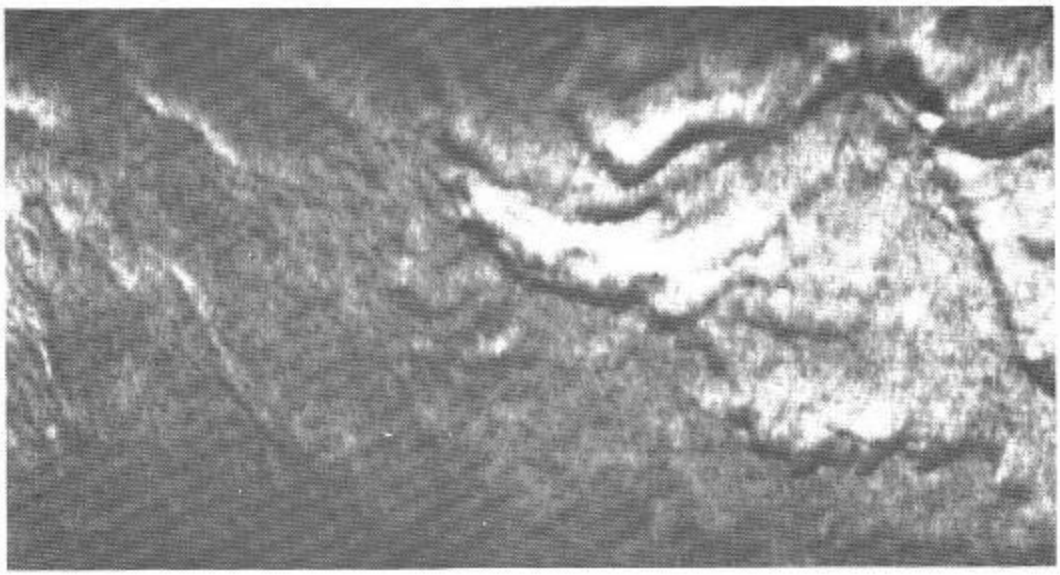

Figure 116. Natural Sea Surface Patterns.
3 August 1962; 0308; 1700 ft; 39°23'N; 71°24'W; AN/AAD-2;
6.25 mm^2 (circular) Ge:Cu; P2V-5F aircraft Bu. No. 131403.

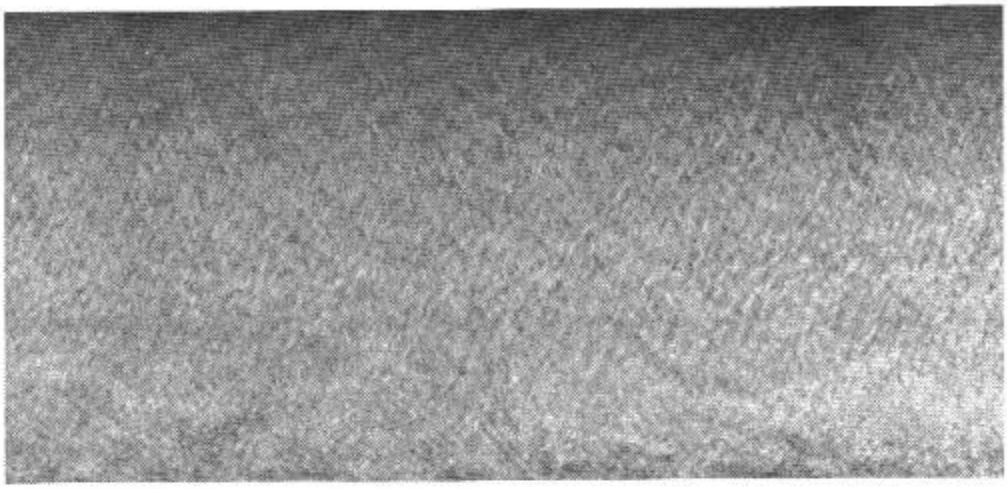

Figure 117. Natural Sea Surface Patterns.
16 May 1962; 2158; 2000 ft; 23°55'N; 81°39'W; AN/AAD-2;
6.25 mm^2 (circular) Ge:Cu; P2V-7 aircraft Bu. No. 140985.
These surface patterns are relatively subdued, perhaps because of violent mixing (state 4 seas) the day before and a lack of sunshine for several days.

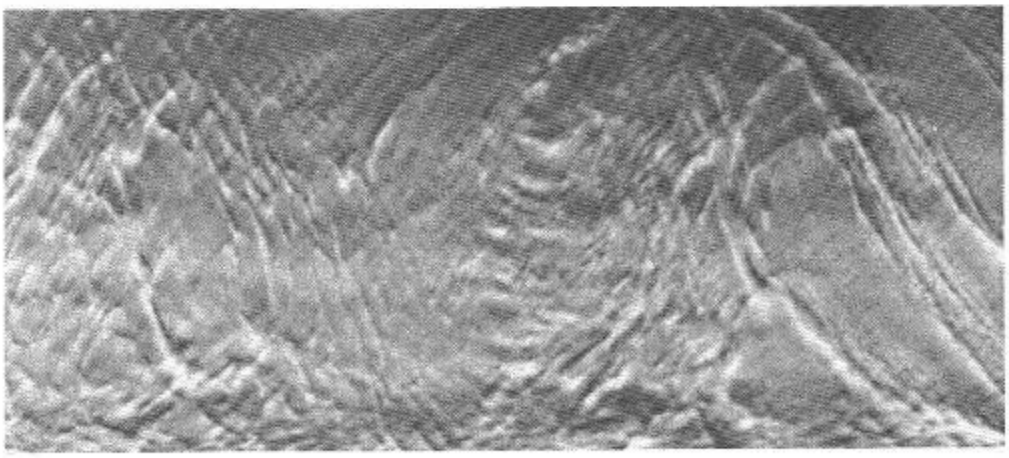

Figure 118. Natural Sea Surface Patterns.
28 March 1962; 2413; 2800 ft; 40°27'N; 73°51'W; AN/AAD-2;
6.25 mm^2 (circular) Ge:Cu; P2V-5F aircraft Bu. No. 131403.

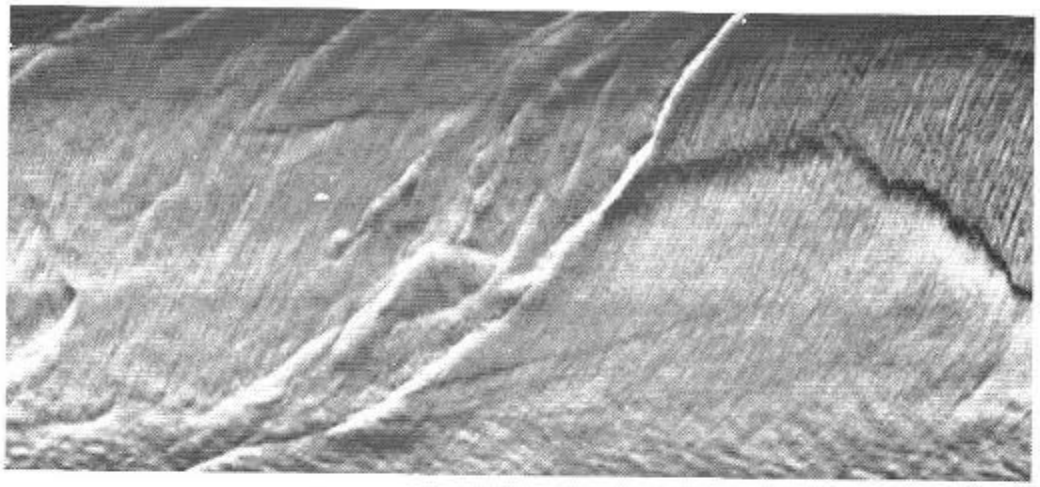

Figure 119. Natural Sea Surface Patterns.
4 April 1962; 2026; 2700 ft; 39°30'N; 71°40'W; AN/AAD-2;
6.25 mm^2 (circular) Ge:Cu; P2V-5F aircraft Bu. No. 131403.

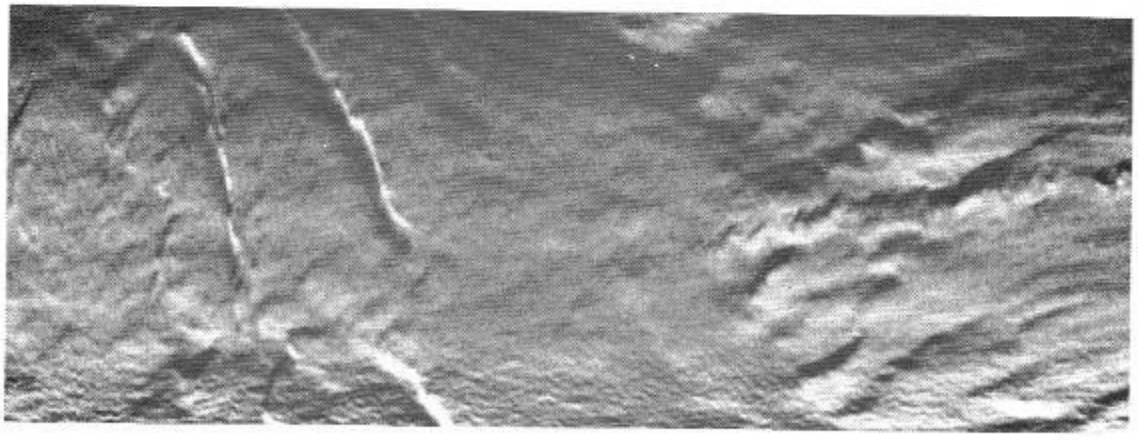

Figure 120. Natural Sea Surface Patterns.
19 April 1962; 2001; 2500 ft; 40°00'N; 71°15'W; AN/AAD-2;
6.25 mm^2 (circular) Ge:Cu; P2V-5F aircraft Bu. No. 131403.

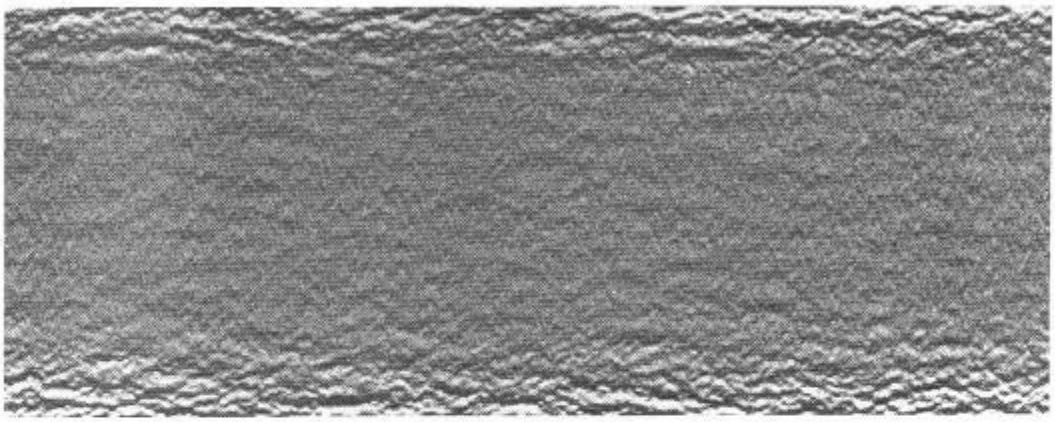

Figure 121. Natural Sea Surface Patterns.
10 May 1966; 38°26'N; 74°03'W; AN/AAR-32;
2.5 X 2.5 mm Ge:Hg; P-3A aircraft Bu. No. 148883.
Notice the enhancement of surface effects near the edges.

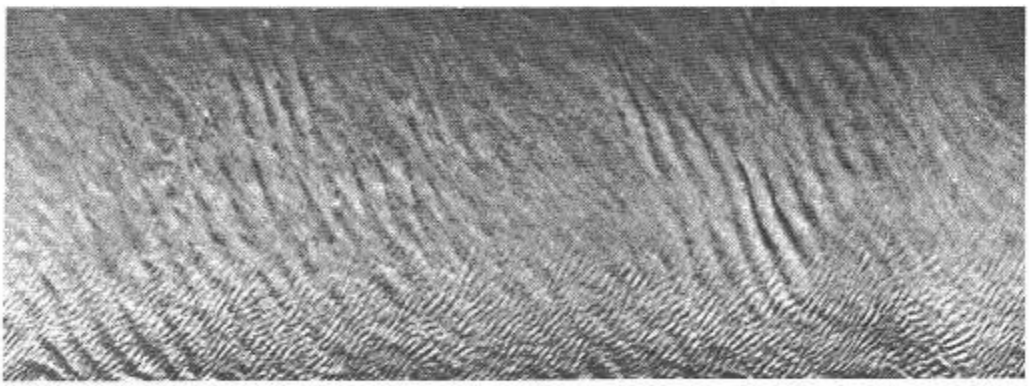

Figure 122. Natural Sea Surface Patterns.
10 May 1962; 2421; 2500 ft; 40°16'N; 71°55'W; AN/AAD-2;
6.25 mm^2 (circular) Ge:Cu; P2V-7 aircraft Bu. No. 140985.
Note the prominence of waves along the lower edge of the picture.

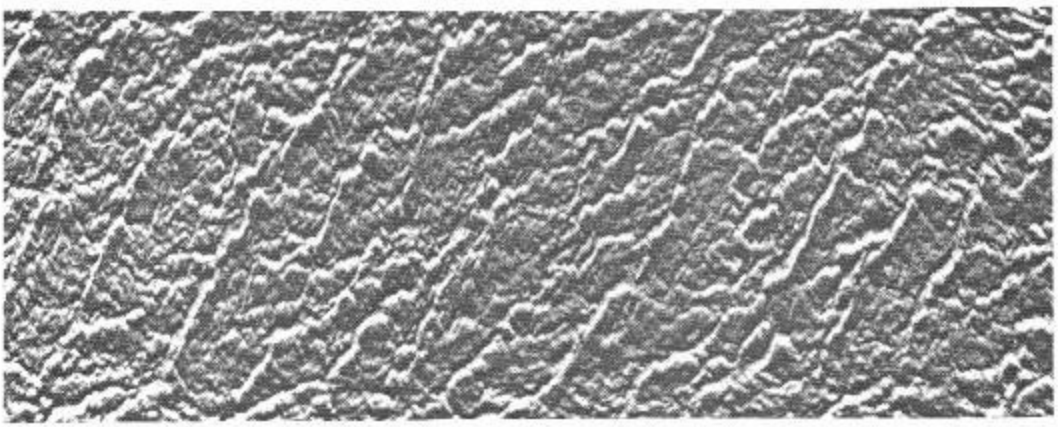

Figure 123. Natural Sea Surface Patterns.
10 May 1966; 38°18'N; 74°11'W; AN/AAR-32; 2.5 X 2.5 mm
Ge:Hg; P-3A aircraft Bu. No. 148883.

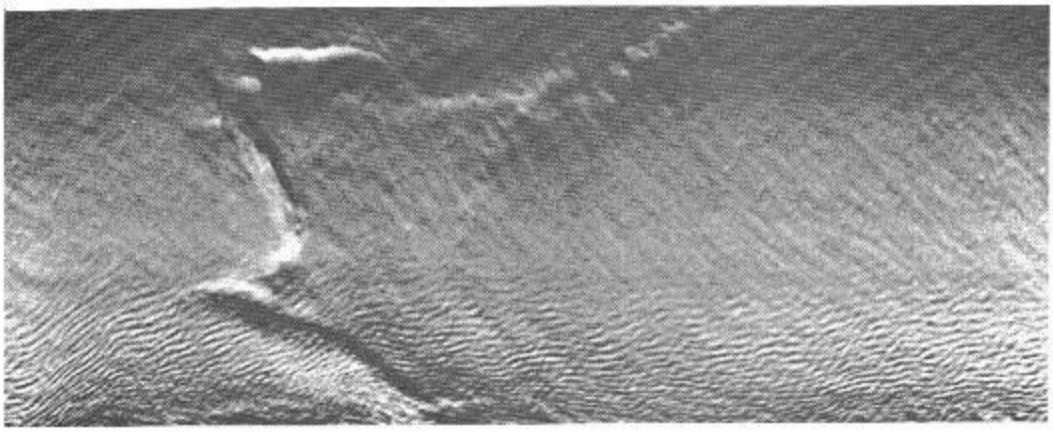

Figure 124. Natural Sea Surface Patterns.
10 May 1962; 2410; 2000 ft; 40°09'N; 71°47'W; AN/AAD-2;
6.25 mm^2 (circular) Ge:Cu; P2V-7 aircraft Bu. No. 140985.
Note the prominence of waves in the lower portion of the
picture.

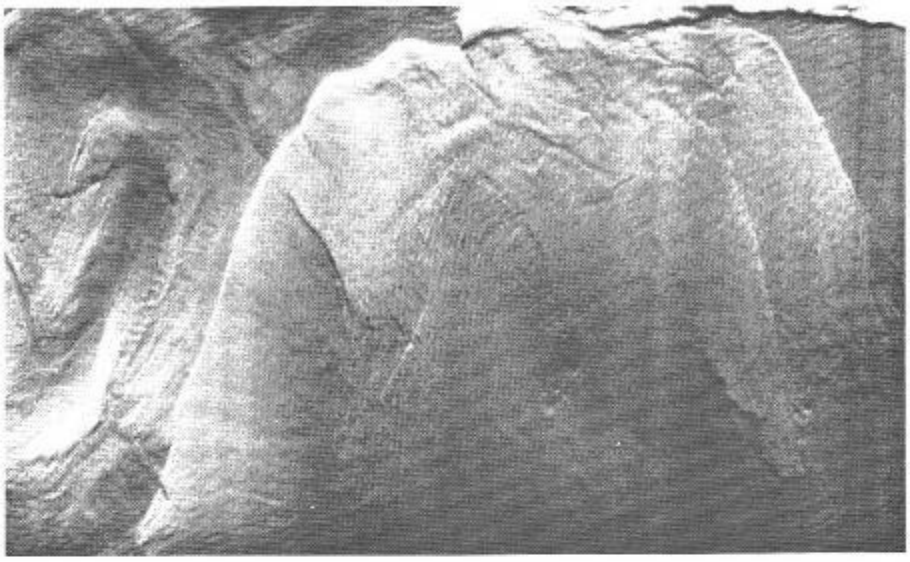

Figure 125. Natural Sea Surface Patterns.
8 April 1970; 1253; 3000 ft; 32°36'N; 79°41'W; AN/AAR-30;
2.5 X 2.5 mm Ge:Hg.

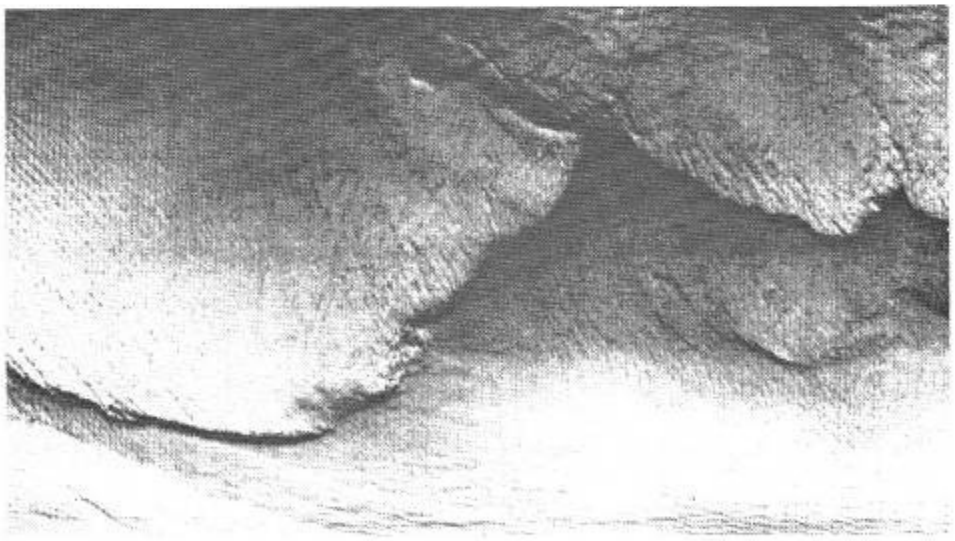

Figure 126. Thermal Front.
22 April 1963; 2230; 41°41'N; 68°17'W; AN/AAR-30;
6.25 mm^2 (circular) Ge:Cu; SP-2E aircraft Bu. No. 131403.

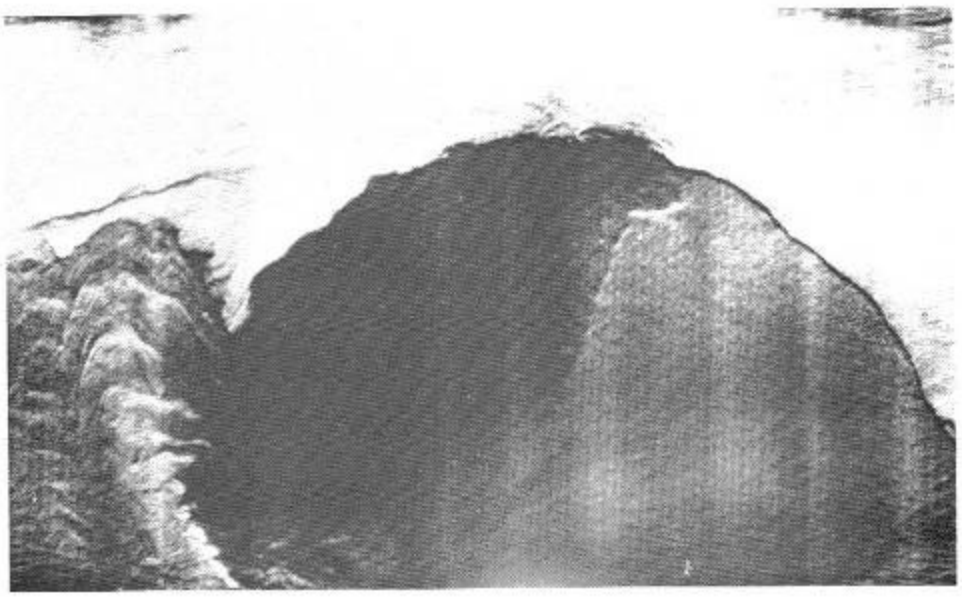

Figure 127. Natural Sea Surface Patterns.
8 April 1970; 1235; 3000 ft; 33°08'N; 78°50'W; AN/AAR-30;
2.5 X 2.5 mm Ge:Hg.

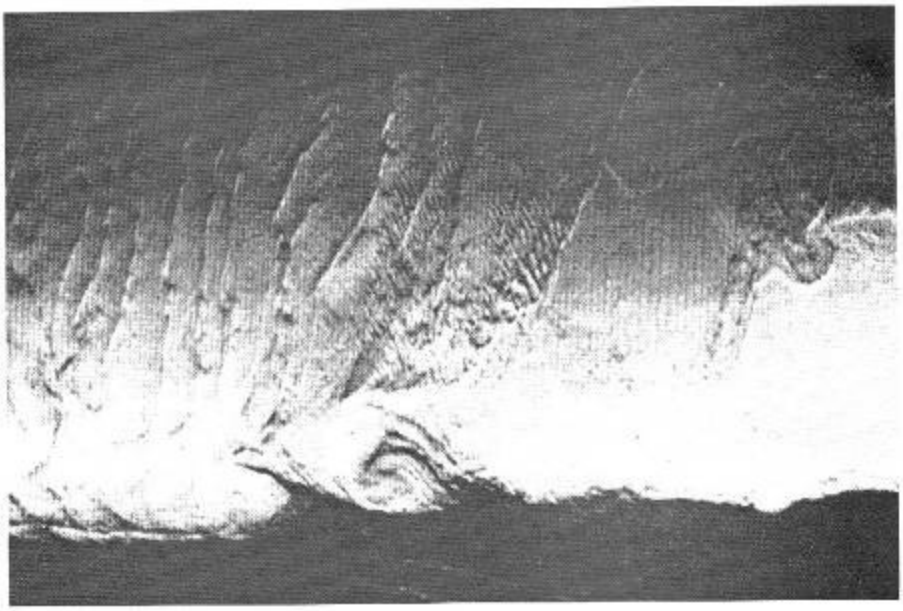

Figure 128. Natural Sea Surface Patterns.
22 April 1963; 2232; 41°41'N; 68°24'W; AN/AAR-30;
6.25 mm^2 (circular) Ge:Cu; SP-2E aircraft Bu. No. 131403.

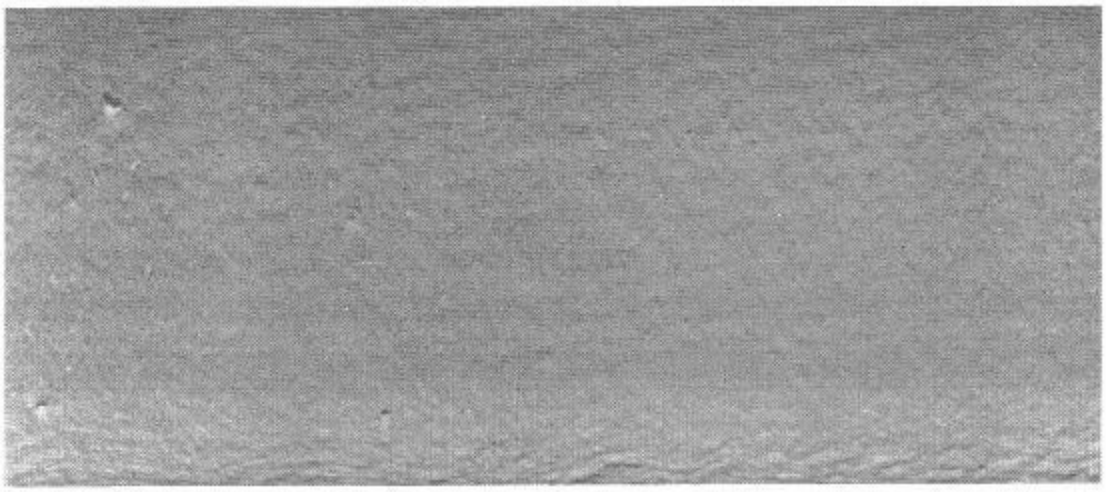

Figure 129. Whitecaps (Most Prominent on Left) and Waves (Lower Portion of Picture).
16 November 1963; 2230; 1000 ft; 23°55'N; 81°30'W; Reconofax IV Mark II; 4 mm^2 (circular) Ge:Cu; NP-2E aircraft Bu. No. 131403.
Sea state: 4.

Figure 130. Natural Sea Surface Patterns.
21 June 1967; 2105; 1000 ft; 25°45'N; 76°10'W; AN/AAR-30; 6.25 mm^2 (circular) Ge:Cu; NP-2E aircraft Bu. No. 131403.
Sea state: 0

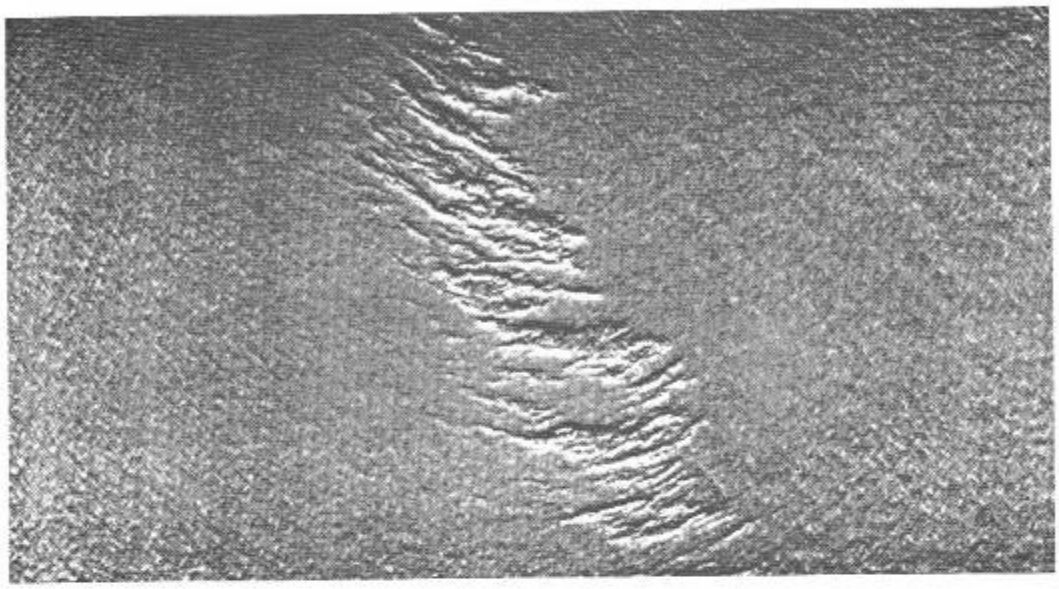

Figure 131. Natural Sea Surface Patterns.
13 January 1967; 0235; 2000 ft; 26°05'N; 79°50'W; AN/AAR-30;
6.25 mm^2 (circular) Ge:Cu; NP-2E aircraft Bu. No. 131403.

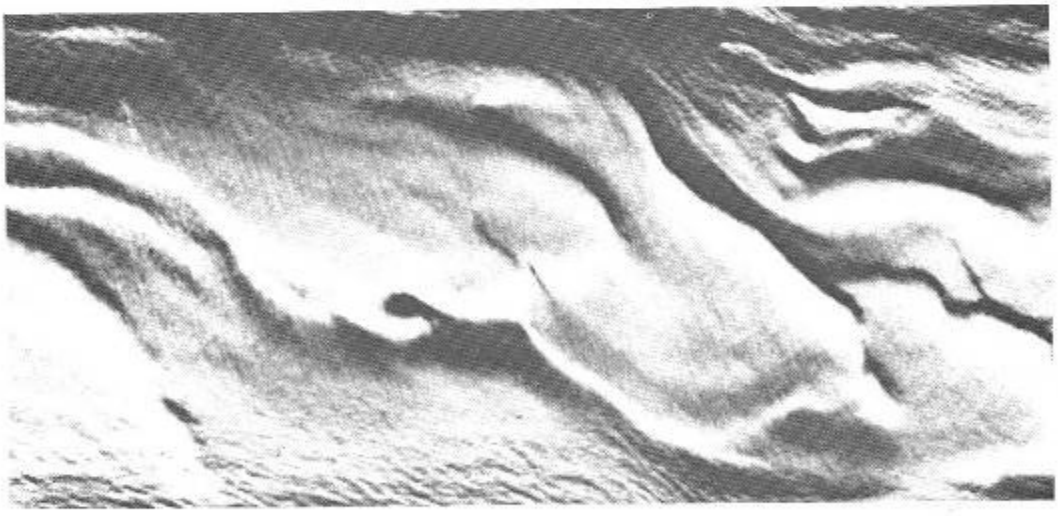

Figure 132. Natural Sea Surface Patterns.
7 May 1962; 2044; 3000 ft; 39°30'N; 70°30'W; AN/AAD-2;
6.25 mm^2 (circular) Ge:Cu; P2V-7 aircraft Bu. No. 140985.

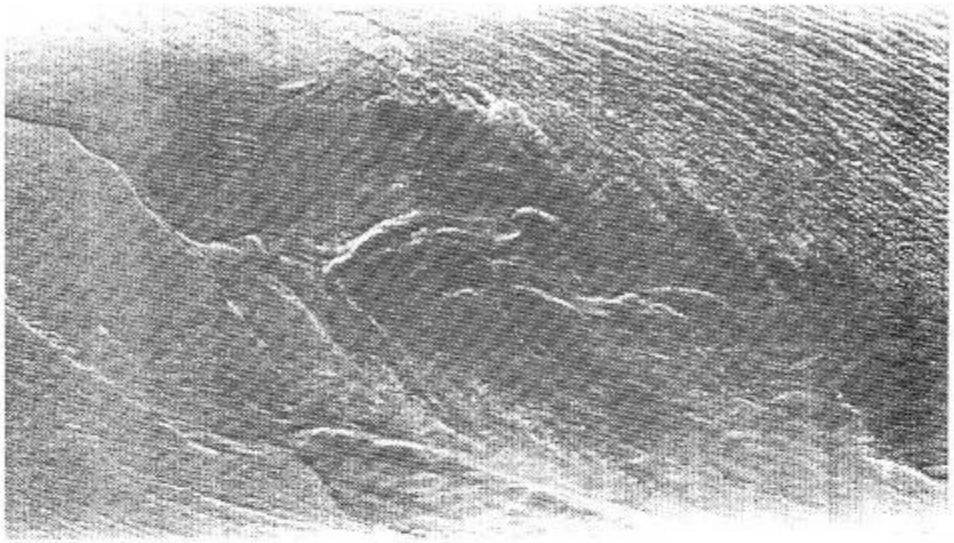

Figure 133. Natural Sea Surface Patterns.
1 September 1964; 2100; 3500 ft; AN/AAR-30; 6.25 mm^2 (circular) Ge:Hg; NP-2E aircraft Bu. No. 131403.

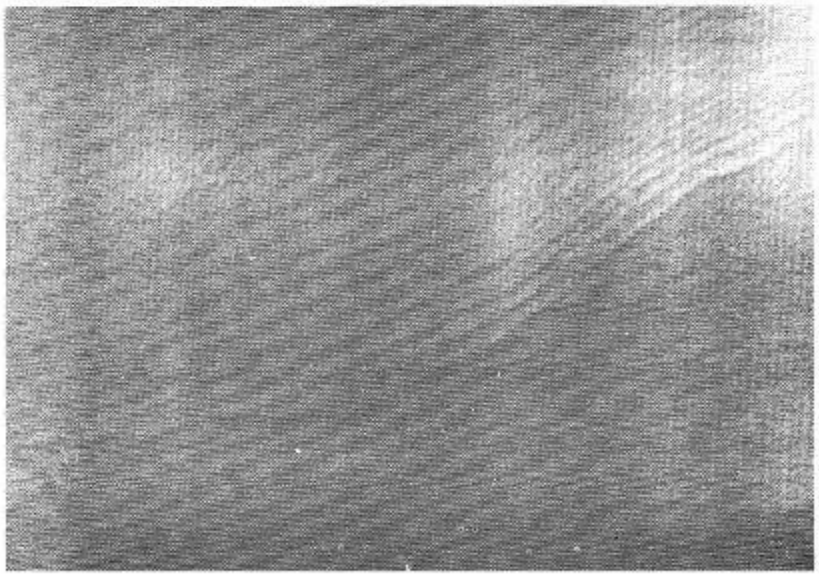

Figure 134. Natural Sea Surface Patterns.
8 April 1970; 1220; 2000 ft; 33°36'N; 78°49'W; AN/AAR-30; 2.5 X 2.5 mm Ge:Hg.

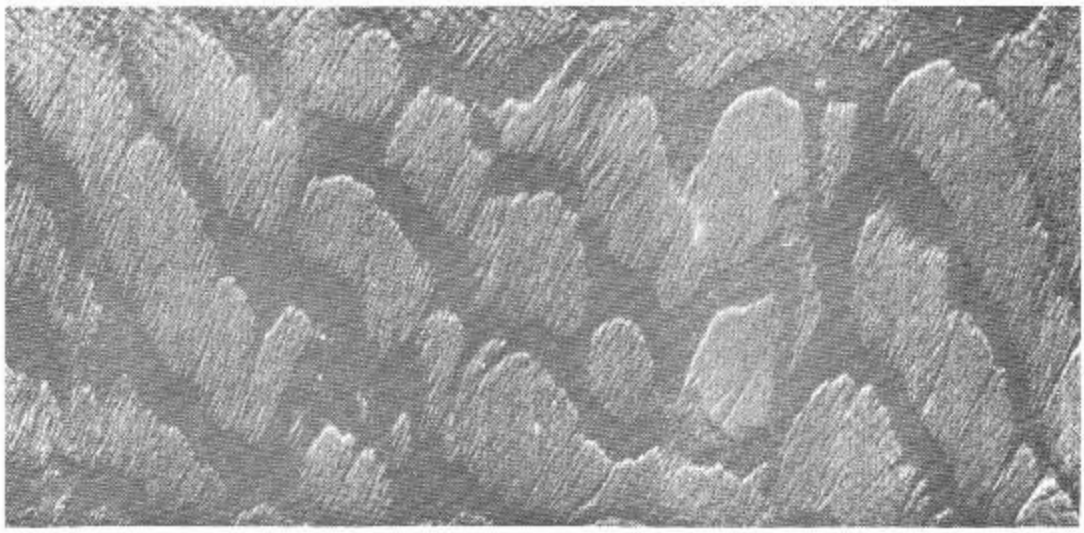

Figure 135. Natural Surface Patterns.
27 April 1972; 1944; 1200 ft; AN/AAR-30;
2.5 X 2.5 mm Ge: Hg.

Figure 136. Natural Sea Surface Patterns.
2 September 1967; 2245; 400 ft; 24°19'N; 82°17'W;
AN/AAR-32; 0.5 mm (diameter) Ge:Hg; NP-2E aircraft
Bu. No. 131403.
Sea state: 1-2.

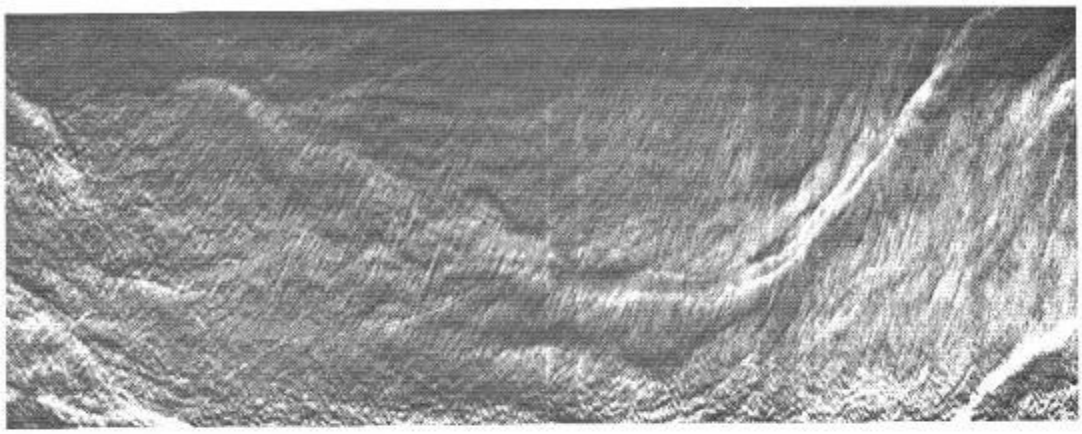

Figure 137. Natural Sea Surface Patterns.
19 April 1962; 1910; 2000 ft; 40°00'N; 71°33'W; AN/AAD-2;
6.25 mm^2 (circular) Ge:Cu; P2V-5F aircraft Bu. No. 131403.
Sea state: 1.

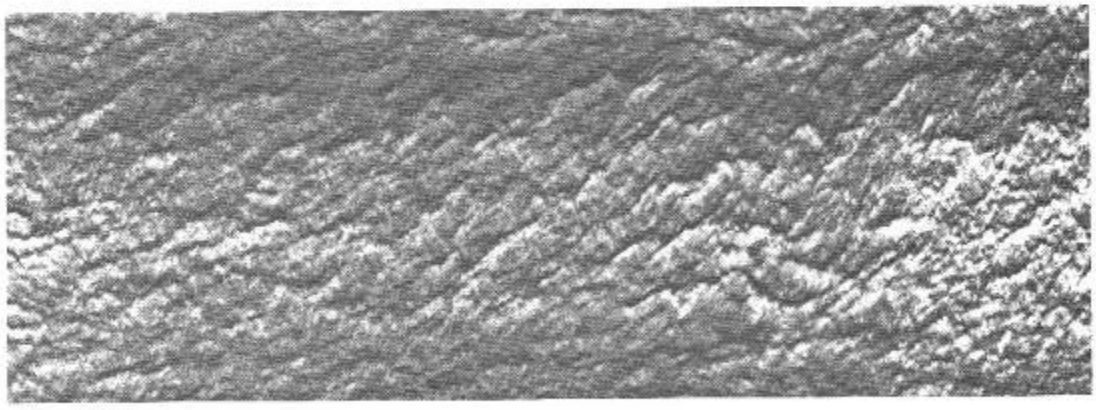

Figure 138. Natural Sea Surface Patterns.
11 October 1967; 2043; 480 ft; 31°42'N; 79°19'W; AN/AAR-32;
0.5 mm (diameter) Ge:Hg; NP-2E aircraft Bu. No. 131403.
Sea state: 1-2.

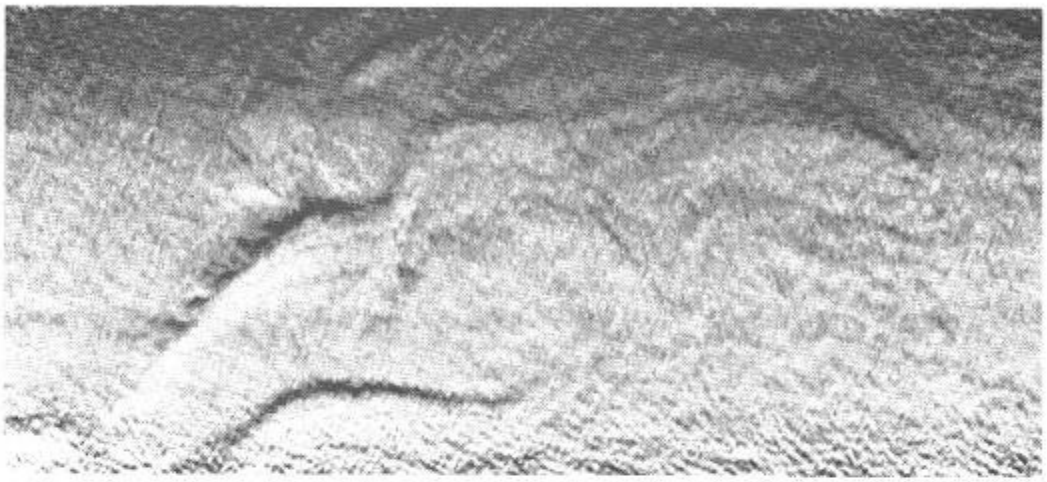

Figure 139. Natural Sea Surface Patterns.
16 April 1962; 2357; 2000 ft; 40°10'N; 71°10'W; AN/AAD-2;
6.25 mm^2 (circular) Ge:Cu; P2V-5F aircraft
Bu. No. 131403.

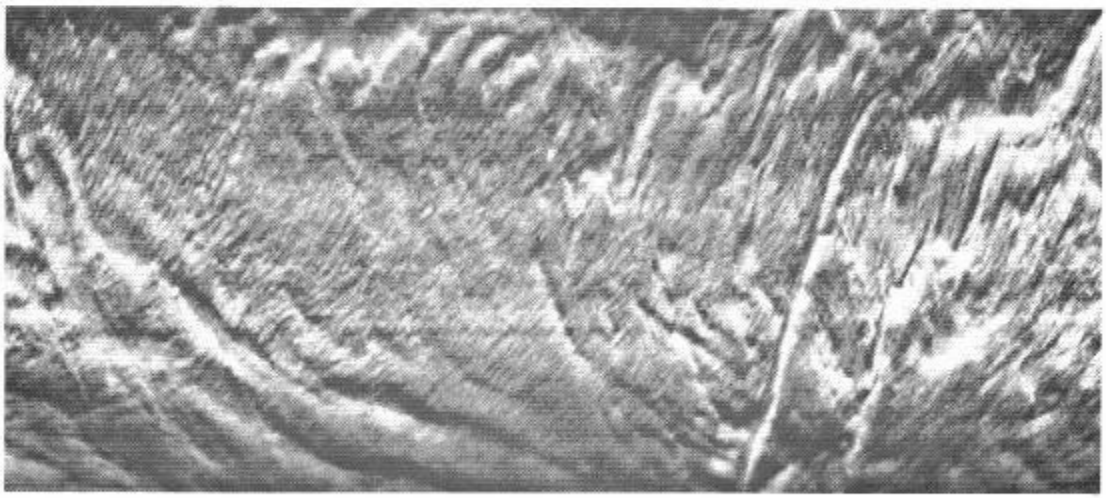

Figure 140. Natural Sea Surface Patterns.
4 September 1967; 2115; 380 ft; 24°18'N; 82°11'W; AN/AAR-32;
0.5 mm (diameter) Ge:Hg; NP-2E aircraft Bu. No. 131403.
Sea state: 0.

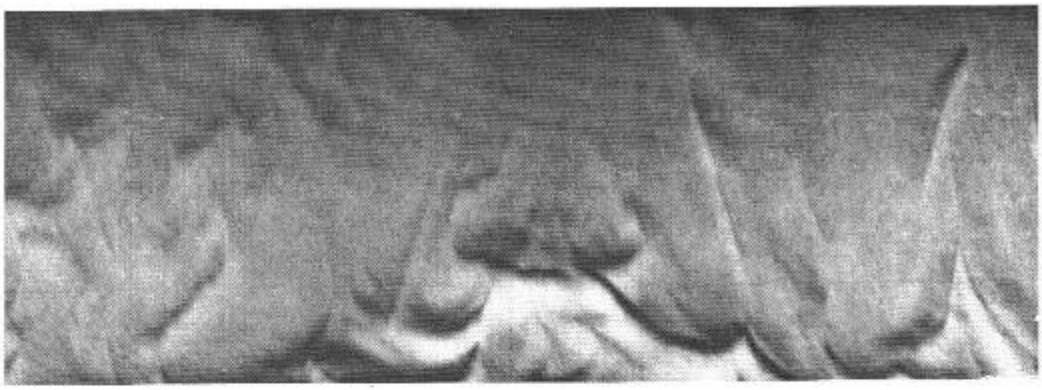

Figure 141. Natural Sea Surface Patterns.
27 July 1962; 0324; 4500 ft; $40^{o}50'$N; $71^{o}30'$W; AN/AAD-2;
6.25 mm^2 (circular) Ge:Cu; P2V-5FS aircraft
Bu. No. 131403.

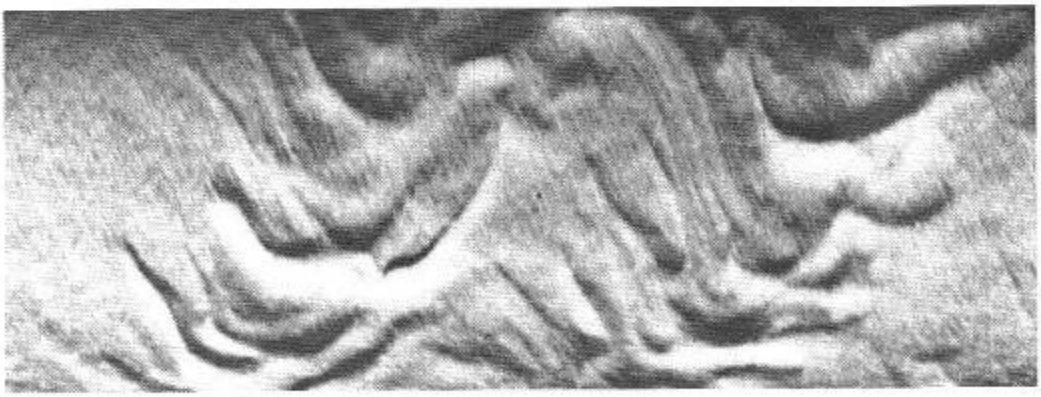

Figure 142. Natural Sea Surface Patterns.
27 July 1962; 0335; 4500 ft; $40^{o}48'$N; $72^{o}01'$W; AN/AAD-2;
6.25 mm^2 (circular) Ge:Cu; P2V-5FS aircraft
Bu. No. 131403.

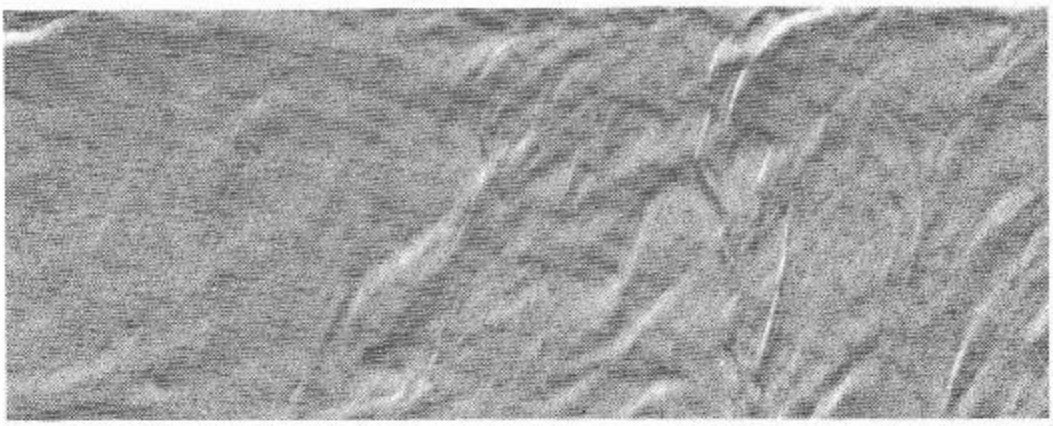

Figure 143. Natural Sea Surface Patterns.
15 July 1965; 1514; 4400 ft; 37°20'; 75°19'W; AN/AAD-2;
4 mm^2 (circular) Ge:Cu; NP-2E aircraft Bu. No. 131403.

Figure 144. Natural Sea Surface Patterns.
12 March 1962; 2227; 2500 ft; 24°33'N; 81°57'W; AN/AAD-2;
6.25 mm^2 (circular) Ge:Cu; P2V-5F aircraft
Bu. No. 131403.

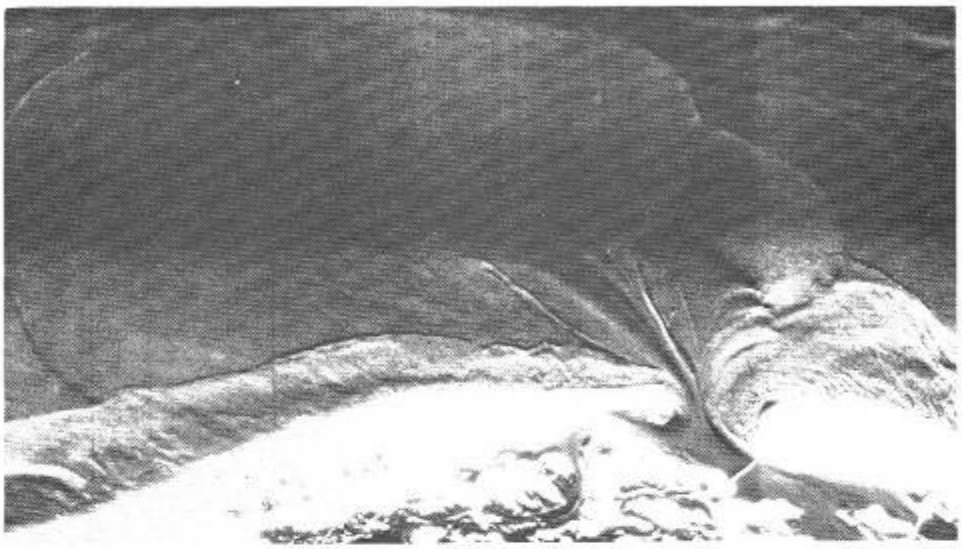

Figure 145. Great Egg Harbor Inlet.
3 October 1963; 2123; 12,000 ft; 39°18'N; 74°33'W; AN/AAR-30;
0.5 mm (diameter) Ge:Cu; NP-2E aircraft Bu. No. 131403.

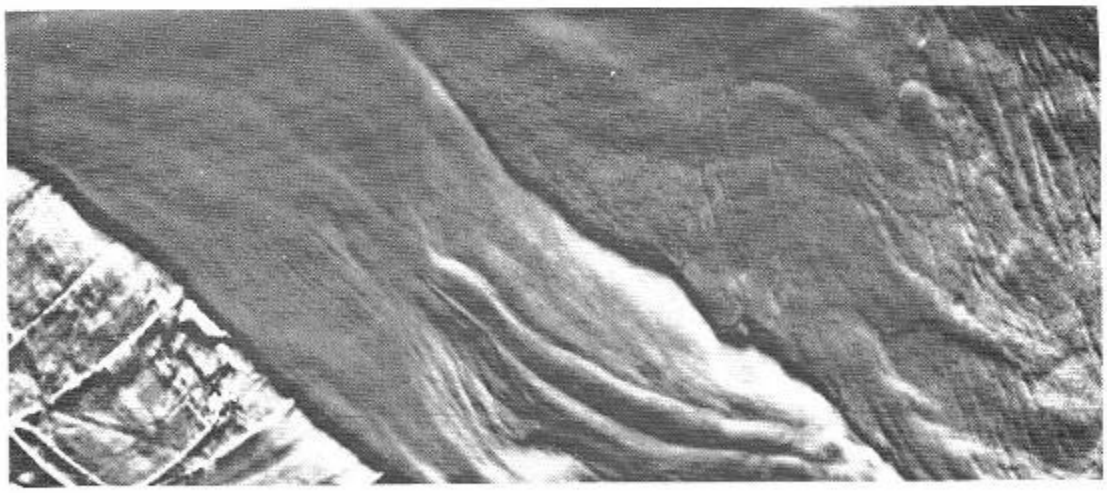

Figure 146. Surface Patterns in the Delaware River.
26 June 1962; 2032; 2000 ft; 39°53'N; 75°11'W; AN/AAD-2;
6.25 mm^2 (circular) Ge:Cu; P2V-7 aircraft Bu. No. 140985.

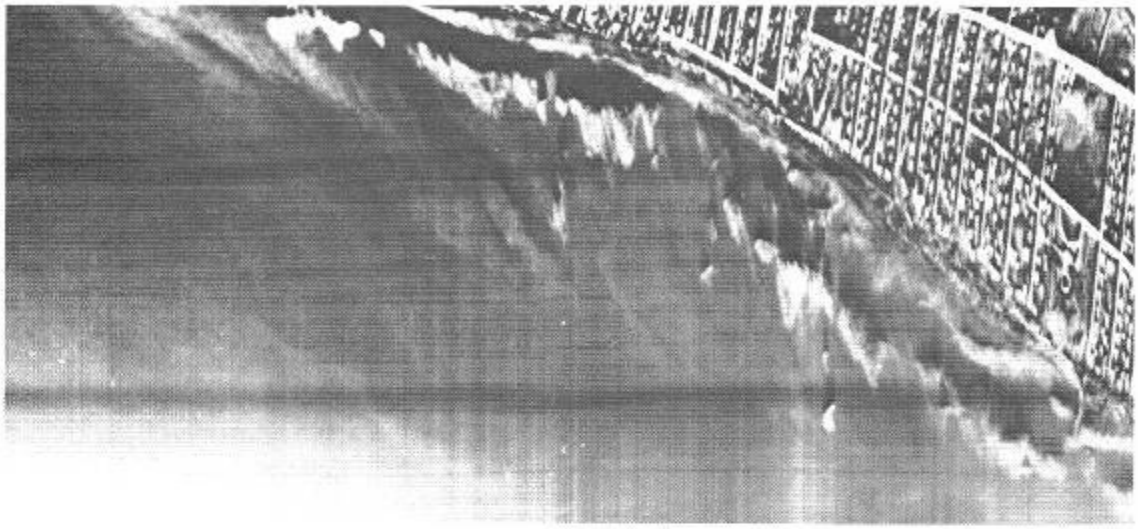

Figure 147. Shoreline, Breakers, and Natural Sea Surface Patterns.
15 February 1962; 1715; 5000 ft; 39°35'N; 74°10'W;
AN/AAD-2; 6.25 mm^2 (circular) Ge:Cu; P2V-5F
aircraft Bu. No. 131403.
Sea state: 3.

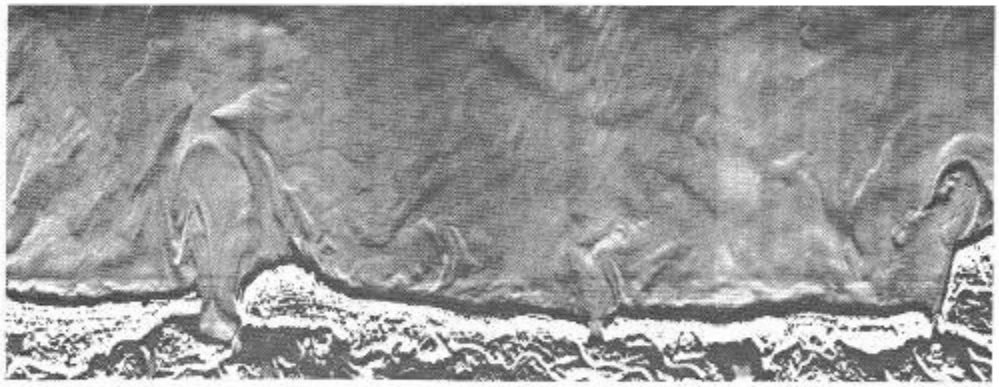

Figure 148. Natural Sea Surface Patterns in the Vicinity of
Ocean City, New Jersey.
1 October 1963; 2213; 12,000 ft; 39°15'N; 74°33'W;
Reconofax IV Mark II; 0.5 mm (diameter) Ge:Cu;
NP-2E aircraft Bu. No. 131403.

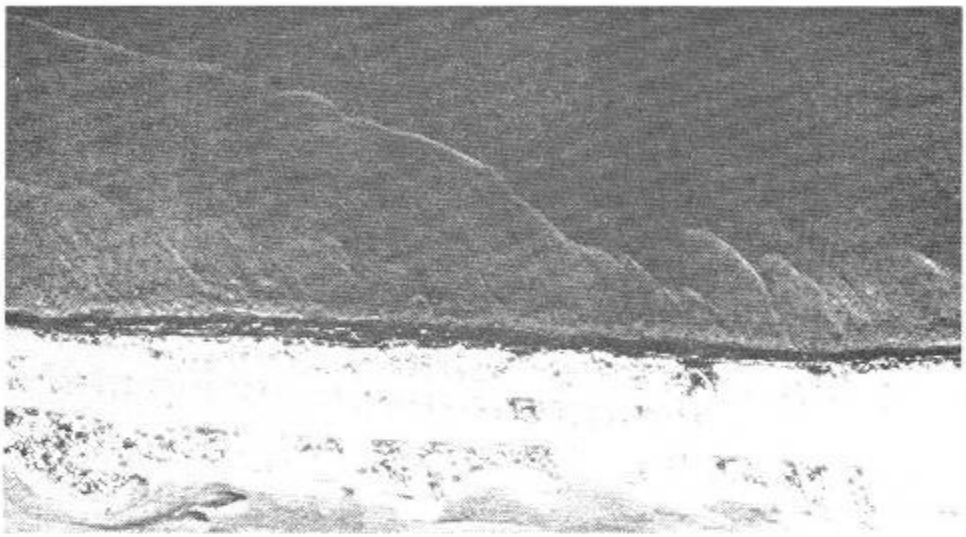

Figure 149. Long Beach, New Jersey, and Adjacent Surface Patterns.
3 October 1963; 1957; 2500 ft; 39°35'N; 74°13'W;
AN/AAR-30; 0.5 mm (diameter) Ge:Cu; NP-2E
aircraft Bu. No. 131403.

Figure 150. Natural Sea Surface Patterns.
7 May 1962; 2205; 3000 ft; 39°33'N; 70°31'W; AN/AAD-2;
6.25 mm^2 (circular) Ge:Cu; P2V-7 aircraft
Bu. No. 140985.

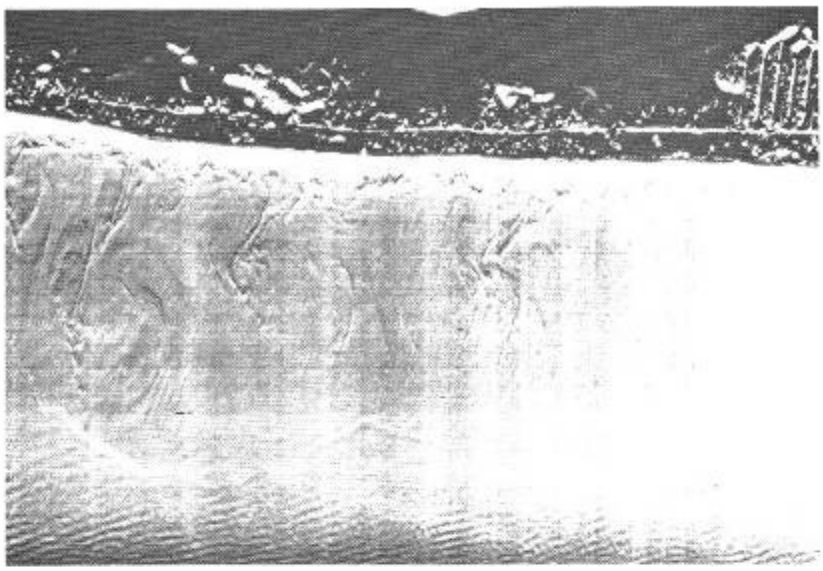

Figure 151. Coastline and Adjacent Sea Surface Patterns.
30 January 1964; 1902; 39°44'N; 74°07'W; AN/AAR-30; 0.5 mm (diameter) Ge:Cu; NP-2E aircraft Bu. No. 131403.
Note evidence of waves along the lower border of the picture.

Figure 152. Interface Between Water Masses of Unequal Temperature.
30 March 1967; 1433; 3300 ft; AN/AAR-32; 0.5 mm (diameter) Ge:Hg; NP-2E aircraft Bu. No. 131403.

Figure 153. Natural Surface Patterns.
24 May 1972; 1848; 7000 ft; AN/AAR-30; 2.5 X 2.5 mm Ge:Hg.

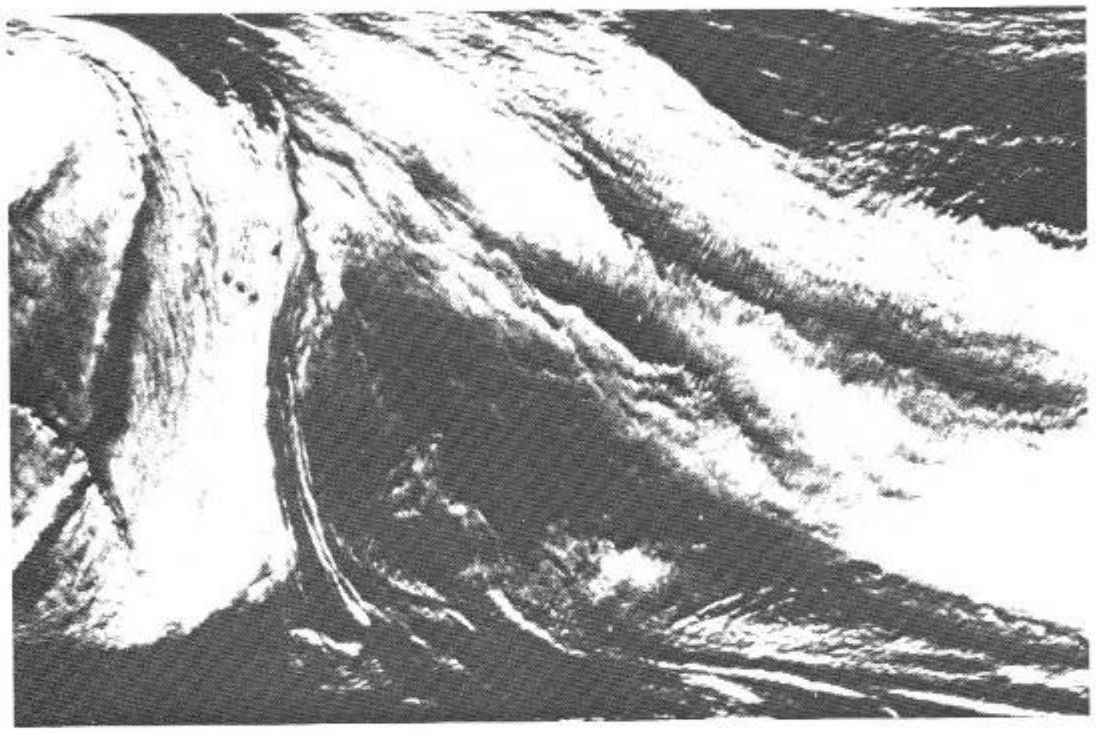

Figure 154. Natural Surface Patterns.
24 May 1972; 1836; 5000 ft; AN/AAR-30; 2.5 X 2.5 mm Ge:Hg.

Figures 155-159 demonstrate the persistence of surface thermal patterns in the Tongue of the Ocean, a region southeast of Florida, over a course of 42 minutes. This series of infrared pictures was recorded at 1000 feet with a mercury doped germanium detector operating in the AN/AAR-32 during the flight of 13 May 1966.

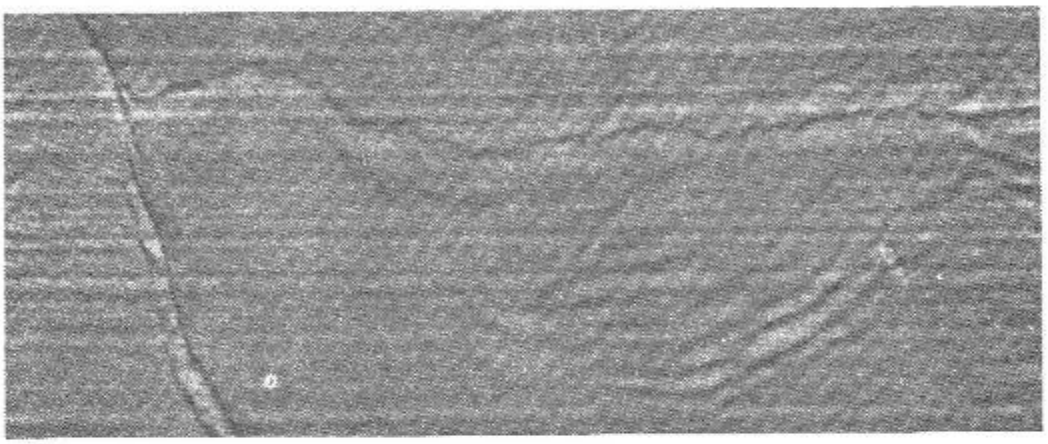

Figure 155. Time: 2307.

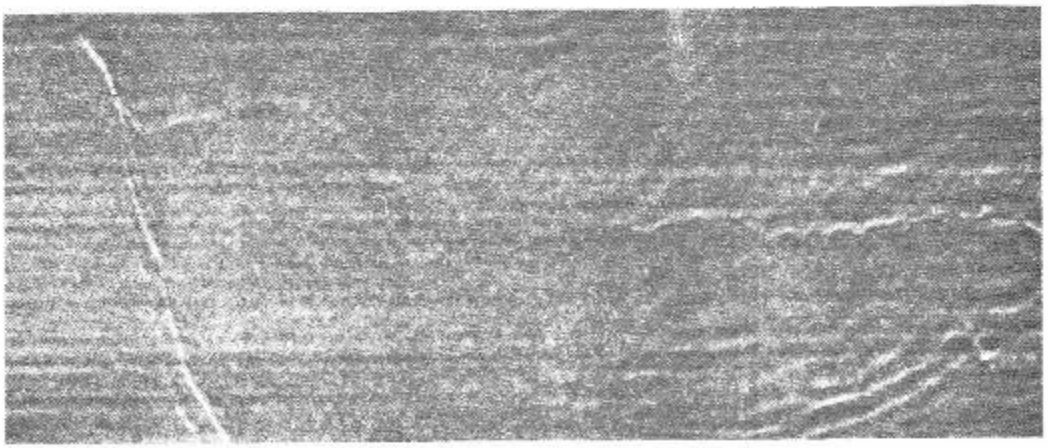

Figure 156. Time: 2314.

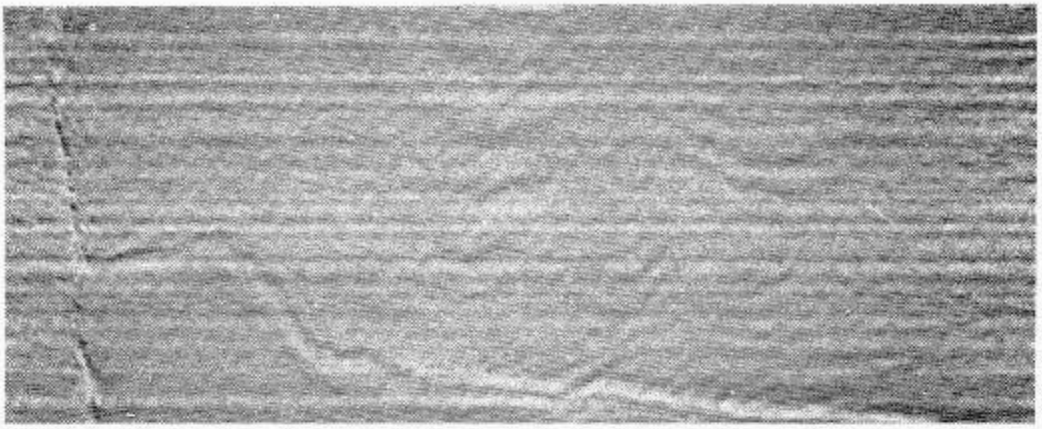

Figure 157. Time: 2327.

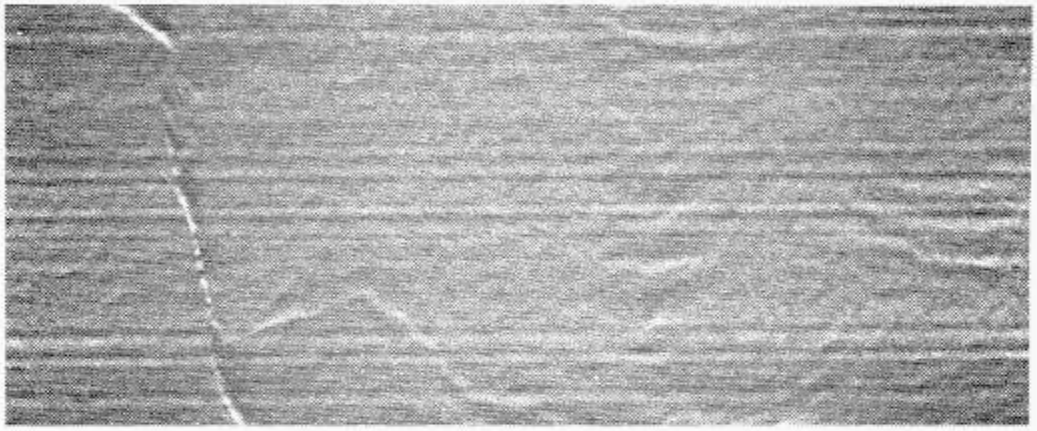

Figure 158. Time: 2334.

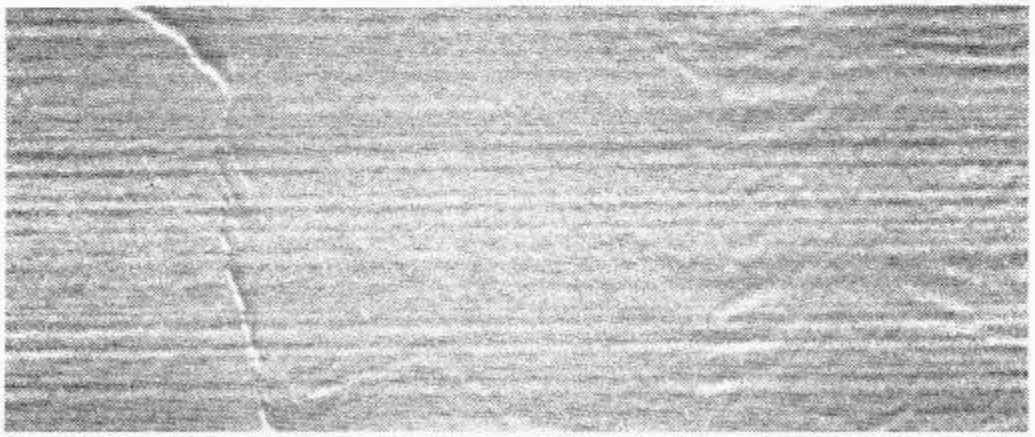

Figure 159. Time: 2349.

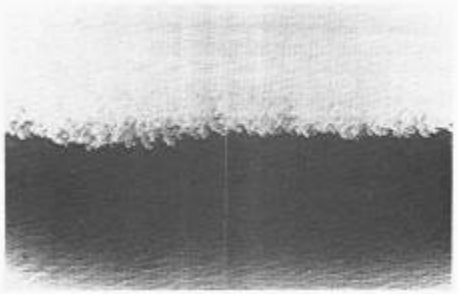

Figure 160. Western Wall of the Gulf Stream.
16 September 1966; 1422; 1500 ft; 37°57'N; 70°31'W;
AN/AAR-30; 2.5 X 2.5 mm Ge:Hg; NP-2E aircraft
Bu. No. 131403.
The water of the Gulf Stream was found to be about 0.5 K
warmer than the coastal waters at the boundary.

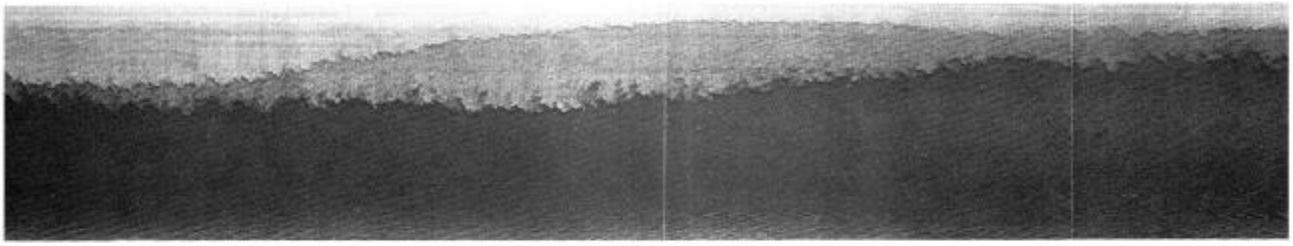

Figure 161. Interface Between the Gulf Stream and cooler coastal
waters.
16 September 1966; 1428; 1500 ft; 38°07'N; 70°22'W;
AN/AAR-30; 2.5 X 2.5 mm Ge:Hg; NP-2E aircraft
Bu. No. 131403.

Figures 162 to 179 were recorded during a series of flights over Bute Inlet in July 1969. For each of the exercises, a 2.5 X 2.5 mm mercury doped germanium detector was used in the Reconofax IV Mark II.

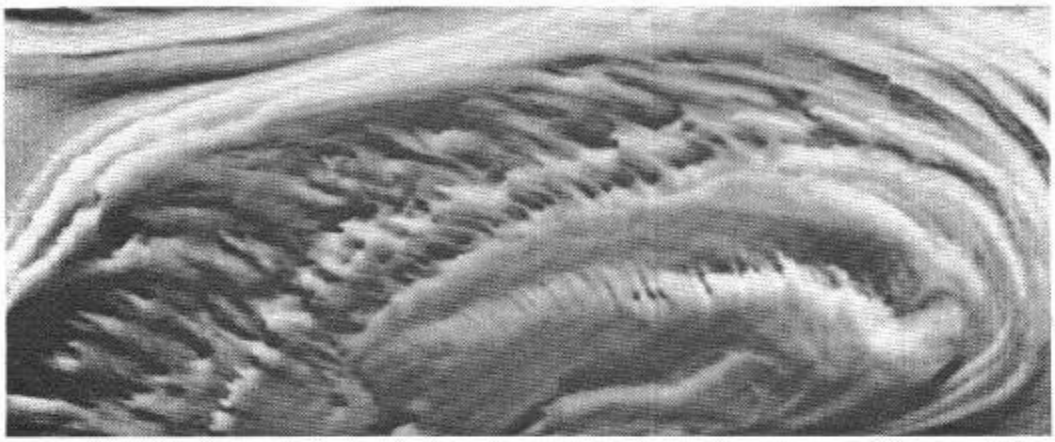

Figure 162. Natural Surface Patterns.
15 July 1969; 1709; 1000 ft.
Sea state: 1.

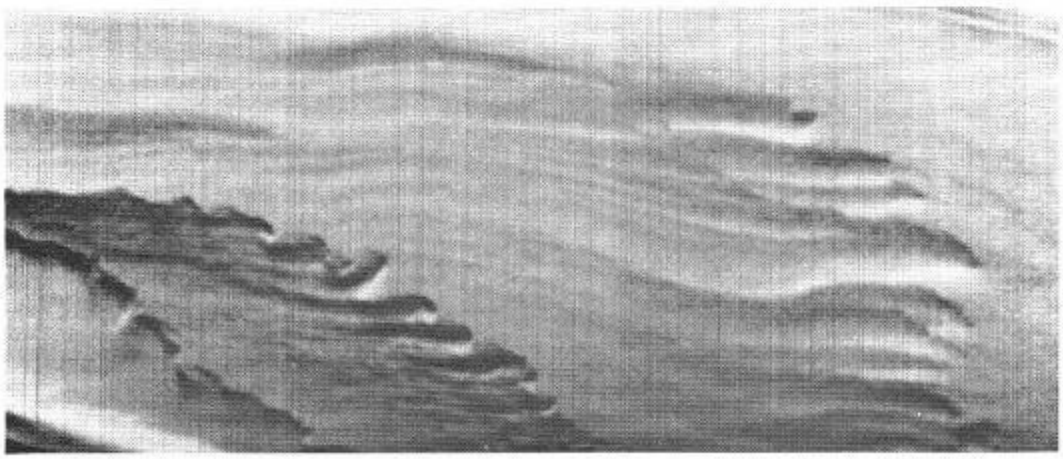

Figure 163. Natural Surface Patterns.
12 July 1969; 1045; 600 ft.
Sea state: 1.

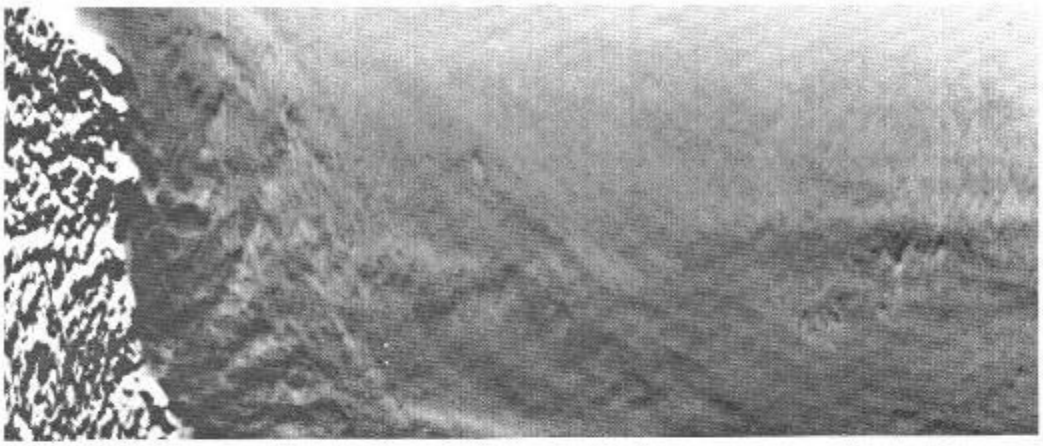

Figure 164. Shoreline and Natural Surface Patterns.
18 July 1969; 1530; 300 ft.
Sea state: 1/4 - 1/2.

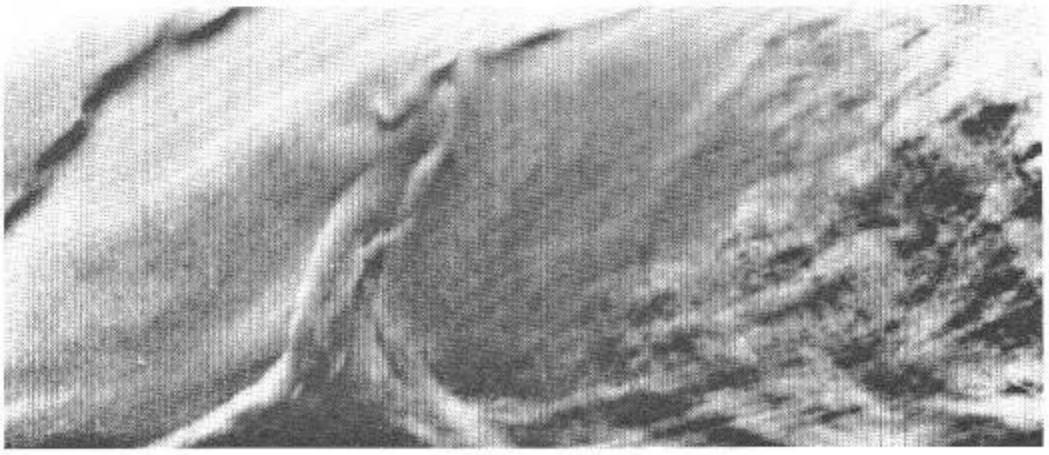

Figure 165. Natural Surface Patterns.
9 July 1969; 1357; 500 ft.
Sea state: 1/4.

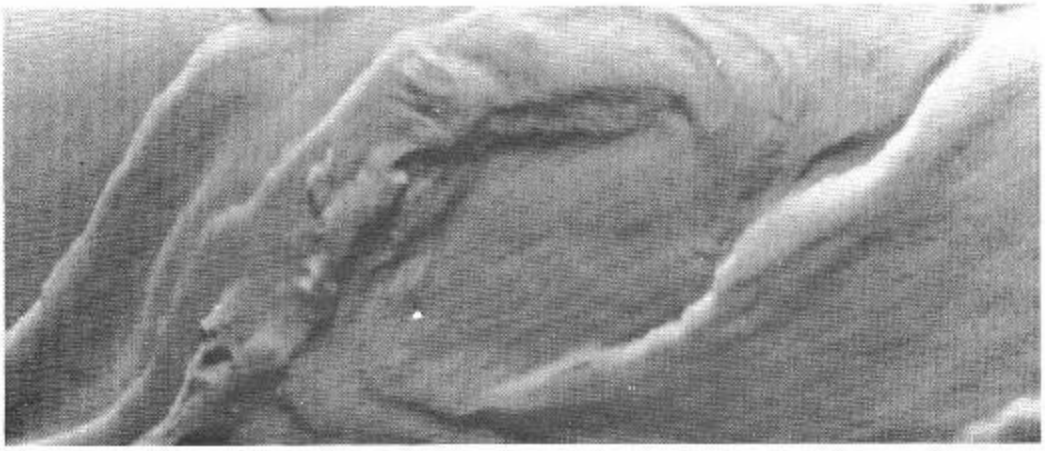

Figure 166. Natural Surface Patterns.
10 July 1969; 1405; 1000 ft.
Sea state: 1-2.

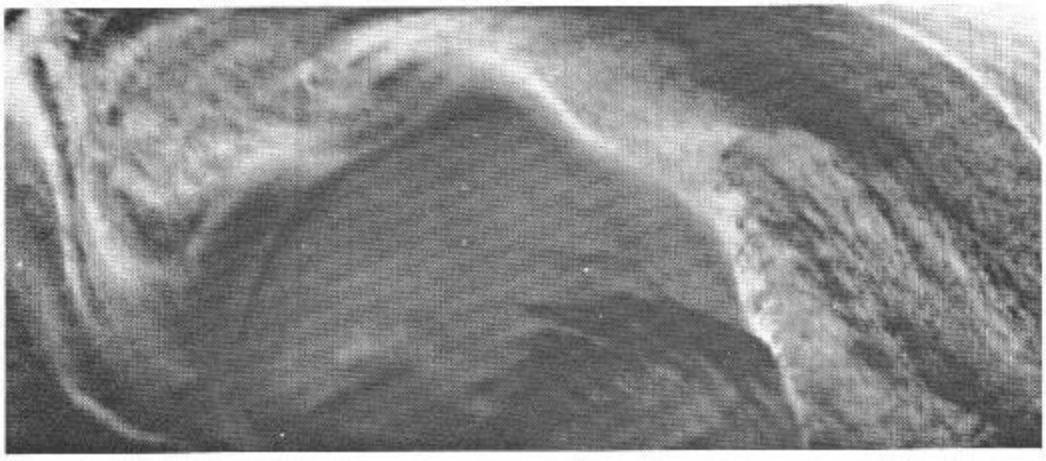

Figure 167. Natural Surface Patterns.
12 July 1969; 0849; 500 ft.
Sea state: 1.

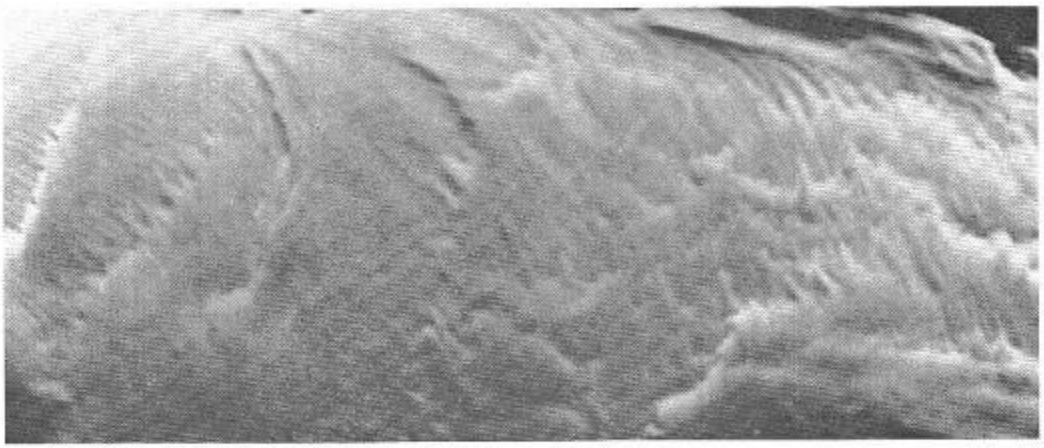

Figure 168. Natural Surface Patterns.
9 July 1969; 1349; 1500 ft.
Sea state: 1/4.

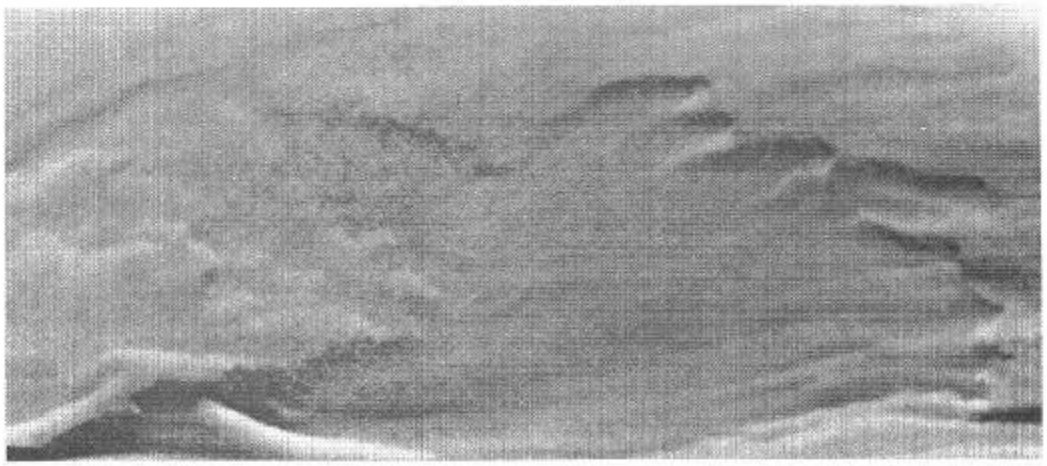

Figure 169. Natural Surface Patterns.
10 July 1969; 1346; 200 ft.
Sea state: 1-2.

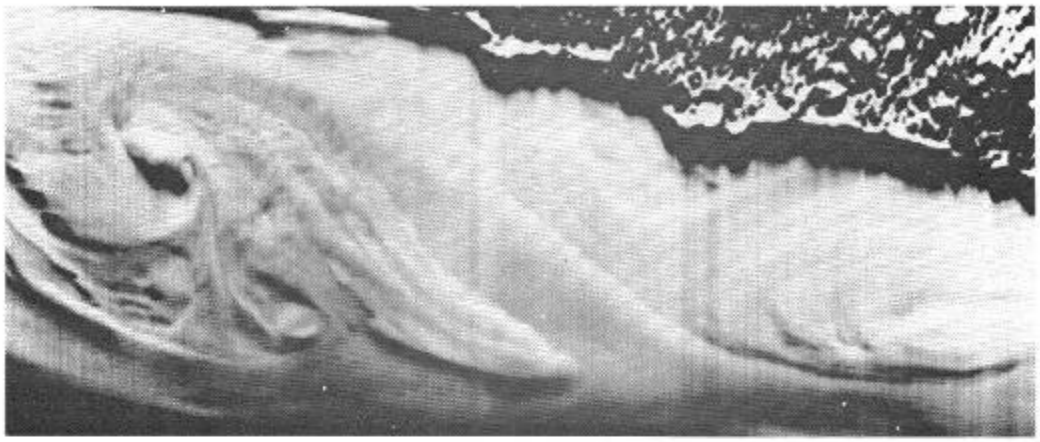

Figure 170. Shoreline and Adjacent Surface Patterns.
15 July 1969; 1710; 1000 ft.
Sea state: 1.

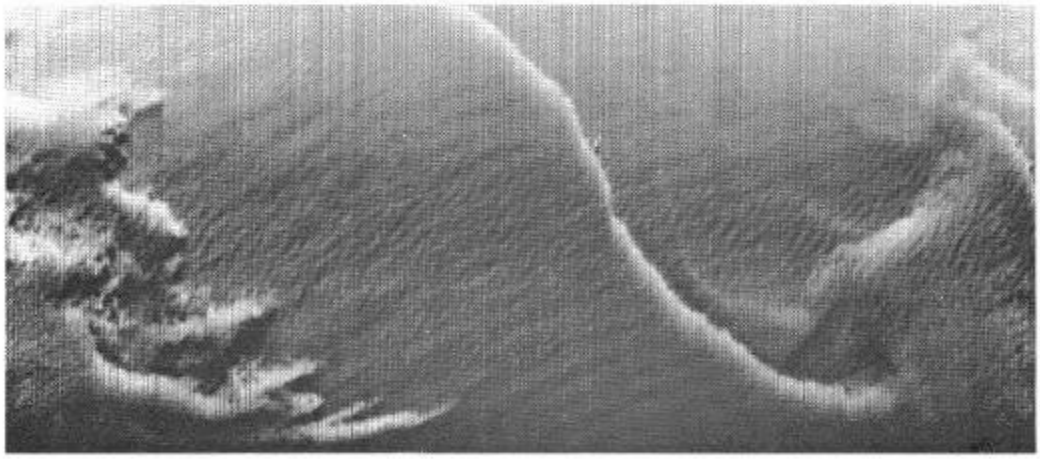

Figure 171. Natural Surface Patterns.
14 July 1969; 1539; 300 ft.
Sea state: 1/2.

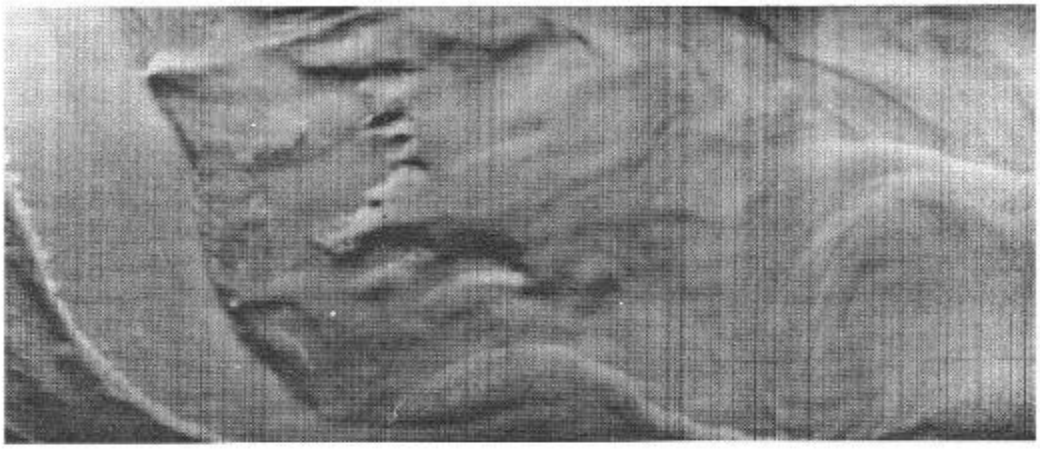

Figure 172. Natural Surface Patterns.
14 July 1969; 1613; 700 ft.
Sea state: 1/2.

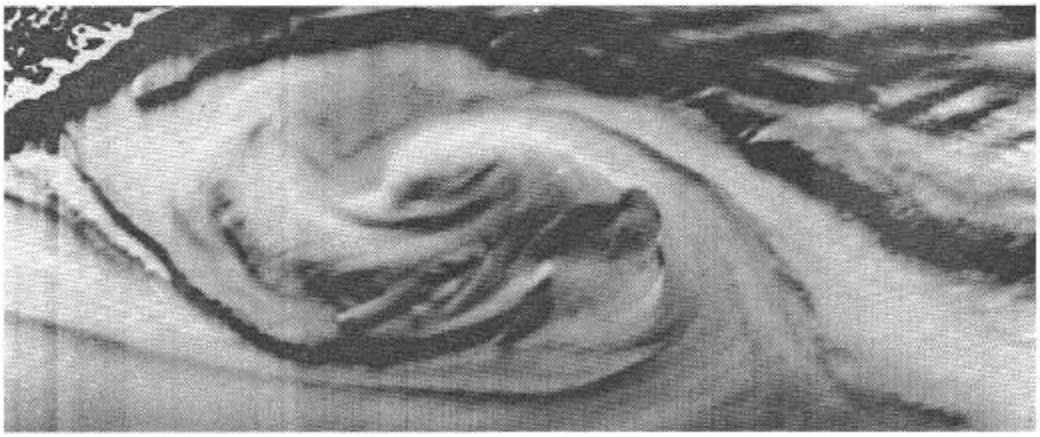

Figure 173. Offshore Eddy.
15 July 1969; 1708; 1000 ft.
Sea state: 1.

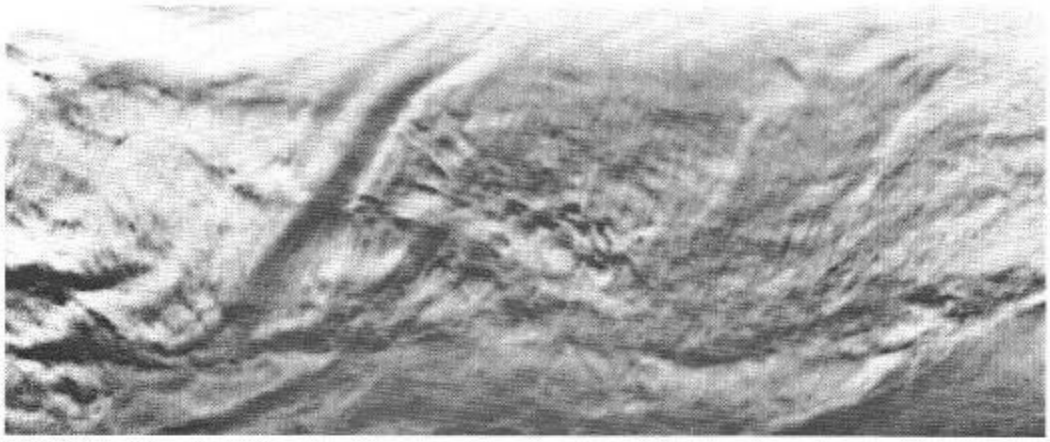

Figure 174. Natural Surface Patterns.
19 July 1969; 1000; 300 ft.
Sea state: 0 - 1/4.

Figure 175. Natural Surface Patterns.
14 July 1969; 1654; 700 ft.
Sea state: 1/2.

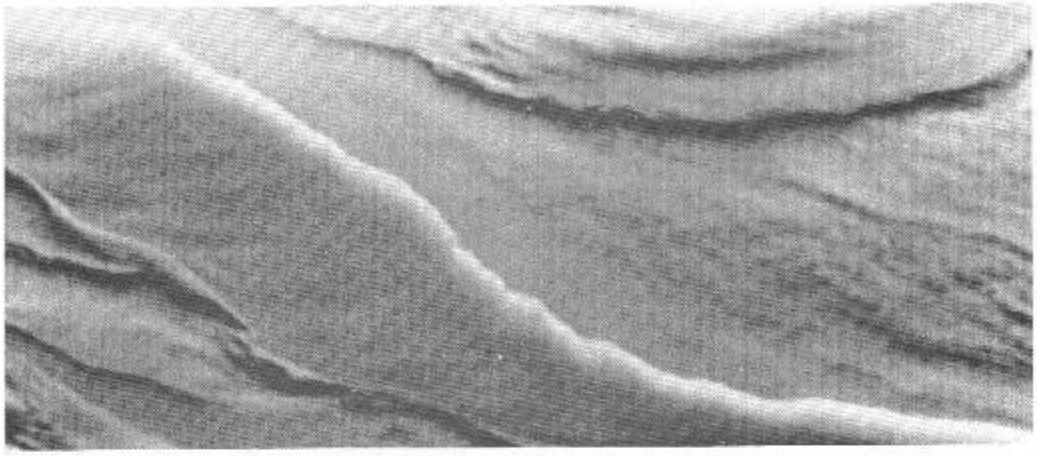

Figure 176. Natural Surface Patterns.
10 July 1969; 1425; 1000 ft.
Sea state: 1-2.

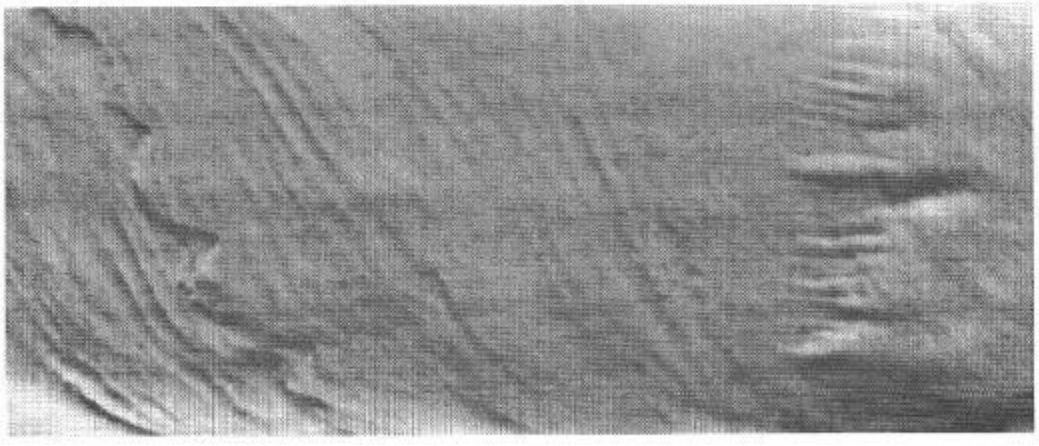

Figure 177. Natural Surface Patterns.
16 July 1969; 1030; 300 ft.
Sea state: 1/2.

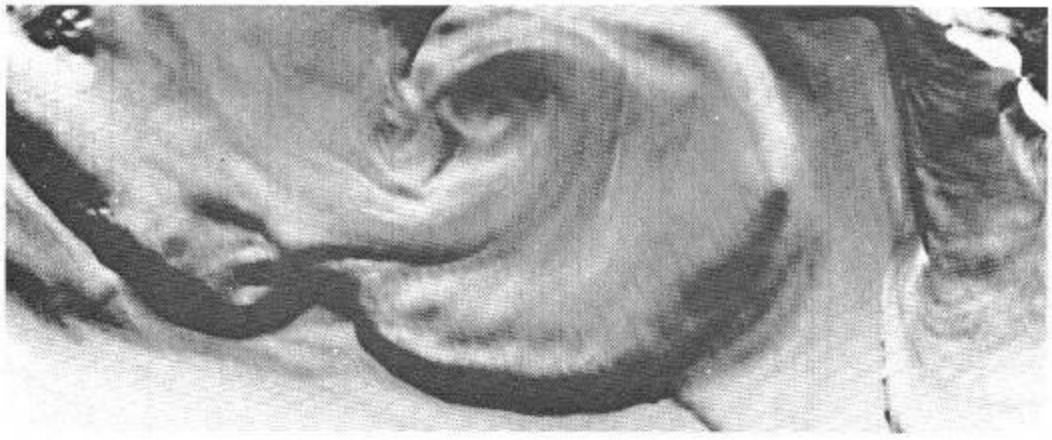

Figure 178. Eddy.
9 July 1969; 1538; 1000 ft.
Sea state: 1/4.

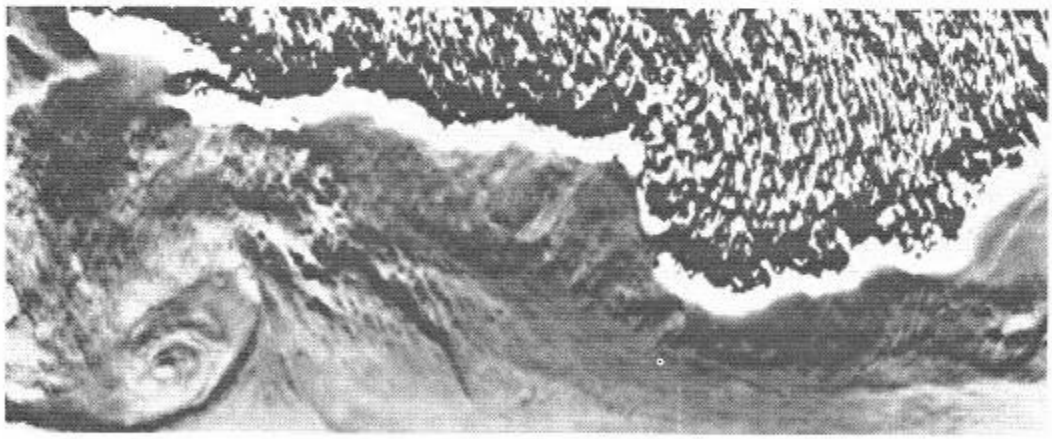

Figure 179. Eddy and Nearby Land Mass.
18 July 1969; 1511; 300 ft.
Sea state: 1/4 - 1/2.

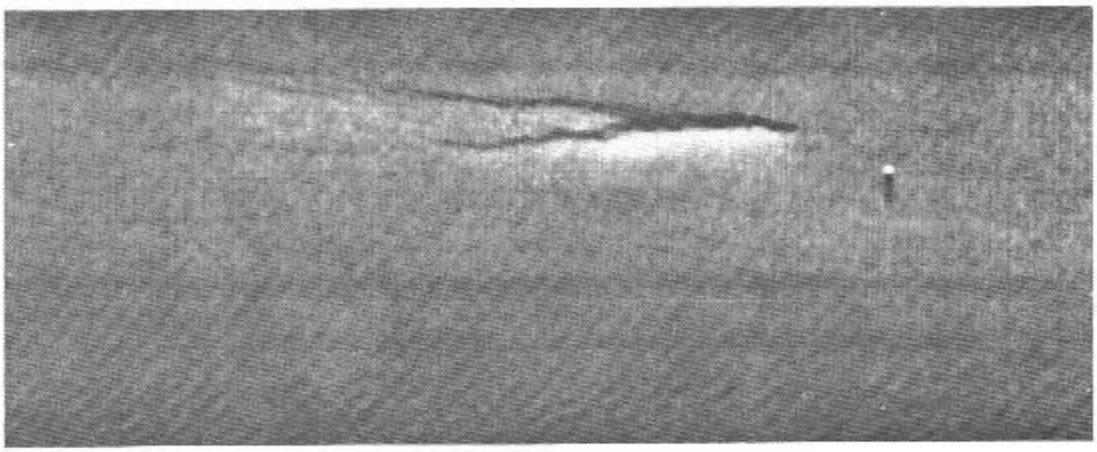

Figure 180. Oil Slick and Smoke Light.
7 February 1963; 2028; 1500 ft; 24°33'N; 81°18'W;
AN/AAD-2; 6.25 mm^2 (circular) Ge:Cu; SP-2H
aircraft Bu. No. 147949.
Note detectability of waves along bottom edge of picture.

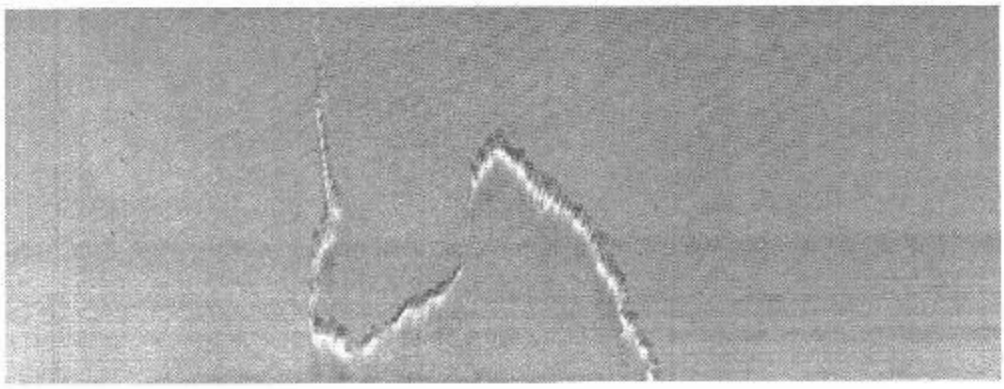

Figure 181. Oil Slick.
3 October 1963; 2006; 2500 ft; 39°17'N; 74°22'W;
Reconofax IV Mark II; Ge:Cu; NP-2E aircraft
Bu. No. 131403.

Figures 182-186 show thermal pictures taken during the flight of 16 December 1971, which was conducted in cooperation with the Environmental Protection Agency to detect possible industrial waste water discharges along the Delaware and Schuylkill Rivers.

Figures 182 and 183 were taken over the Schuylkill River on 16 December 1971; 1500 ft; AN/AAR-30; 2.5 X 2.5 mm Ge:Hg; NP-2E aircraft Bu. No. 131403. In Figure 182, note effectively "warm" water flowing from a point near the bottom center of the picture. In Figure 183 warm water is being discharged into the river at a point to the right of center.

Figure 182. Time: 1712

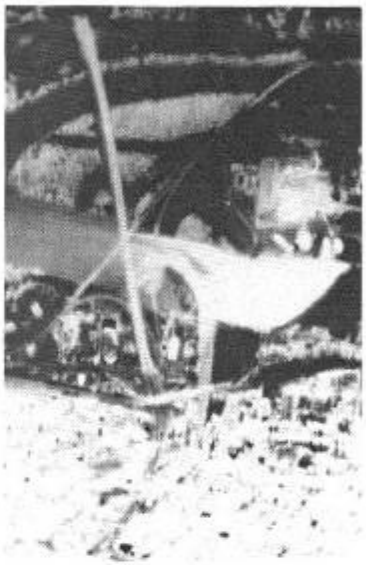

Figure 183. Time: 1717

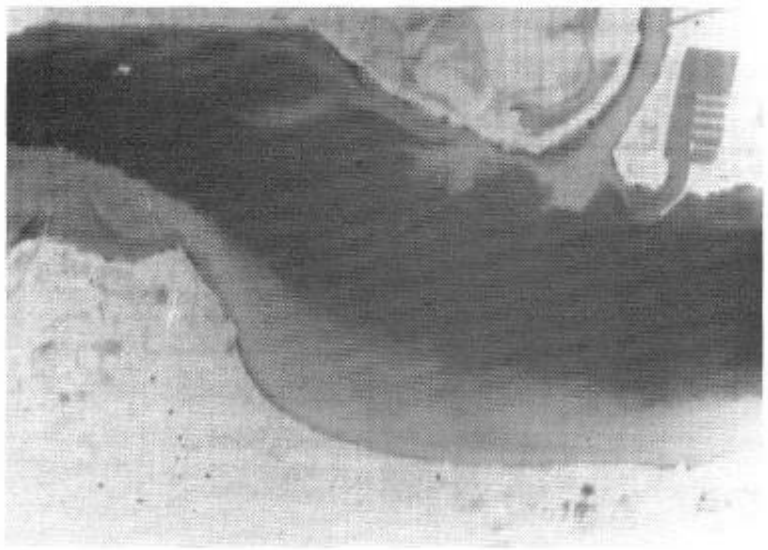

Figure 184. Delaware River.
16 December 1971; 1904; 1500 ft; AN/AAR-30; 2.5 X 2.5 mm Ge:Hg; NP-2E aircraft Bu. No. 131403.
This scene shows the Neshaminy Creek (upper right) emptying into the Delaware River. Along the opposite shore, heated water from a power plant upstream (to the right) can be seen.

Figures 185 and 186 were recorded over an oil refinery on the Delaware River at different times and with different equipment.

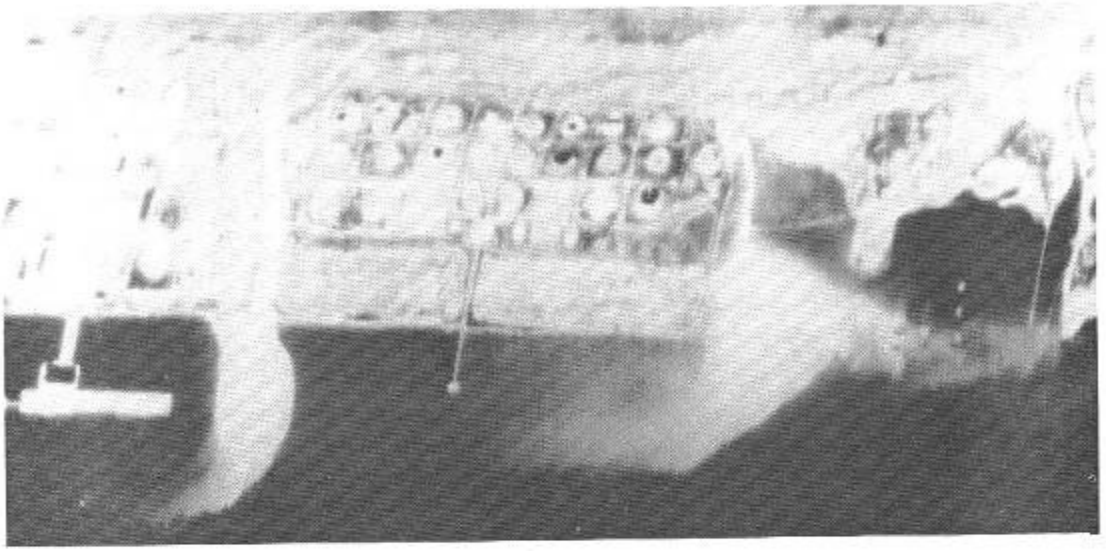

Figure 185. 16 December 1971; 1856; 1500 ft; AN/AAR-30; 2.5 X 2.5 mm Ge:Hg; NP-2E aircraft Bu. No. 131403.

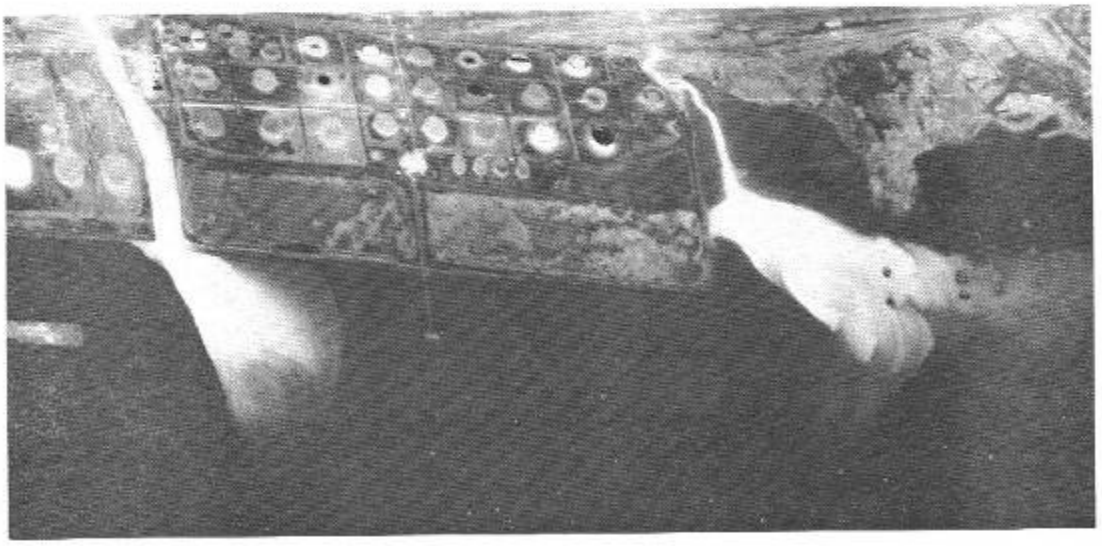

Figure 186. 16 December 1971; 1933; 1500 ft; AN/AAR-35; 0.3 X 0.3 mm Ge:Hg; NP-2E aircraft Bu. No. 131403.

Figures 187 to 193 were reproduced from the film record of the flight of 8 March 1971. The AN/AAR-35 was operated over a region centered at 68° 55'N, 18°20'W. The black spots in the pictures are fragments of thick, multi-year ice; light gray areas represent young ice; the darker gray sections are first year ice; and white patches correspond to open water or new ice.

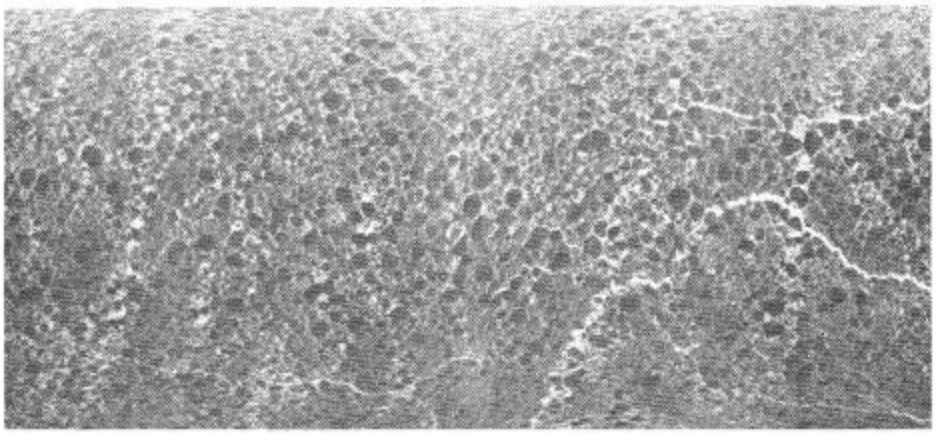

Figure 187. Time: 1930
Altitude: 1000 ft.

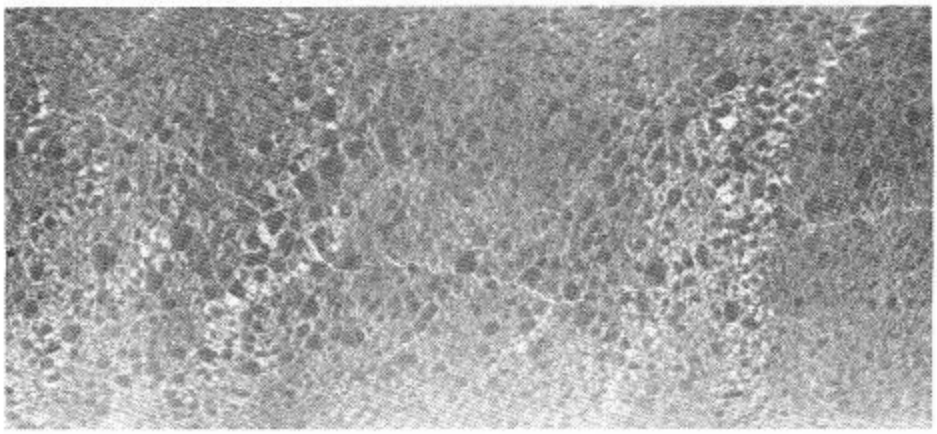

Figure 188. Time: 1931
Altitude: 1000 ft.

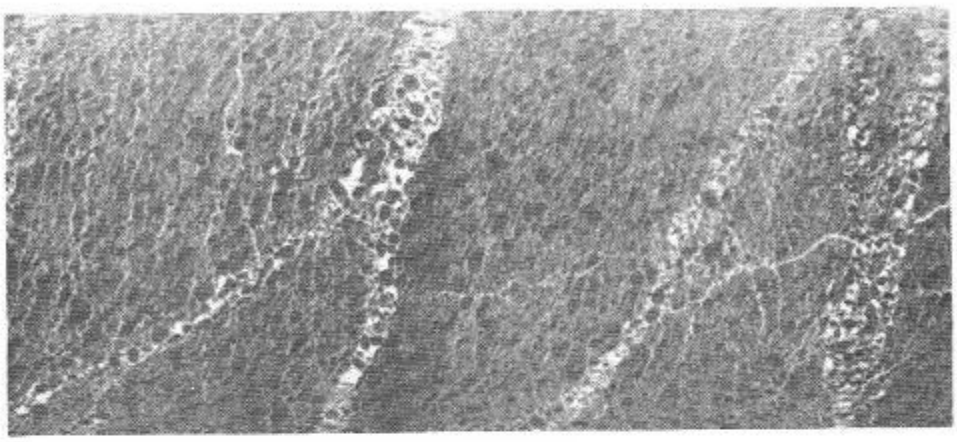

Figure 189. Time 1932
Altitude: 1000 ft.

Figure 190. Time 1748
Altitude: 5000 ft.

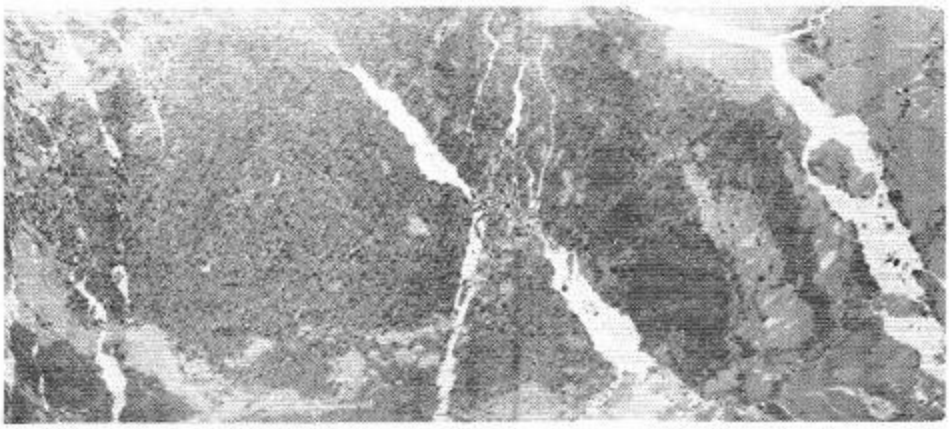

Figure 191. Time: 1750
Altitude: 5000 ft.

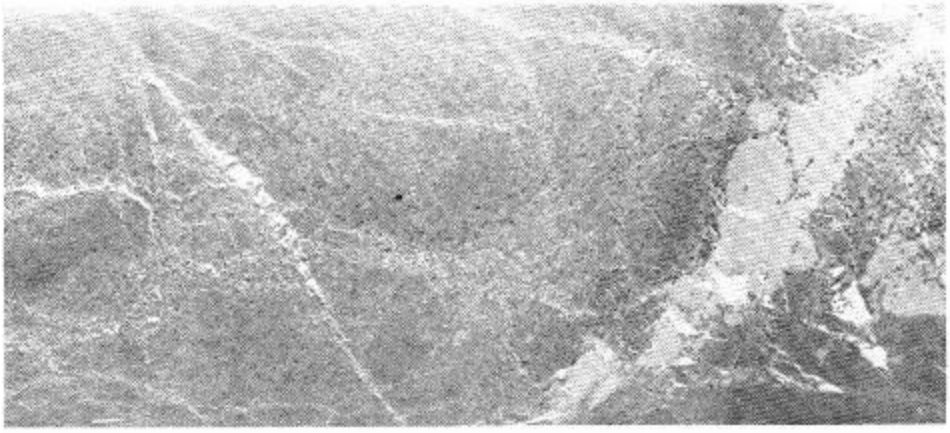

Figure 192. Time: 1752
Altitude: 5000 ft.

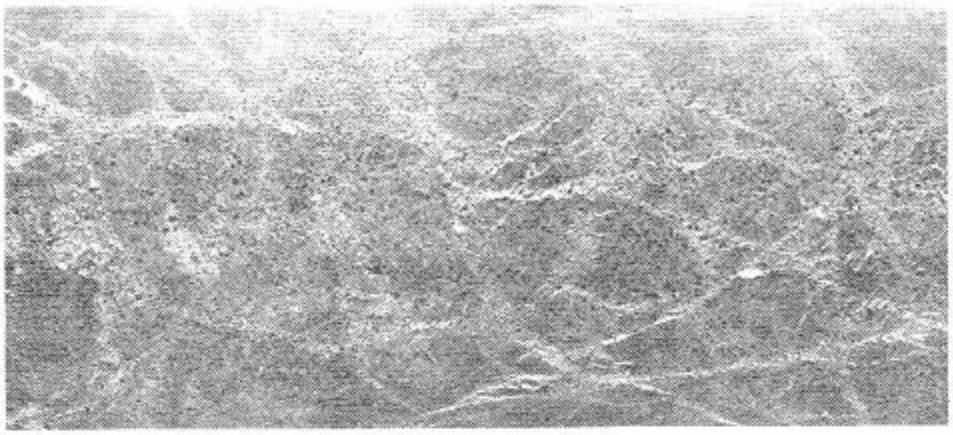

Figure 193. Time: 1754
Altitude: 5000 ft.

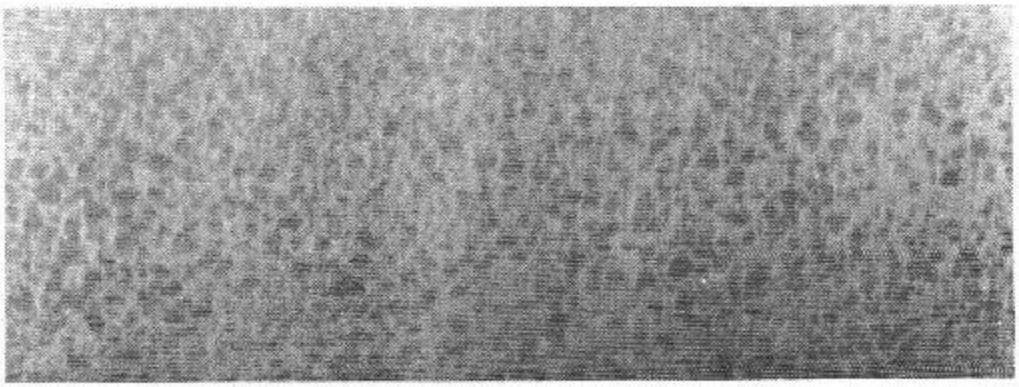

Figure 194. Chunks of Ice Floating on Water East of Greenland.

DISTRIBUTION LIST

REPORT NO. NADC-78226-30

AIRTASK NO. A-35-370E/001B/9F11-100-000
Work Unit No. WF11-100-000/ZU701

	No. of Copies
NAVAIRSYSCOM	10
(2 for retention)	
(3 for AIR-370)	
(3 for AIR-53335)	
(1 for AIR-360)	
(1 for AIR-370D)	
CNA, OP-03EG	1
CNM, MAT-08TE	3
MAT-08T214	
MAT-08T245	
CNO, OP-095	5
OP-098	
OP-35E	
OP-955	
OP-986	
FLEWEACEN (CAPT R. Hughes)	1
NAC, Code 802	1
NATC, SA83	2
AT51	
NAVOCEANO	3
NAVSEA, Code 0313	2
Code 03415	
NCSC	1
NIC, Code 01	1
NISC, Code 70	1
NLEX, Code 3042 (2 copies)	3
PME 107-52	
NORDA, Code 331	3
Code 332	
Code 335	
NOSC, Code 14	7
Code 015	
Code 407	
Code 811	
Code 6514	
Code 7313	
Code 1603B	
NPC	1
NPGS, 61 Ct	1
NRL, 1409W	17
Code 5300	
Code 5500	
Code 5501	
Code 5553	
Code 5530	
Code 5560	
Code 6110	

	No. of Copies
NRL, Code 7905	
Code 8000	
Code 8300	
Code 8301	
Code 8304	
Code 8310	
Code 8320	
Code 8340	
Code 8400	
NSRDC, Code 2833	1
NSWC/DL, N-54	1
NSWC/WOL, CR-34	2
CR-42	
NUSC, Code 343	1
NWC, Code 315 (4 copies)	9
Code 33	
Code 3311	
Code 3175	
Code 394 (2 copies)	
ONR, Code 103T	5
Code 421	
Code 460	
Code 480	
Code 481	
ONR, Bay St. Louis (Mr. Stanley Wilson)	1
ONR, Boston (Dr. M. B. White)	1
ONR, Chicago (Dr. J.E. Ivory)	1
ONR, London (Dr. R.S. Hughes)	1
ONR, New York (Mr. I. Rowe)	1
ONR, Pasadena (CDR Kenneth G. Robinson)	1
PMTC, Code 1233	1
OUSDRE (R&AT)	1
DARPA	2
NV&EOL	1
AFAL	1
AFGL	1
EPA	1
ERIM	3
IDA	3
IRIA	2
NASA	1
NOAA	1
APL/JHU (Dr. Richard Gasparovic)	1
Scripps Institution of Oceanography	1
Woods Hole Oceanographic Institution	4
DDC	
University of Wisconsin, Marine Studies Center (Dr. Theodore Green III)	1